

**YILDIRIM BEYAZIT UNIVERSITY  
GRADUATE SCHOOL OF NATURAL AND APPLIED  
SCIENCES**



**ANALYTICAL AND NUMERICAL ANALYSIS OF  
SWAGE AUTOFRETTAGE PROCESS APPLIED  
TO THICK WALLED CYLINDERS**

**M.Sc. THESIS by  
Halil YILDIRIM**

**Department of Mechanical Engineering**

**ANKARA, 2015**

# **ANALYTICAL AND NUMERICAL ANALYSIS OF SWAGE AUTOFRETTAGE PROCESS APPLIED TO THICK WALLED CYLINDERS**

**A Thesis Submitted to the  
Graduate School of Natural and Applied Sciences of Yildirim Beyazıt  
University  
In Partial Fulfillment of the Requirements for the Degree of Master of Science  
in Mechanical Engineering, Department of Mechanical Engineering**

**by**

**Halil YILDIRIM**

**ANKARA, 2015**

## M.Sc THESIS EXAMINATION RESULT FORM

We have read the thesis entitled “**Analytical and Numerical Analysis of Swage Autofrettage Process Applied Thick Walled Cylinders**” completed by **Halil YILDIRIM** under supervision of **Prof. Dr. Veli ÇELİK** and we certify that in our opinion it is fully adequate, in scope and in quality, as a thesis for the degree of Master of Science.

.....  
Prof. Dr. Veli ÇELİK

\_\_\_\_\_  
Supervisor

.....  
Prof. Dr. Osman YİĞİT

\_\_\_\_\_  
(Jury Member)

.....  
Prof. Dr. M. Hüsnü DİRİKOLU

\_\_\_\_\_  
(Jury Member)

\_\_\_\_\_  
Prof.Dr. Fatih V. ÇELEBİ

Director

Graduate School of Natural and Applied Sciences

## ACKNOWLEDGEMENTS

I would like to thank all those people who made this thesis possible and provided an important experience for me.

First of all, I would like to express the deepest appreciation to my supervisor Professor **Veli ÇELİK** for his guidance, encouragement, and support and for helping me complete my work.

Besides my advisor, I am deeply grateful to Professor **Osman YİĞİT**. He always shared his knowledge and experience with me. His creative ideas, valuable criticism, irreplaceable encouragement and friendly approach contributed to the completion of the present work.

I am grateful to **Onur GÜNGÖR** who works in The Machinery and Chemistry Industry Institution for sharing his great experiences about Finite Element Methods.

Finally, I would like to thank **my wife Nur** and **my family** who gave me great continuous support, and encouragement more than I need throughout my study.

# **ANALYTICAL AND NUMERICAL ANALYSIS OF SWAGE AUTOFRETTAGE PROCESS APPLIED TO THICK WALLED CYLINDERS**

## **ABSTRACT**

Autofrettage is the process of residual stress formation on the walls of the thick walled cylinders before their usage. These residual stresses help to increase the pressure bearing capacity of the thick walled cylinders by eliminating some stresses during the high pressure applications. In practice, there are two different autofrettage methods as hydraulic and swage. Swage autofrettage is a more economical method to form beneficial residual stresses in the thick walled cylinders when it is compared with the hydraulic autofrettage method.

In this study, it is investigated how the residual stresses, that occur as a result of the swage autofrettage during manufacturing of a heavy armour barrel, affect the stress distributions that occur at the operating conditions of the barrel. At first, the stress distributions are obtained analytically for both Tresca and Von Mises criteria. Then, the verification of the analytical model is performed by making use of a commercial software which uses the finite element method.

In the calculations, the mandrel's outer radius is considered as constant but the bore value of the cylinder is changed and the results for different % interference ratios are compared. The obtained results show that the maximum equivalent stress in an autofrettaged cylinder at operating pressure occurs in the elastic-plastic junction region.

The equivalent stress distributions are obtained at 400 MPa operating pressure for different % interference values. The equivalent stress distributions are obtained by the analytical model for both Tresca and Von Mises criteria and the optimum interference value is found as 1% with respect to both two yielding criteria. However, in result of finite element model, the optimum interference value is found as 1% for Tresca criterion whereas it is found as 1,5% for Von Mises criterion.

Bauschinger effect is represented by the kinematic hardening model in both analytical model and finite element model. According to the results that are obtained by analytical model, Bauschinger effect does not cause a secondary plastic yielding. However, according to the results that are obtained by finite element model, it is seen that Bauschinger effect causes a secondary plastic yielding.

**Keywords: swage autofrettage, mandrel, elasto-plastic cylinders, residual stress, thick walled cylinders, pressure vessels, bilinear hardening model, elastic perfectly plastic model, elastic-plastic radius, secondary yielding, bauschinger effect, interference ratio**

# KALIN CİDARLI SİLİNDİRLERE UYGULANAN MEKANİK OTOFRETAJ İŞLEMİNİN ANALİTİK VE NÜMERİK ANALİZİ

## ÖZ

Otofretaj, kalın cidarlı silindirlerin cidarlarında, kullanım öncesi kalıcı gerilmeler oluşturma işlemidir. Bu kalıcı gerilmeler, yüksek basınçların kullanıldığı uygulamalarda ortaya çıkan gerilmelerin bir kısmının yok edilmesi suretiyle, kalın cidarlı silindirlerin basınç taşıma kapasitelerinin artırılmasına yardımcı olmaktadır. Pratikte hidrolik ve mekanik olmak üzere iki farklı ofofretaj yöntemi vardır. Mekanik ofofretaj tekniği, kalın cidarlı silindirlerde faydalı kalıcı gerilmeler oluşturmak için hidrolik ofofretaj tekniğine göre daha ekonomik bir yöntemdir.

Bu çalışmada bir ağır silah namlusunun üretimi sırasında uygulanan mekanik ofofretaj işlemi sonucu ortaya çıkan kalıcı gerilmelerin, namlunun çalışma şartlarında oluşan gerilme dağılımlarını ne şekilde etkilediği araştırılıyor. İlk başta gerilme dağılımları Tresca ve Von Mises akma kriterlerinin her ikisi için analitik yöntemle elde ediliyor. Daha sonra sonlu elemanlar metodunu kullanan ticari bir bilgisayar yazılımı yardımıyla analitik modelin doğrulaması yapılıyor.

Hesaplamalarda mandrel dış çapı sabit alınırken, silindir iç çap değerleri değiştirilerek farklı % arakesit değerleri için elde edilen sonuçlar karşılaştırılıyor. Elde edilen sonuçlar, ofofretaj görmüş silindirde çalışma basıncında oluşan maksimum eşdeğer gerilmenin elastik-plastik yarı çap bölgesinde oluştuğunu göstermektedir.

Farklı % arakesit değerleri için 400 MPa çalışma basıncında eşdeğer gerilme dağılımları elde ediliyor. Analitik model kullanılarak, Von Mises ve Tresca kriterlerinin her ikisi için ayrı ayrı eşdeğer gerilme dağılımları elde ediliyor ve her iki akma kriterine göre optimum arakesit değeri %1 olarak bulunuyor. Sonlu elemanlar yönteminde ise Tresca kriteri için optimum arakesit değeri %1 olarak bulunurken, Von Mises kriteri için %1.5 olarak bulunuyor.

Hem analitik modelde ve hem de sonlu elemanlar modelinde Bauschinger etkisi kinematik pekleşme modeli ile temsil ediliyor. Analitik model kullanılarak elde edilen sonuçlara göre Bauschinger etkisi ikincil bir plastik akmaya neden olmazken, sonlu elemanlar modeli ile elde edilen sonuçlara göre Bauschinger etkisinin ikincil plastik akmaya neden olduğu görülüyor.

**Anahtar Kelimeler : mekanik otofretaj, mandrel, elasto-plastik silindirler, kalıntı gerilme, kalın cidarlı silindirler, basınçlı kaplar, bilineer pekleşme modeli, elastik-mükemmel plastik model, elastik-plastik yarıçap, ikincil akma, bauschinger etkisi, arakesit oranı**



## CONTENTS

THESIS EXAMINATION RESULT FORM .....	ii
ACKNOWLEDGEMENTS .....	iii
ABSTRACT.....	iv
ÖZ .....	vi
CONTENTS.....	vii
LIST OF TABLES .....	xi
LIST OF FIGURES .....	xii
SYMBOLS.....	xiv
<b>1. INTRODUCTION .....</b>	<b>1</b>
1.1 Wire Winding Method .....	2
1.2 Autofrettage Method .....	2
1.2.1 Hydraulic Autofrettage .....	2
1.2.2 Swage Autofrettage .....	3
1.3 Compound Cylinder Method.....	3
1.4 Purpose of the Thesis .....	3
1.5 Methodology .....	4
1.6 Literature Research.....	6
<b>2. INTRODUCTION TO PLASTICITY .....</b>	<b>10</b>
2.1 Yielding Criteria .....	11
2.1.1 Strain Energy .....	11
2.1.2 The Components of Strain Energy .....	13
2.1.2.1 Distortion Energy.....	14
2.1.3 Distortion Energy Theory (von Mises).....	14

2.1.4 Maximum Shear Stress Theory (Tresca) .....	16
2.2 Bauschinger Effect .....	17
2.3 Strain Hardening.....	17
2.4 Ideal Material Models .....	18
2.4.1 Kinematic Hardening Model .....	18
2.4.2 Elastic-Perfectly Plastic Model .....	19
2.4.3 Elastic-Linear Plastic Model .....	20
<b>3. ANALYTICAL MODELLING .....</b>	<b>21</b>
3.1 Equilibrium Equations in Polar Coordinates.....	21
3.2 Strain Displacement Relations in Polar Coordinates .....	22
3.3 Analytical Relations for Thick Walled Cylindrical Vessels .....	23
3.3.1 Cylinders Subjected to Internal Pressure only.....	25
3.3.2 Cylinders Subjected to External Pressure only .....	25
3.4 Analytical Relations For Swage Autofrettage Process.....	26
3.4.1 Elastic-Perfectly Plastic Model .....	27
3.4.1.1 The Stresses in the Plastic Region in Loading Condition.....	27
3.4.1.2 The Stresses in the Elastic Region in Loading Condition.....	29
3.4.1.3 Determination of the Elastic-Plastic Junction.....	29
3.4.1.4 Residual Stresses.....	33
3.4.1.5 Elastic Recovery without Reyielding.....	33
3.4.1.5.1 Residual Stresses in the Plastic Region.....	33
3.4.1.5.2 Residual Stresses in the Elastic Region .....	33
3.4.1.6 Elastic Recovery with Reyielding.....	34
3.4.1.6.1 Stresses in ( $a \leq r \leq d$ ) Region.....	34
3.4.1.6.2 Stresses in ( $d \leq r \leq c$ ) Region.....	35
3.4.1.6.3 Stresses in ( $c \leq r \leq b$ ) Region.....	36
3.4.1.7 Bauschinger Effect in Autofrettage Process .....	36
3.4.1.7.1 Secondary Yielding Resulting from Bauschinger Effect.....	37
3.4.1.7.2 Stresses in ( $a \leq r \leq d$ ) Region.....	38
3.4.1.7.3 Stresses in ( $d \leq r \leq c$ ) Region.....	38
3.4.1.7.4 Stresses in ( $c \leq r \leq b$ ) Region.....	38

3.4.2 Bilinear Hardening Model .....	38
3.4.2.1 Stresses in the Plastic Region .....	40
3.4.2.2 Stresses in the Elastic Region .....	41
3.4.2.3 Determination of Elastic-Plastic Junction.....	42
3.4.2.4 Residual Stresses in the Plastic Region .....	42
3.4.2.5 Residual Stresses in the Elastic Region .....	42
3.4.2.6 Secondary Yielding Resulting from Bauschinger Effect.....	43
3.4.2.6.1 Stresses in ( $a \leq r \leq d$ ) Region.....	43
3.4.2.6.2 Stresses in ( $d \leq r \leq c$ ) Region.....	43
3.4.2.6.3 Stresses in ( $c \leq r \leq b$ ) Region.....	43
3.4.2.7 Determination of Bauschinger Effect Factor for Bilinear Kinematic Hardening Model.....	43
3.4.3 Effect of Turning Process on the Residual Stresses .....	44
3.4.3.1 The Stresses Due to Only Internal Turning .....	44
3.4.3.2 The Stresses Due to Only External Turning .....	45
3.4.4 Stresses Occurring at Service Pressure.....	45
3.4.5 Derivation of the Equations in Accordance with Von Mises Criterion...	46
<b>4. RESULTS and DISSCUSSIONS .....</b>	<b>47</b>
4.1 Results of Analytical Model.....	47
4.1.1 Autofrettage and Steel Barrel Draft.....	47
4.1.2 Determination of the Elastic-Plastic Junctions at Different Interference Values.....	49
4.1.3 Investigation of Bauschinger Effect for Different Interference Values...	50
4.1.4 Stress Distributions at Different Stages of Autofrettage .....	52
4.1.4.1 Stresses in Loading Condition .....	52
4.1.4.1.1 Radial Stresses .....	52
4.1.4.1.2 Hoop Stresses .....	54
4.1.4.1.3 Axial Stresses .....	55
4.1.4.2 Residual Stresses.....	57
4.1.4.2.1 Radial Stresses .....	57
4.1.4.2.2 Hoop Stresses .....	58

4.1.4.2.3 Axial Stresses .....	59
4.1.4.3 Optimization of Interference .....	61
4.1.4.4 Investigation of the Stress Distributions in Case of Secondary Yielding Due to Bauschinger Effect .....	63
4.1.4.5 Investigation of the Benefit of Autofrettage.....	65
4.1.4.6 Lightening the Barrel by External Turning .....	65
4.2 Results of Finite Element Model.....	68
4.2.1 Residual Stresses .....	69
4.2.1.1 Radial Stresses .....	69
4.2.1.2 Hoop Stresses.....	70
4.2.1.3 Axial Stresses.....	71
4.2.2 Equivalent Stresses at Operating Pressure.....	71
4.3 Comparison of Results of Analytical Model and Finite Element Model .....	73
4.3.1 Residual Stresses .....	73
4.3.1.1 Radial Stresses .....	73
4.3.1.2 Hoop Stresses.....	74
4.3.1.3 Axial Stresses.....	75
4.3.1.4 Comparison of Elastic-Plastic Radius Values.....	77
4.4 Conclusions .....	77
4.5 Recommendations .....	78
<b>REFERENCES.....</b>	<b>79</b>

## LIST OF TABLES

4.1 Geometrical data of Autofrettage draft .....	47
4.2 Material properties of cylinder and mandrel .....	49
4.3 Elastic-plastic radius values corresponding to various interference ratios.....	49
4.4 Bauschinger effect factors corresponding to various interference ratios .....	50
4.5 The effect of BEF on secondary yielding in various interference ratios according to Tresca criteria.....	51

4.6 The effect of BEF on secondary yielding in various section values according to Von Mises criteria.....	51
4.7 Maximum pressure bearing capacity before and after autofrettage .....	65
4.8 Tolerable maximum pressure values after removing material .....	66
4.9 Comparison of elastic-plastic radius values .....	77

## LIST OF FIGURES

1.1 Various pressure vessel samples .....	1
2.1 $\sigma - \epsilon$ curve of a elasto-plastic material.....	10
2.2 Stress-strain curve .....	12
2.3 Geometrical representation of distortion energy theory.....	16
2.4 Geometrical representation of maximum shear stress theory .....	17
2.5 Graphical representation of Bauschinger effect .....	18
2.6 Bilinear kinematic hardening model .....	19
2.7 Elastic-Perfect plastic model .....	20
2.8 Elastic-Linear plastic model.....	20
3.1 Stress element in polar coordinates .....	21
3.2 Deformed element in two dimensions.....	23
3.3 Stress distribution in internal pressure state .....	25
3.4 Stress distribution in external pressure state .....	26
4.1 Representation of autofrettage and steel barrel draft.....	47
4.2 35NiCrMoV12.5 Stress-Strain Diagram .....	48
4.3 Mandrel cross section picture.....	48
4.4 Radial stresses for 1% interference ratio.....	52
4.5 Radial stresses for 1.5% interference ratio.....	53
4.6 Radial stresses for 2% interference ratio.....	53
4.7 Hoop stresses for 1% interference ratio .....	54
4.8 Hoop stresses for 1.5% interference ratio .....	54

4.9 Hoop stresses for 2% interference ratio .....	55
4.10 Axial stresses for 1% interference ratio .....	55
4.11 Axial stresses for 1.5% interference ratio .....	56
4.12 Axial stresses for 2% interference ratio .....	56
4.13 Residual radial stresses for 1% interference ratio .....	57
4.14 Residual radial stresses for 1.5% interference ratio .....	57
4.15 Residual radial stresses for 2% interference ratio .....	58
4.16 Residual hoop stresses for 1% interference ratio .....	58
4.17 Residual hoop stresses for 1.5% interference ratio .....	59
4.18 Residual hoop stresses for 2% interference ratio .....	59
4.19 Residual axial stresses for 1% interference ratio.....	60
4.20 Residual axial stresses for 1.5% interference ratio.....	60
4.21 Residual axial stresses for 2% interference ratio.....	61
4.22 Tresca equivalent stresses in operating pressure.....	62
4.23 Von Mises equivalent stresses in operating pressure .....	62
4.24 Residual radial stresses in case of secondary yielding .....	63
4.25 Residual hoop stresses in case of secondary yielding .....	64
4.26 Residual axial stresses in case of secondary yielding .....	64
4.27 Tresca equivalent stresses in service pressure in case of secondary yielding ... .....	65
4.28 Tresca equivalent stress distribution of 1% interference autofrettaged cylinder after 22.5 mm material is removed .....	67
4.29 Von Mises equivalent stress distribution of 1% interference autofrettaged cylinder after 22.5 mm material is removed .....	67
4.30 Movement of mandrel and tube constraints during swage autofrettage.....	68
4.31 Abaqus ¼ cross-sectioned calculation model .....	68
4.32 Mesh model .....	69
4.33 Representation of stresses during calculations .....	69
4.34 Residual radial stresses for % 1 , % 1.5, and % 2 interference ratios .....	70
4.35 Residual hoop stresses for % 1 , % 1.5, and % 2 interference ratios .....	71
4.36 Residual axial stresses for % 1 , % 1.5, and % 2 interference ratios.....	71
4.37 Tresca equivalent stresses occurring in the service pressure.....	72

4.38 Von Mises equivalent stresses occurring in the service pressure .....	72
4.39 Residual radial stresses for 1% interference ratio .....	73
4.40 Residual radial stresses for 1.5% interference ratio .....	73
4.41 Residual radial stresses for 2% interference ratio .....	74
4.42 Residual hoop stresses for 1% interference ratio .....	74
4.43 Residual hoop stresses for 1.5% interference ratio .....	75
4.44 Residual hoop stresses for 2% interference ratio .....	75
4.45 Residual axial stresses for 1% interference ratio.....	76
4.46 Residual axial stresses for 1.5% interference ratio.....	76
4.47 Residual axial stresses for 2% interference ratio.....	77

## SYMBOLS

- $U$  : Strain energy  
 $U_0$  : Strain energy density  
 $U_h$  : Dilatational energy density  
 $U_d$  : Distortion energy density  
 $\sigma_h$  : Hydrostatic stress  
 $\sigma_{VM}$  : Von Mises stress  
 $E$  : Modulus of elasticity  
 $E_t$  : Tangent modulus  
 $\nu$  : Poisson's ratio  
 $a$  : Inner radius of the vessel  
 $b$  : Outer radius of the vessel  
 $c$  : Elastic-plastic radius  
 $d$  : Secondary elastic-plastic radius  
 $P_i$  : Internal pressure  
 $P_e$  : External pressure  
 $\sigma_r$  : Radial stress  
 $\sigma_\theta$  : Hoop stress  
 $\sigma_z$  : Axial stress

$\epsilon_r$  : Radial strain  
 $\epsilon_r^p$  : Plastic radial strain  
 $\epsilon_r^e$  : Elastic radial strain  
 $\epsilon_\theta$  : Hoop strain  
 $\epsilon_\theta^p$  : Plastic hoop strain  
 $\epsilon_\theta^e$  : Elastic hoop strain  
 $\epsilon_z$  : Axial strain  
 $\sigma_0$  : Yielding stress  
 $P_a$  : Internal pressure which causes yielding of material at the inner surface  
 $\sigma_{r_c}$  : Radial stress on the elastic-plastic junction  
 $P_c$  : Pressure acting on the elastic-plastic junction  
 $P^*$  : Internal pressure which causes yielding of tube wall up to elastic-plastic junction  
 $\sigma_r^*$  : Radial stress caused by the  $P^*$   
 $I$  : Interference  
 $r_m$  : Outer radius of the mandrel  
 $G$  : Shear modulus  
 $\epsilon_{\theta_t}$  : Hoop strain of the tube  
 $\epsilon_{\theta_m}$  : Hoop strain of the mandrel  
 $\Delta P$  : Pressure difference on the secondary elastic-plastic junction for elastic-perfectly plastic model ( without Bauschinger effect)  
 $f$  : Bauschinger effect factor  
 $\Delta P^*$  : Pressure difference on the secondary elastic-plastic junction for elastic-perfectly plastic model (with Bauschinger effect)  
 $\bar{\epsilon}^p$  : Equivalent plastic strain  
 $\dot{P}$  : Autofrettage pressure for bilinear hardening model  
 $\widehat{\Delta P}$  : Pressure difference on the secondary elastic-plastic junction for bilinear model hardening model (with Bauschinger effect)  
 $\sigma_h$  : Stress difference between yielding stress and maximum stress  
 $\ddot{\Delta P}$  : Pressure difference occurring at the turning surface  
 $P_{\acute{a}_1}$  : Pressure in the  $\acute{a}$  occurring before internal turning



$P_{a_2}$  : Pressure in the  $\acute{a}$  after internal turning

$P_{b_1}$  : Pressure in the  $\acute{b}$  occurring before external turning

$P_{b_2}$  : Pressure in the  $\acute{b}$  after external turning

$P_{ser}$  : Service pressure

$\sigma_{total}$  : Total stress occurring after application of the service pressure

**BEF** : Bauschinger effect factor



## CHAPTER 1

### 1. INTRODUCTION

Pressure vessels are sealed structures that are used to store, transfer and process the fluids under high pressure and high temperature conditions. In accordance with the industrial needs, there exist different pressure vessel designs and one of the most commonly used type is thick walled pressure vessels. Thick walled pressure vessels are widely used in nuclear power plants and chemistry, gas and defense industries (Partovi, 2012).

The inner diameter surface has the highest hoop stress in the thick walled pressure vessels at service pressure. This region has the highest potential for the cracks as well. There are three fundamental methods to prevent those kind of defects in the thick walled pressure vessels and to increase their pressure holding capacity (Partovi, 2012).



**Figure 1.1 Various pressure vessel samples (Partovi , 2012)**

## **1.1 Wire Winding Method**

Wire winding is a manufacturing method used in the production of open and close ended pressure vessels. Wire wound cylinders are commonly used especially in arms industry. The process includes winding of the wire on pressure vessel where the wire is stressed on a male mandrel. During the process, as the wire on the carriage moves on the horizontal axis and creates the desired pattern, the mandrel also rotates. The most commonly used wires are carbon and glass fiber ones and they are shielded by synthetic resin as they are wound. The mandrel is usually placed in an oven to harden the resin. As the resin hardens, mandrel is taken out and the process is finished. The winding angle of the wire has an important effect on the final product's specifications (Wikipedia, Filament Winding).

## **1.2 Autofrettage Method**

In autofrettage method, the internal regions of the cylinder is subject to pressure, resulting some plastic deformation inside. Once the pressure is released, this region of the cylinder can not recover to its original geometry because of the plastic deformation. Therefore, residual compressive stress on the inner region and residual tensile stress on the outer region will be observed. As a result, when the cylinder is subjected to an internal pressure, the total stress on the inner surface will decrease down to certain amount due to superposition of the tensile stress due to this pressure and the residual compressive stress due to the autofrettage.

### ***1.2.1 Hydraulic Autofrettage***

Hydraulic autofrettage method involves hydrostatic pressure application to the inner surface of the cylinder hole. Therefore, the equivalent stress value exceeds the material's yielding point and the plastic deformation starts. With the increased pressure, the plastic region on the inside wall of the cylinder spreads to the outer diameter. To pressurize the tube, a non-corrosive oil which has a highly compression capability compared to gases is used. During the hydraulic autofrettage, a spacer is placed into the center of the tube. The spacer decreases the volume of the fluid that will be pumped into the tube. Before the process, both ends of the tube should be

sealed. The resistance of the sealing elements against the axial force during the process should also be considered (Gibson, 2008).

### ***1.2.2 Swage Autofrettage***

Swage autofrettage is a method that was developed to expand the autofrettage application limits to higher pressure applications and to eliminate the problems that occur in the high pressure intervals. In this method, the use of the mechanical advantage of the mandrel decreases the pressure need dramatically compared to the hydraulic autofrettage method. This technique is based on obtaining the expected hole expanding due to slipping a relatively big forging tool all through the cylinder bore. The necessary force to move the mandrel can be accomplished by a unit or a mechanical loading tool that provides direct hydraulic pressure. Although a lubricant is used to decrease the friction between the mandrel and the tube, the cylinder, which is fixed on one end, is subject to extremely big axial forces. The choice of constraint location, either the mandrel entry or exit end, determines whether the deformed length of tube is held in tension or the undeformed length is compressed (Gibson, 2008).

### **1.3 Compound Cylinder Method**

In compound cylinder method, two or more cylinders are shrunk into each other to form a single cylinder. This process is accomplished by either interference fit method or having temperature difference between the cylinders. Under normal conditions, the outer diameter of the inner cylinder is a little bigger than the inner diameter of the outer cylinder. After the shrinkage, the residual stresses due to the interference cause a decrease in the total stress value on the compound cylinder's inner surface which is subject to service pressure (Yayla, 2014).

### **1.4 Purpose of the Thesis**

The barrel is the most basic component of a firearm. Barrels are cylindrical vessels with one end open and other is closed. They are resistant to high pressure and enable the bullet to travel to the aimed target with the desired speed. To realize the design of an firearm barrel, stress distribution on the walls of the barrel at service

pressure and the parameters that affect these stress distribution should be analyzed in detail at first.

When the stresses that occur in the thick walled cylindrical vessels subject to only internal pressure are examined, it is observed that maximum stress was on the inner walls and plastic yielding occurred on this region as well. To increase the maximum pressure that the barrel will hold in elasticity limits, the wall thickness should be increased. Since the increase of the wall thickness will result in an increase also in the barrel weight, there will be a negative effect on the portability of the firearm system. Since this situation will also lead to an increase in the cost of manufacturing, it will be an undesired result in the firearm systems. To increase the pressure bearing capacity of the barrel without an increase in the wall thickness, various methods were developed by the researchers. These are wire winding, autofrettage and compound cylinder methods that were explained previously in detail. The use of these methods provides an opportunity to decrease the wall thickness of the barrels. This result means a significant decrease in the barrel weight.

In this thesis study, swage autofrettage implementation to a heavy armor barrel that belongs to 105 mm obus class will be examined. To gain the maximum benefit of the autofrettage process, the optimum interference ratio between the barrel and the mandrel will be tried to obtain.

## **1.5 Methodology**

The procedural steps that will be followed in accordance with the determined objective are listed below :

- 1.** First, the mathematical relations that provide stress distribution of a thick walled cylindrical tube will be achieved. The thick walled cylindrical tube is subject to only internal and only external pressure and has not been autofrettaged before.

- 2.** Thick walled cylindrical tube's stress components, that are partially plastic deformed during the autofrettage process, are expressed mathematically in accordance with the elastic perfectly plastic model.

**3.** The mathematical expression, that gives the approximate radius value of the plastic region of the cylindrical tube which is partially plastic deformed after the autofrettage process, is derived with the assumption that the material complies with the elastic perfectly plastic model.

**4.** The equations, that give the residual stresses after the removal of the load in the autofrettage process, are obtained for elastic perfectly plastic model.

**5.** After the removal of the load in the autofrettage process, the necessary conditions to let a secondary plastic yielding to begin are examined and in case of the secondary yielding, the mathematical expressions that give the residual stresses in the cylindrical tube are obtained.

**6.** The necessary conditions for Bauschinger effect to start a secondary plastic yielding are examined for the elastic perfectly plastic model and the residual stresses, that occur with the secondary yielding as a result of Bauschinger effect, are obtained.

**7.** The stress equations, that were obtained for the elastic perfectly plastic material model, are obtained for the bilinear hardening model.

**8.** The effect of internal or external surface turning after the autofrettage process on the residual stress distribution is examined.

**9.** The formulation, that will be used to determine the stress distributions at the operating pressure after the autofrettage, is approached.

**10.** Barrel material and barrel geometry are described and analytical solutions are obtained for each step of the autofrettage process with the use of MATLAB program.

**11.** Stress distributions are obtained for each step of the autofrettage process with the use of ABAQUS finite element analysis program.

**12.** The results that were obtained through Abaqus and Matlab are compared and the optimum dimensions of the barrel is determined to gain the maximum efficiency of autofrettage process.

## 1.6 Literature Research

The problem of determination of the stresses and strains of a thick walled cylindrical elastic tube that is subject to internal and external pressure was first solved by the French scientists Lamé and Clapeyron in 1833.

In 1963, T.E. Davidson, D.P. Kendall and A.N. Reiner compared the theoretical results with the results of the experiments that they performed to see how the residual stresses that occur during the swage autofrettage change with respect to over-strains and diameter ratio. The experimental determination of the residual stresses was based on the measurement of the changes of stresses on the exterior side of the swage autofrettaged cylindrical tube after some machining of the interior surface. D.P. Kendall and his friends applied hydrostatic pressure to the inner surface of the cylinder that was autofrettaged before as well and they examined the reyielding characteristics of the swage autofrettaged cylinders.

In the report, that was prepared by Graham Clark in 1982, analytical approaches in accordance with the elastic perfectly plastic model were presented to predict the residual stresses in the swage autofrettaged thick walled cylinders. In the report, by ignoring the elastic compression of the mandrel in the swage autofrettage, the mathematical relation between the interference value and elastic plastic junction was derived. Furthermore, Bauschinger effect that causes a reyielding on the inner diameter after the removal of the load in autofrettage process was discussed analytically. In the study, the residual stresses were experimentally obtained as well with the X-Ray measurement method.

In the report that was prepared by G.S.Jost, in 1988, in the organization named “Department of Defense Science and Technology Organization Aeronautical Research Laboratory”, stresses and strains that occur during the hole expanding process were examined analytically in detail. While the equations were being derived, the material was considered as elastic-perfectly plastic and Von Mises yielding criterion was based. The relation between the interference value of the hole and the mandrel and elasto-plastic junction that occurs during the process was

expressed mathematically. In the report, deductions about the conditions under which there will be a new yielding after the removal of the load were made. Analytical results were compared with the results that were obtained by the numerical method and it was confirmed that they are consistent.

In the report that Anthony P. Parker and John H. Underwood prepared in 1997, for the elastic perfectly plastic model, they included Bauschinger effect into the analytical method that was developed to predict the residual stresses due to autofrettage process and they mathematically expressed that this effect reduces the strength of the compressive yielding and thereby a secondary yielding is triggered around the inner diameter of the cylinder. Then, correlating the Bauschinger effect with the fatigue life, they determined the optimum over strain amount to maximize the fatigue life.

In the article that was published by Hamid Jahed and Ghader Ghanbari in 2003, a simple forward-reverse torsion test was performed to determine the unloading behavior of NiCrMoV125 steel. As the result of the performed test, it was identified that the material exhibited the perfect plastic behavior during loading but it exhibited a nonlinear behavior during the unloading. The experimentally obtained real material behavior was used in the analysis to get the residual stress distribution that occurs after the autofrettage. The results of the analysis that were performed with the real material model and the results that were obtained by the use of the ideal models such as isotropic hardening were compared and it was determined that the ideal models deviated dramatically from the residual stress values that were calculated with respect to the real model. The change, that will occur in the residual stress distribution of the autofrettaged cylinders after turning, was discussed in the article as the final topic.

In the article that was published by X.P. Huang and W.C.Cui in 2006, the residual stress after the autofrettage is expressed mathematically for different material models. In the article, it was tried to establish the most proper analytic model in accordance with the real material behavior and Bauschinger effect was also included in the calculations. Additionally, the model allows the residual stress calculations



with respect to different yielding criteria. The obtained stress distributions were established by both numerical and experimental methods. The results of the used three methods were compared and it was seen that the results matched each other.

In the article that was published by Amran Ayob and M. Kabashi Elbasheer in 2007, stress distribution of autofrettaged thick walled cylinders at operating pressure was examined and it was determined that the maximum equivalent stress at the operating pressure occurred on the elastic-plastic junction. Depending on the elastic-plastic junction change, minimum point of the maximum equivalent stress distribution of autofrettaged cylinder at operating pressure was analytically determined and this point was accepted as the optimum autofrettage radius. The optimum autofrettage pressure was correlated with the optimum radius and formulated mathematically. Finally, the optimum radius that was found by the analytical method and the optimum pressure values were compared with the finite element analysis results.

In the article that was published by Abu Rayhan Md. Ali, Nidul Ch. Ghosh, Tanvir-E-Alam in 2010, the factors such as ratio of outer radius to inner radius of the cylinder tube, operation pressure, material model and autofrettage level were dwelled on to see how they affect the benefit of the autofrettage process. As a result of the analysis that were performed by using finite element method, it was observed that the maximum Von Mises stress decreased up to a certain pressure value as the autofrettage pressure increased and after that value it started to increase. The increases in the outer radius to inner radius ratio, operating pressure and the slope of the plastic region in the material's hardening curve lead to an increase of the optimum autofrettage pressure.

Deniz Öztörün, in his Master of Science study that he presented in 2013, established the interior ballistics curves of the barrel first to accomplish the design of a heavy armor barrel with different methods and then tried to determine the optimum barrel dimensions making use of a finite element software. Öztörün determined the maximum operating pressure that the barrel was subject to and examined how the

different autofrettage levels affect the stress distribution of the barrel during the bursting, as a result of the interior ballistics curves.

In 2014, Zahong Hu and Chandra Penumarthy accomplished the swage autofrettage simulation, that would be applied to a heavy armour barrel, with the use of a finite element software. Nonlinear kinematic hardening model was used in the analysis. The residual stresses that would occur during the swage autofrettage were calculated for different interference values. In the article, the force applied to the mandrel by the driver was determined for different interference values with respect to displacement change of the mandrel. After the accomplishment of the autofrettage simulation, the maximum pressure that can be applied to the cylinder in the elastic limits was determined and the cylinder's internal surface was re-pressurized by this pressure value. The equivalent Von Mises stresses that occur at the operating pressure were determined for different interference values in the autofrettaged barrel. With the comparison of maximum Von Mises equivalent stresses for different interference values, The lowest value of Maximum Von Mises equivalent stresses was determined and this value was accepted as the optimum value.

## CHAPTER 2

### 2. INTRODUCTION TO PLASTICITY

When an object is subject to external loads, it is deformed. If the deformation is independent of time and it can be recovered, i.e. the deformation disappears suddenly as the load is removed, the deformation is named as elastic. A reversible but time dependent deformation is known as viscoelastic. The deformation after the application of the load increases by time and it decreases slowly after the removal of the load in viscoelastic deformation. If the deformation is irreversible or permanent, it is called a plastic deformation (Khan, 1995).

Plasticity theory studies the stress-strain and load-deflection relations of plastically deformed ductile material or the structures. The following two steps should be followed to build these relations: 1-Experimental Observation 2-Mathematical Representation. The obtained stress situations are generally simple and uniform in any experiment. However, the final aim of any plasticity theory is to present the general mathematical formulation that provides the estimation for plastic deformation that will occur under the complex loading and boundary conditions (Khan, 1995).

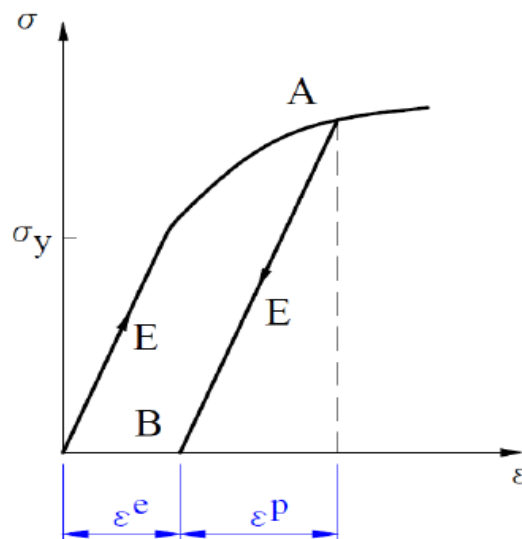


Figure 2.1  $\sigma - \varepsilon$  curve of an elasto-plastic material (Partovi, 2012)

As it is seen in Figure 2.1, the material behaves linearly up to the yielding point. At this stage, removal of the load will cause the material to follow the same line and go back to the starting point in the stress-strain diagram. However, a bigger loading value will carry the material to the plastic region. In the case of removal of the load at a random point like point A in the plastic region, material behavior is different from the elastic region. As it is shown in the figure, there is a recovery to as elastically in case of unloading at point A. The recovery line has the same slope with the loading case and therefore, the recovery will end at any point else which is not the same point where the loading started. This point is shown as Point B in Figure 2.1. The deformation that occurs after the application of the load is partially reversed with the unloading. After all, permanent deformations occurs in the object. The total strain value at point A is equal to the sum of plastic strain and elastic strain.

## **2.1 Yielding Criteria**

If an object is subject to a uniaxial tensile load, plastic yielding will start when the stress value reaches to the yielding point in the stress-strain diagram. However, in triaxial state of stress, one stress component is not enough to predict the yielding status. In a complex stress state, the relation established between the stress components to predict the yielding status of the material is called yielding criteria. There are two important yielding criteria used for the ductile materials. These are Von Mises and Tresca yielding criteria.

### ***2.1.1 Strain Energy***

When force is applied to an object, the object deforms. In the meantime, work is done on the object in proportion to the force and the deformation. The work done by the force is stored as potential energy on the object. The energy stored in the body of this object is named as strain energy. The strain energy stored on the object may not be distributed uniformly. Due to this reason, a term called strain energy density was proposed. The strain energy density is the strain energy per unit volume and represented with  $U_0$ . The total strain energy of an object can be obtained by the following integration (Kim, 2015).

$$U = \iiint U_o(x, y, z) dV \quad (2.1)$$

In the uniaxial stress case, strain energy density is equal to the area that is under the strain energy curve (Kim, 2015).

$$U_o = \frac{1}{2} \sigma \varepsilon \quad (2.2)$$

For general three dimensional case, the strain energy density is expressed as the following (Kim, 2015).

$$U_o = \frac{1}{2} [\sigma_x \varepsilon_x + \sigma_y \varepsilon_y + \sigma_z \varepsilon_z + \tau_{xy} \gamma_{xy} + \tau_{yz} \gamma_{yz} + \tau_{xz} \gamma_{xz}] \quad (2.3)$$

If the material is elastic, the strain energy will be totally regained when the load on the object is removed. If we think about a coordinate system that is parallel to the principal stress directions and there is no shear components in this coordinate system, Eq. (2.3) can be expressed in a simpler form as follows (Kim, 2015).

$$U_o = \frac{1}{2} [\sigma_1 \varepsilon_1 + \sigma_2 \varepsilon_2 + \sigma_3 \varepsilon_3] \quad (2.4)$$

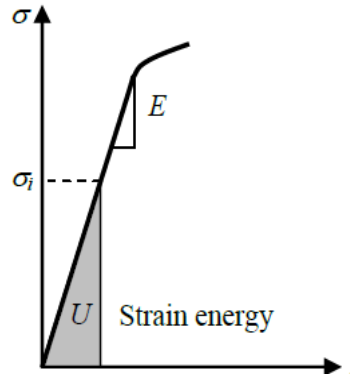


Figure 2.2 Stress-strain curve (Kim, 2015)

The relations between stress and strains that is known as the Generalized Hook Law in the elastic region are expressed with Eq.(2.5) (Kim, 2015).

$$\begin{cases} \varepsilon_1 = \frac{1}{E} (\sigma_1 - \nu \sigma_2 - \nu \sigma_3) \\ \varepsilon_2 = \frac{1}{E} (\sigma_2 - \nu \sigma_1 - \nu \sigma_3) \\ \varepsilon_3 = \frac{1}{E} (\sigma_3 - \nu \sigma_1 - \nu \sigma_2) \end{cases} \quad (2.5)$$

If Eq.(2.5) is substituted in Eq.(2.4), we can write the strain energy density in terms of principal stresses as follows (Kim, 2015).

$$U_0 = \frac{1}{2E} [\sigma_1^2 + \sigma_2^2 + \sigma_3^2 - 2\nu(\sigma_1\sigma_2 + \sigma_2\sigma_3 + \sigma_1\sigma_3)] \quad (2.6)$$

It can be thought that the strain energy density is composed of two components. These are dilatation strain energy density and distortion strain energy density. Dilatation strain energy density is related with the change in the volume. Distortion strain energy density is responsible for the change in the form. Many experiments showed that the ductile materials can be loaded hydrostatically beyond the ultimate strength points without any failure observed in the material. This is achieved because the sample does not change its form but only its value decreases due to the hydrostatic stress (Kim, 2015).

### 2.1.2 The Components of Strain Energy

Strain energy density of a point on a solid can be decomposed into two: dilatation strain energy density  $U_h$  which causes the volume changes and distortion strain energy density  $U_d$  which is responsible for the change in the form. We can decompose the stress matrix similarly as dilatation stress matrix  $\sigma_h$  and distortion stress matrix  $\sigma_d$  as well to calculate these components (Kim, 2015).

$$\begin{bmatrix} \sigma_1 & 0 & 0 \\ 0 & \sigma_2 & 0 \\ 0 & 0 & \sigma_3 \end{bmatrix} = \begin{bmatrix} \sigma_h & 0 & 0 \\ 0 & \sigma_h & 0 \\ 0 & 0 & \sigma_h \end{bmatrix} + \begin{bmatrix} \sigma_{1d} & 0 & 0 \\ 0 & \sigma_{2d} & 0 \\ 0 & 0 & \sigma_{3d} \end{bmatrix} \quad (2.7)$$

Dilatation component  $\sigma_h$  is defined as the following (Kim, 2015).

$$\sigma_h = \frac{\sigma_1 + \sigma_2 + \sigma_3}{3} \quad (2.8)$$

If the hydrostatic stress components are substituted in Eq.(2.6), dilatation energy density is obtained as in Eq.(2.9) (Kim, 2015).

$$\begin{aligned} U_h &= \frac{1}{2E} [\sigma_h^2 + \sigma_h^2 + \sigma_h^2 - 2\nu(\sigma_h\sigma_h + \sigma_h\sigma_h + \sigma_h\sigma_h)] \\ &= \frac{3(1-2\nu)}{2E} \sigma_h^2 \end{aligned} \quad (2.9)$$

By using the relation in Eq.(2.8), Eq.(2.9) can be written as follows (Kim, 2015).

$$\begin{aligned}
 U_h &= \frac{3(1-2\nu)}{2E} \left( \frac{\sigma_1 + \sigma_2 + \sigma_3}{3} \right)^2 \\
 &= \frac{(1-2\nu)}{6E} [\sigma_1^2 + \sigma_2^2 + \sigma_3^2 - 2(\sigma_1\sigma_2 + \sigma_2\sigma_3 + \sigma_1\sigma_3)]
 \end{aligned} \tag{2.10}$$

### 2.1.2.1 Distortion Energy

Distortion component of the strain energy is obtained by the subtraction of Eq.(2.10) from Eq.(2.6) (Kim, 2015).

$$U_d = U_0 - U_h \tag{2.11}$$

$$U_d = \frac{(1+\nu)}{3E} (\sigma_1^2 + \sigma_2^2 + \sigma_3^2 - \sigma_1\sigma_2 - \sigma_2\sigma_3 - \sigma_1\sigma_3) \tag{2.12}$$

$$U_d = \frac{(1+\nu)}{3E} \frac{[(\sigma_1 - \sigma_2)^2 + (\sigma_2 - \sigma_3)^2 + (\sigma_3 - \sigma_1)^2]}{2} = \frac{(1+\nu)}{3E} \sigma_{VM}^2 \tag{2.13}$$

### 2.1.3 Distortion Energy Theory (von Mises)

According to Von Mises' theory, yielding will start when the distortion energy density of a ductile solid reaches to a critical value for this material. Since this situation should be valid also for a uniaxial stress case, the critical value of the distortion energy can be obtained from a uniaxial tension test. In a uniaxial tension test, the stress will be as follows, as the yielding starts :  $\sigma_1 = \sigma_y$  ,  $\sigma_2 = 0$  ,  $\sigma_3 = 0$  . The energy density at the moment of yielding is expressed with the following (Kim, 2015).

$$U_d = \frac{(1+\nu)}{3E} \sigma_y^2 \tag{2.14}$$

The energy density given in the above equation is the critical value of the distortion energy density for the material. According to Von Mises yielding criteria, the material starts yielding in the multi axial loading case as the distortion energy density reaches to the critical value (Kim, 2015).

$$\frac{(1+\nu)}{3E} \sigma_{VM}^2 \geq \frac{(1+\nu)}{3E} \sigma_y^2 \tag{2.15}$$

$$\sigma_{VM} \geq \sigma_y \tag{2.16}$$

Distortion Energy Theory foresees that the yielding will start when Von Mises stress value exceeds the yielding stress value that is obtained from a uniaxial tension test. Von Mises stress that is given with the Eq. (2.13) can be written with respect to all stress components as the following (Kim, 2015).

$$\sigma_{VM} = \sqrt{\frac{(\sigma_{xx}-\sigma_{yy})^2+(\sigma_{yy}-\sigma_{zz})^2+(\sigma_{zz}-\sigma_{xx})^2+6(\tau_{xy}^2+\tau_{yz}^2+\tau_{zx}^2)}{2}} \quad (2.17)$$

For a two dimensional plane stress case,  $\sigma_3 = 0$ , Von Mises stress can be defined as following with respect to the principle stresses (Kim, 2015).

$$\sigma_{VM} = \sqrt{\sigma_1^2 - \sigma_1\sigma_2 + \sigma_2^2} \quad (2.18)$$

For a two dimensional plane stress case,  $\sigma_3 = 0$ , Von Mises stress can be defined as following with respect to the general stress components (Kim, 2015).

$$\sigma_{VM} = \sqrt{\sigma_{xx}^2 - \sigma_{xx}\sigma_{yy} + \sigma_{yy}^2 + 3\tau_{xy}^2} \quad (2.19)$$

Two dimensional distortion energy equation defines also an ellipse drawn on the  $\sigma_1$ - $\sigma_2$  plane (Figure 2.3). The inner region of the ellipse defines the combined biaxial stress region where the material is safe against yielding in case of static loading (Kim, 2015).

If we handle the situation in which there is no normal stresses but only a shear stress, the principle stresses will be  $\sigma_1 = -\sigma_2 = \tau$  and  $\sigma_3 = 0$ . This pure shear on the  $\sigma_1$ - $\sigma_2$  plane is represented by a straight line passing through the origin at  $-45^\circ$  as shown in Figure 2.3. This line intercepts von Mises ellipse at two points A and B as shown in Figure 2.3. The amplitudes of the  $\sigma_1$  and  $\sigma_2$  stresses at these points can be obtained from Eq.(2.18) (Kim, 2015).

$$\sigma_y^2 = \sigma_1^2 - \sigma_1\sigma_1 + \sigma_1^2 = 3\sigma_1^2 = 3\tau_{max}^2 \quad (2.20)$$

$$\tau_{max} = \sigma_1 = \frac{\sigma_y}{\sqrt{3}} = 0.577\sigma_y \quad (2.21)$$



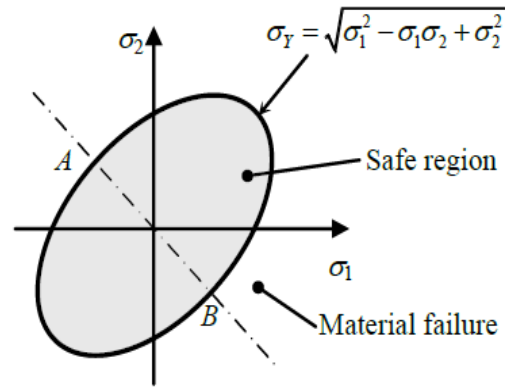


Figure 2.3 Geometrical representation of distortion energy theory

#### 2.1.4 Maximum Shear Stress Theory (Tresca)

According to the Maximum Shear Stress Theory, yielding will start when the maximum shear stress of a material reaches to a critical value for this material. Since this situation should be valid also for a uniaxial stress case, the allowable maximum shear stress can be obtained from a uniaxial tension test. In a uniaxial tension test, the stress will be as :  $\sigma_1 = \sigma_y$  ,  $\sigma_2 = 0$  ,  $\sigma_3 = 0$  as the yielding starts. The maximum shear stress is expressed by the following equation (Kim, 2015).

$$\tau_{max} = \frac{\sigma_1 - \sigma_3}{2} \geq \tau_y = \frac{\sigma_y}{2} \quad (2.22)$$

Maximum shear stress value is also called the material's yielding shear stress and it is expressed by  $\tau_y$  symbol. Tresca yielding criterion foresees that the material will start to yield when the maximum shear stress value exceeds the yielding shear strength of the material. According to the maximum shear stress theory, the two-dimensional stress case is represented by the hexagon in Figure 2.4. The ellipse that corresponds to Von Mises theory is represented in the same way as well. The hexagon is drawn in the ellipse and all six corners of it contact the ellipse. Since the combinations of principle stresses  $\sigma_1$  and  $\sigma_2$  in the hexagon will not cause yielding, the shaded region in the hexagon is accepted as the safe region according to the maximum shear stress theory. According to the theory, yielding will start when the compound stress reaches to the borders of the hexagon. In the graphical representation in Figure 2.4, it is seen clearly that this theory is a more conservative failure theory than the maximum distortion energy theory. In case of pure shear

stress; the shear stress value at points A and B in Figure 2.3 is  $0.577\sigma_y$  with respect to distortion energy theory whereas the shear stress value at points C and D in Figure 2.4 corresponds to  $0.5\sigma_y$  with respect to maximum shear stress theory (Kim, 2015).

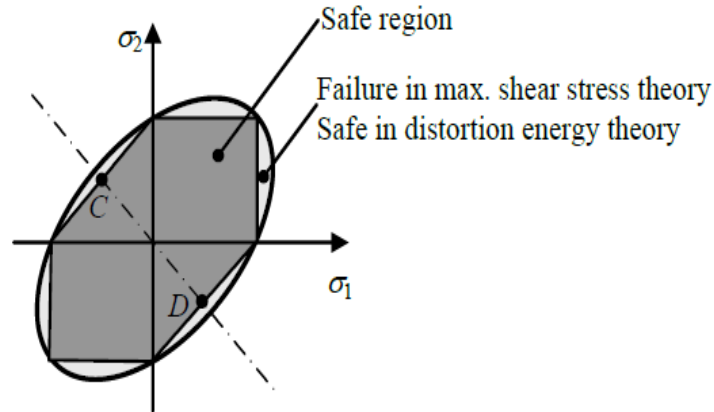


Figure 2.4 Geometrical representation of maximum shear stress theory (Kim, 2015)

## 2.2 Bauschinger Effect

If the compressive or tensile load on a material sample in the plastic region is removed and the sample is reloaded in the reverse direction until the yielding point, it will be observed that the yielding stress that was measured for the reloading will have a smaller value than the yielding stress value in the original direction has. This phenomenon is named as Bauschinger Effect. Figure 2.5 sets forth the Bauschinger effect very clearly. In the elastic region, the tensile yielding stress is equal to the compressive yielding stress ( $OA = OF$  or  $S_{et} = S_{ec}$ ). If the material loaded up to the point B which is beyond the elastic limit and then the load is removed, the new tensile yielding strength of the material will be higher than what it had before it moved to the plastic region (BC). However, a decrease will be observed in the compressive yielding strength. As seen in Figure 2.5, the material's compressive yielding strength is at the value shown with  $S_{ec}$  and decreases to the value  $S_{ec}'$  (Abdelselam, 2012).

## 2.3 Strain Hardening

The experimental results show that if a solid object is loaded up to a point that is beyond the yielding strength and then it is totally unloaded and loaded in the same direction for reyielding, an increase in the strength of the solid object against

deformation will be observed. Namely, as a result of this process the object's yielding strength will increase. This occurrence which is very commonly met in metals is called strain hardening. As seen in Figure 2.5, if the sample is subject to some plastic stress up to the point B by using the tensile test and then it is subject to again a tensile stress, then the secondary yielding will occur at point B. The trajectory of the distance between point A and point B on the tensile stress axis is equal to the increase in the material's yielding strength due to the material's strain hardening (Abdelselam, 2012).

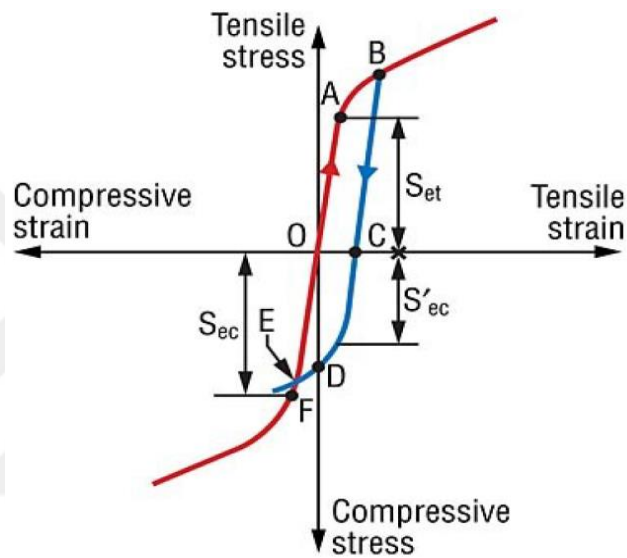


Figure 2.5 Graphical representation of Bauschinger effect (Abdelselam, 2012)

## 2.4 Ideal Material Models

The difficulties of mathematical modeling of the real stress-strain behavior of the materials caused the raise of some ideal material acceptances. Below are given the general information about some ideal material models that have the most common usage.

### 2.4.1 Kinematic Hardening Model

The existence of Bauschinger effect makes modelling of plastic deformation harder. Kinematic hardening model which is a simplified model of Bauschinger effect was proposed to unclutter this complication. According to this model, the decrease of the yielding stress in the reverse direction is equal to increase of the

stress level of the sample that was loaded going beyond the yielding stress in the original direction and starting from the first yielding point (Jahed, 1997).

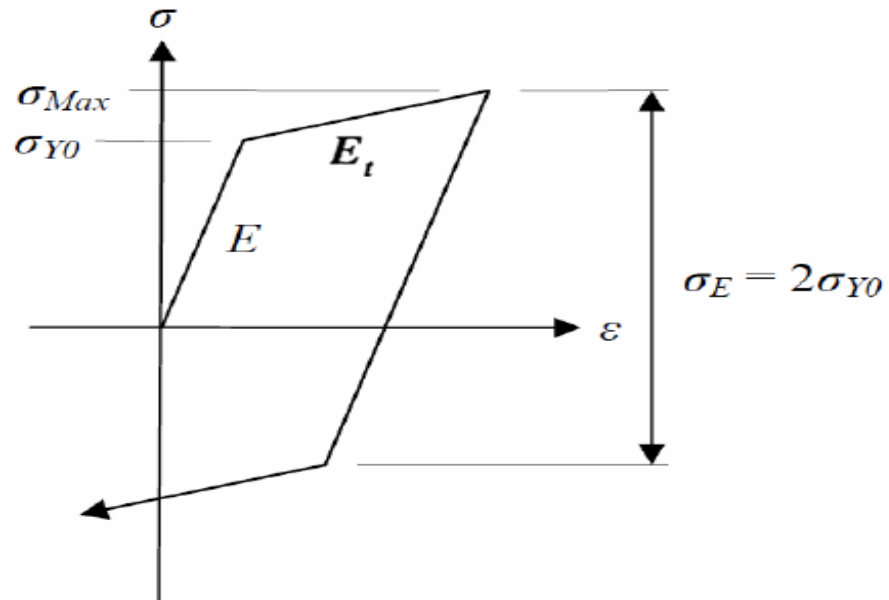


Figure 2.6 Bilinear kinematic hardening model (Abdelselam, 2012)

#### 2.4.2 Elastic-Perfectly Plastic Model

The simplest model to handle a material's behavior is elastic-perfectly plastic model. This model's behavior is shown in Figure 2.7. According to this model, the yielding point's value does not change with respect to plastic strain. Idealization of the plastic behavior of the materials, that do not exhibit much strain hardening, with this model will not cause major deviations in the results obtained. Stress-strain relation for the elastic-perfectly plastic model can be expressed as follows (Jahed, 1997)

$$\varepsilon = \frac{\sigma}{E} \quad (\sigma < \sigma_0) \quad (2.23)$$

$$\varepsilon = \frac{\sigma}{E} + \varepsilon^p \quad (\sigma > \sigma_0) \quad (2.24)$$

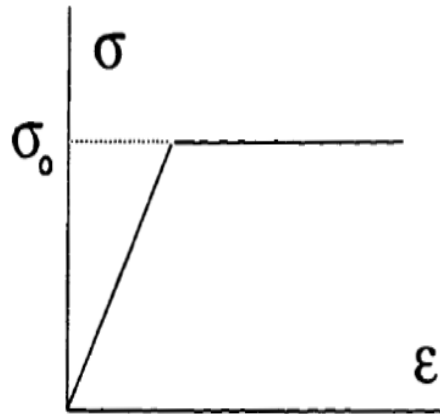


Figure 2.7 Elastic-perfectly plastic model (Jahed, 1997)

### 2.4.3 Elastic-Linear Plastic Model

Elastic-linear plastic model is a more real like stress-strain model when it is compared to elastic-perfectly plastic model. In this model, the stress-strain curve is represented by two lines. Although the transition from the elastic to the plastic region is generally soft in the real stress-strain curve, the transition in this model is sharp. The first linear region of the idealized diagram has the same slope with the material's elastic module. The second region which represents the idealized hardening behavior has a slope which is equal to the tangent module  $E_t$ . The stress-strain relation for the elastic-linear plastic model can be expressed as follows (Jahed, 1997).

$$\varepsilon = \frac{\sigma}{E} \quad (\sigma < \sigma_0) \quad (2.25)$$

$$\varepsilon = \frac{\sigma}{E} + \frac{1}{E_t}(\sigma - \sigma_0) \quad (\sigma > \sigma_0) \quad (2.26)$$

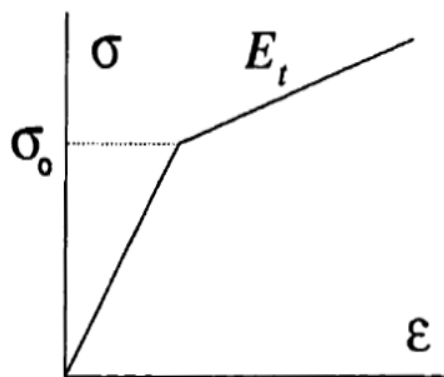


Figure 2.8 Elastic-linear plastic model (Jahed, 1997)

## CHAPTER 3

### 3. ANALYTICAL MODELLING

#### 3.1 Equilibrium Equations in Polar Coordinates

A two dimensional state of stress in an infinitesimal element abcd is shown in Figure 3.1. The  $r$  and  $\theta$  directed body forces are denoted by  $F_r$  and  $F_\theta$ . Following equation are obtained by taking advantage of equilibrium of radial forces (Ugural, 2012).

$$\begin{aligned} & \left( \sigma_r + \frac{\partial \sigma_r}{\partial r} dr \right) (r + dr) d\theta - \sigma_r r d\theta - \left( \sigma_\theta + \frac{\partial \sigma_\theta}{\partial \theta} d\theta \right) dr \sin \frac{d\theta}{2} - \sigma_\theta dr \sin \frac{d\theta}{2} + \\ & \left( \tau_{r\theta} + \frac{\partial \tau_{r\theta}}{\partial \theta} d\theta \right) dr \cos \frac{d\theta}{2} - \tau_{r\theta} dr \cos \frac{d\theta}{2} + F_r r dr d\theta = 0 \end{aligned} \quad (3.1)$$

Because  $d\theta$  is small,  $\sin(d\theta/2)$  may be replaced by  $d\theta/2$  and  $\cos(d\theta/2)$  by 1. Additional simplification is performed by dropping terms containing higher-order infinitesimals. A similar analysis may be performed for the tangential direction. When both equilibrium equations are divided by  $rdrd\theta$ , following equations are obtained (Ugural, 2012).

$$\frac{\partial \sigma_r}{\partial r} + \frac{1}{r} \frac{\partial \tau_{r\theta}}{\partial \theta} + \left( \frac{\sigma_r - \sigma_\theta}{r} \right) + F_r = 0 \quad (3.2)$$

$$\frac{1}{r} \frac{\partial \sigma_\theta}{\partial \theta} + \frac{\partial \tau_{r\theta}}{\partial r} + \frac{2\tau_{r\theta}}{r} + F_\theta = 0 \quad (3.3)$$

In the absence of the body forces and the shear stresses, the equilibrium equation can be written in the following way (Ugural, 2012):

$$\frac{\partial \sigma_r}{\partial r} + \frac{\sigma_r - \sigma_\theta}{r} = 0 \quad (3.4)$$

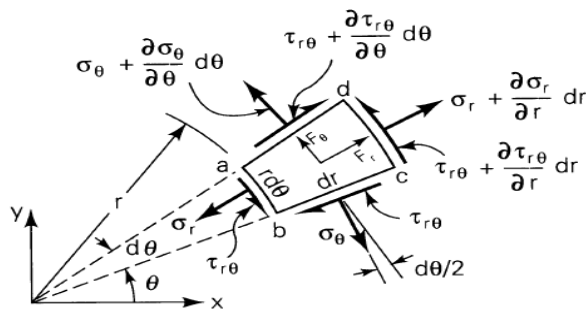


Figure 3.1 Stress element in polar coordinates

### 3.2 Strain Displacement Relations in Polar Coordinates

As shown in Figure 3.2, consider now the deformation of the infinitesimal element ABCD, denoting the  $r$  and  $\theta$  displacements by  $u$  and  $v$ , respectively. In the analysis that follows, the small angle approximation  $\sin\theta \approx \theta$  is employed, and arcs AB and CD are assumed straight lines. The radial strain  $\varepsilon_r$ , the deformation per unit length of side AC, is associated only with the  $u$  displacement (Sitharam, 2015):

$$\varepsilon_r = \frac{\partial u}{\partial r} \quad (3.5)$$

The tangential strain due to displacement  $u$  per unit length is stated as follows (Sitharam, 2015).

$$(\varepsilon_\theta)_u = \frac{(r+u)d\theta - rd\theta}{rd\theta} = \frac{u}{r} \quad (3.6)$$

Tangential strain due to displacement  $v$  is given by Eq.(3.7) (Sitharam, 2015).

$$(\varepsilon_\theta)_v = \frac{\left(\frac{\partial v}{\partial \theta}\right)d\theta}{rd\theta} = \frac{1}{r} \frac{\partial v}{\partial \theta} \quad (3.7)$$

Hence, the resultant strain is stated as follows (Sitharam, 2015).

$$\varepsilon_\theta = (\varepsilon_\theta)_u + (\varepsilon_\theta)_v \quad (3.8)$$

$$\varepsilon_\theta = \frac{u}{r} + \frac{1}{r} \left(\frac{\partial v}{\partial \theta}\right) \quad (3.9)$$

Similarly, the shearing strains can be calculated due to displacements  $u$  and  $v$  as below. Component of shearing strain due to  $u$  is given by Eq.(3.10) (Sitharam, 2015).

$$(\gamma_{r\theta})_u = \frac{\left(\frac{\partial u}{\partial \theta}\right)d\theta}{rd\theta} = \frac{1}{r} \left(\frac{\partial u}{\partial \theta}\right) \quad (3.10)$$

Component of shearing strain due to  $v$  is given by Eq.(3.11) (Sitharam, 2015).

$$(\gamma_{r\theta})_v = \frac{\partial v}{\partial r} - \left(\frac{v}{r}\right) \quad (3.11)$$

Therefore, the total shear strain is stated as follows (Sitharam, 2015).

$$\gamma_{r\theta} = (\gamma_{r\theta})_u + (\gamma_{r\theta})_v \quad (3.12)$$

$$\gamma_{r\theta} = \frac{1}{r} \left(\frac{\partial u}{\partial \theta}\right) + \frac{\partial v}{\partial r} - \left(\frac{v}{r}\right) \quad (3.13)$$

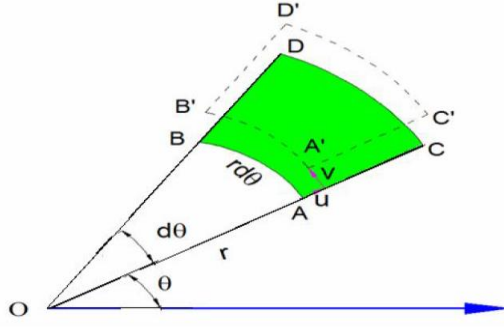


Figure 3.2 Deformed element in two dimensions (Sitharam, 2015)

### 3.3 Analytical Relations for Thick Walled Cylindrical Vessels

According to Generalized Hook's Law, Stresses can be written in the following form (Yayla, 2014).

$$\sigma_r = \frac{E}{(1+\nu)(1-2\nu)} [(1-\nu)\varepsilon_r + \nu(\varepsilon_\theta + \varepsilon_z)] \quad (3.14)$$

$$\sigma_\theta = \frac{E}{(1+\nu)(1-2\nu)} [(1-\nu)\varepsilon_\theta + \nu(\varepsilon_r + \varepsilon_z)] \quad (3.15)$$

$$\sigma_z = \frac{E}{(1+\nu)(1-2\nu)} [(1-\nu)\varepsilon_z + \nu(\varepsilon_r + \varepsilon_\theta)] \quad (3.16)$$

In the axial symmetry state, Eq.(3.5) and Eq.(3.6) will be used for  $\varepsilon_r$  and  $\varepsilon_\theta$ . We can assume that  $\varepsilon_z = 0$  (plane strain condition) and Shear stresses and shear strains don't exist. If we substitute Eq.(3.5) and Eq.(3.6) into Eq.(3.14), Eq.(3.15), Eq.(3.16) then,

$$\sigma_r = \frac{E}{(1+\nu)(1-2\nu)} \left[ (1-\nu) \frac{\partial u}{\partial r} + \nu \frac{u}{r} \right] \quad (3.17)$$

$$\sigma_\theta = \frac{E}{(1+\nu)(1-2\nu)} \left[ (1-\nu) \frac{u}{r} + \nu \frac{\partial u}{\partial r} \right] \quad (3.18)$$

$$\sigma_z = \frac{E}{(1+\nu)(1-2\nu)} \left[ \nu \left( \frac{u}{r} + \frac{\partial u}{\partial r} \right) \right] \quad (3.19)$$

Since r is the only independent variable, Eq.(3.4) can be written as the following .

$$\frac{\partial}{\partial r} (r\sigma_r) - \sigma_\theta = 0 \quad (3.20)$$

Substituting Eq.(3.14) and Eq.(3.15) into Eq.(3.20), we will get the following equation.

$$\frac{\partial^2 u}{\partial r^2} + \frac{1}{r} \frac{\partial u}{\partial r} - \frac{u}{r^2} = 0 \quad (3.21)$$



u can be found from Eq.(3.21) as

$$u = c_1 r + \frac{c_2}{r} \quad (3.22)$$

Substituting Eq.(3.22) into Eq.(3.17), Eq.(3.18), Eq.(3.19)

$$\sigma_r = \frac{E}{(1+\nu)(1-2\nu)} \left[ c_1 - \frac{c_2}{r^2} (1 - 2\nu) \right] \quad (3.23)$$

$$\sigma_\theta = \frac{E}{(1+\nu)(1-2\nu)} \left[ c_1 + \frac{c_2}{r^2} (1 - 2\nu) \right] \quad (3.24)$$

$$\sigma_z = \frac{E}{(1+\nu)(1-2\nu)} (2\nu c_1) \quad (3.25)$$

$c_1$  and  $c_2$  are integration constants and can be found out by applying boundary conditions.

When  $r = a$ ,  $\sigma_r = -P_i$

When  $r = b$ ,  $\sigma_r = -P_e$

So,

$$\frac{E}{(1+\nu)(1-2\nu)} \left[ c_1 - \frac{c_2}{r^2} (1 - 2\nu) \right] = -P_i \quad (3.26)$$

$$\frac{E}{(1+\nu)(1-2\nu)} \left[ c_1 - \frac{c_2}{r^2} (1 - 2\nu) \right] = -P_e \quad (3.27)$$

When Eq.(3.26) and Eq.(3.27) are solved, integration constants are obtained.

$$c_1 = \frac{(1+\nu)(1-2\nu)}{E} \left[ (P_i - P_e) \left( \frac{b^2}{b^2 - a^2} \right) - P_i \right] \quad (3.28)$$

$$c_2 = \frac{(1+\nu)}{E} \left( \frac{a^2 b^2}{b^2 - a^2} \right) (P_i - P_e) \quad (3.29)$$

Integration constants are substituted into Eq.(3.23) , Eq.(3.24) , and Eq.(3.25), we get following equations.

$$\sigma_r = \frac{P_i a^2 - P_e b^2}{b^2 - a^2} - \frac{a^2 b^2}{r^2} \left( \frac{P_i - P_e}{b^2 - a^2} \right) \quad (3.30)$$

$$\sigma_\theta = \frac{P_i a^2 - P_e b^2}{b^2 - a^2} + \frac{a^2 b^2}{r^2} \left( \frac{P_i - P_e}{b^2 - a^2} \right) \quad (3.31)$$

$$\sigma_z = 2\nu \left( \frac{P_i a^2 - P_e b^2}{b^2 - a^2} \right) \quad (3.32)$$

### 3.3.1 Cylinders Subjected to Internal Pressure only

In this case  $P_e = 0$  and  $P_i = P$

Hence,

$$\sigma_r = \left( \frac{Pa^2}{b^2 - a^2} \right) \left( 1 - \frac{b^2}{r^2} \right) \quad (3.33)$$

$$\sigma_\theta = \left( \frac{Pa^2}{b^2 - a^2} \right) \left( 1 + \frac{b^2}{r^2} \right) \quad (3.34)$$

$$\sigma_z = 2\nu \left( \frac{Pa^2}{b^2 - a^2} \right) \quad (3.35)$$

Since  $b^2/r^2 \geq 1$ ,  $\sigma_r$  is negative (compressive) for all  $r$  except  $r = b$ , in which case  $\sigma_r = 0$ . The maximum stress occurs at  $r = a$ . This is illustrated in Figure 3.3 (Sun, 2015).

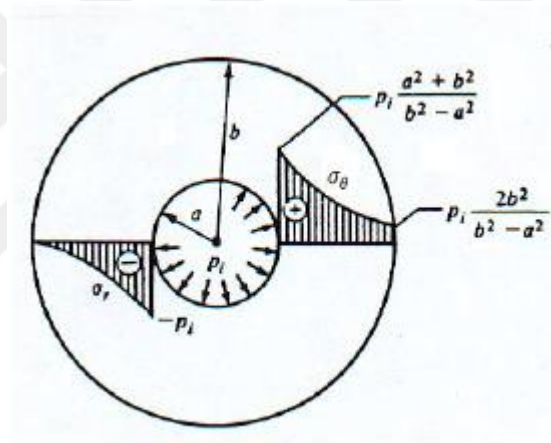


Figure 3.3 Stress distribution in internal pressure state (Sun, 2015)

### 3.3.2 Cylinders Subjected to External Pressure only

In this case  $P_e = P$  and  $P_i = 0$

Hence,

$$\sigma_r = \left( \frac{-Pb^2}{b^2 - a^2} \right) \left( 1 - \frac{a^2}{r^2} \right) \quad (3.36)$$

$$\sigma_\theta = \left( \frac{-Pb^2}{b^2 - a^2} \right) \left( 1 + \frac{a^2}{r^2} \right) \quad (3.37)$$

$$\sigma_z = 2\nu \left( \frac{-Pb^2}{b^2 - a^2} \right) \quad (3.38)$$

The maximum radial stress occurs at  $r = b$  and is compressive for all  $r$ . The maximum  $\sigma_\theta$  is found at  $r = a$ , and is likewise compressive. And this is illustrated in the Figure 3.4 (Sun, 2015).

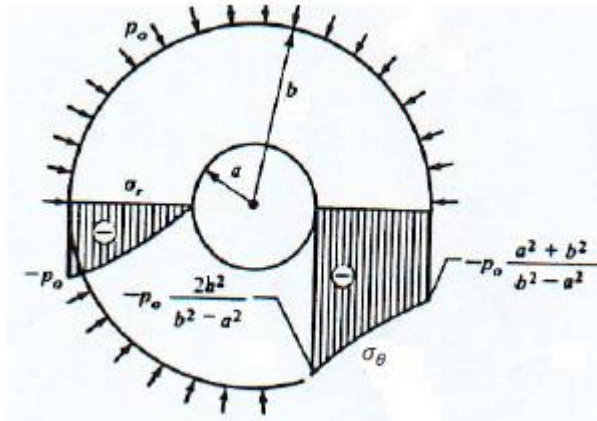


Figure 3.4 Stress distribution in external pressure state (Sun, 2015)

### 3.4 Analytical Relations For Swage Autofrettage Process

Swage autofrettage is a spatial axisymmetric elasto-plastic contact problem. To simplify the problem it's made some assumptions.

1. The sum of the plastic strain components is zero.

$$(\varepsilon_r^p + \varepsilon_\theta^p + \varepsilon_z^p = 0) \quad (3.39)$$

2. During the process, the axial strain is being ignored and cylinder is being assumed in the plane strain condition ( $\varepsilon_z = 0$ ). The axial stress  $\sigma_z$  is expressed by the following equation in the plane strain condition. This equation is being assumed to be valid both in the elastic and plastic regions.

$$\sigma_z = \nu(\sigma_r + \sigma_\theta) \quad (3.40)$$

3. According to the Coulomb friction model, the friction force is proportional to the contact pressure that is applied to the cylinder by the mandrel. If the friction coefficient is shown as  $\mu$ , the shear stress that will occur due to the friction can be expressed as  $(\tau_{rz} = \mu\sigma_r)_{r=a}$ . However, the shear stress value due to the friction can be ignored since it is very small compared to the other stress components.

4. By simplification of the swage autofrettage, the contact pressure that occurs when the mandrel passes through the cylinder is treated as the hydrostatic pressure and the equations that are used for the solution of the hydrostatic autofrettage were made use of.

5. It is assumed that the mandrel behaves elastically during the process.

6. When the pressure on the inner wall of the cylinder is released, the recovery behavior of the material in the stress-strain graphic is assumed to be linear.

### 3.4.1 Elastic-Perfectly Plastic Model

The contact pressure of the cylindrical tube reaches to the yielding point on the inner wall of the cylinder at first. In a cylinder that is subject to only internal pressure, the necessary yielding condition is defined by the following equation (Jost, 1988).

$$\sigma_{\theta} - \sigma_r = \sigma_0 \quad (3.41)$$

When the radial and the tangential stresses given by Eq.(3.33) and Eq.(3.34) are substituted for  $(r = a)$  in Eq.(3.41), the pressure value that will start yielding is obtained (Jost, 1988).

$$P_a = \frac{\sigma_0}{2} \left( 1 - \frac{a^2}{b^2} \right) = -\sigma_r \quad (3.42)$$

If the pressure on the inner wall of the cylinder is increased more, there will be a plastic region that spreads to the outer diameter of the cylinder. The thickness of the plastic region that occurs in the cylinder is related with the difference between outer radius of the mandrel that was used for the swage autofrettage and inner radius of the cylinder. This difference is named as interference. The interference of the cylinder and the mandrel is bigger, the higher the contact pressure on the inner wall of the cylinder is. The higher contact pressure means a deeper plastic region (Jost, 1988).

#### 3.4.1.1 The Stresses in the Plastic Region in Loading Condition

The yielding criterion expressed by Eq.(3.41) should be valid for the whole plastic region occurs in the cylinder. However, the equilibrium equation in Eq.(3.4), is valid

for both the elastic and the plastic region. If the Eq.(3.41) is substituted in Eq.(3.4) and integrated, the following equation is obtained (Jost, 1988).

$$\frac{\partial \sigma_r}{\partial r} - \frac{\sigma_0}{r} = 0 \quad (3.43)$$

$$\sigma_r = \sigma_0 \ln r + c_1 \quad (3.44)$$

If radius  $a$  is substituted by radius  $c$  (elastic-plastic radius) in Eq.(3.42) which states the pressure that starts the plastic yielding in  $r = a$ , the new equation will give  $-\sigma_r$  value on the elastic-plastic junction. This boundary condition is used to determine the  $c_1$  integration constant (Jost, 1988).

$$\sigma_{rc} = \frac{\sigma_0}{2} \left( -1 + \frac{c^2}{b^2} \right) \quad (3.45)$$

When  $r$  is substituted with  $c$  in Eq.(3.44) and  $\sigma_r$  is substituted with  $\sigma_{rc}$  in Eq.(3.45),  $c_1$  constant is obtained (Jost, 1988).

$$c_1 = \frac{\sigma_0}{2} \left( -1 + \frac{c^2}{b^2} - \ln c^2 \right) \quad (3.46)$$

If the  $c_1$  constant which is given in Eq.(3.46) is substituted in Eq.(3.44),  $\sigma_r$  expression in the plastic region is obtained Eq.(3.47) (Jost, 1988).

$$\sigma_r = \frac{\sigma_0}{2} \left( -1 + \frac{c^2}{b^2} + \ln \frac{r^2}{c^2} \right) \quad (3.47)$$

If Eq.(3.47) is substituted in Eq.(3.41), tangential stress expression for the plastic region is obtained (Jost, 1988).

$$\sigma_\theta = \frac{\sigma_0}{2} \left( 1 + \frac{c^2}{b^2} + \ln \frac{r^2}{c^2} \right) \quad (3.48)$$

When the radial and tangential stress expressions that are valid in the plastic region are substituted in Eq.(3.40),  $\sigma_z$  expression for the plastic region is obtained.

$$\sigma_z = \sigma_0 \nu \left( \frac{c^2}{b^2} + \ln \frac{r^2}{c^2} \right) \quad (3.49)$$

Eq.(3.47), Eq.(3.48) and Eq.(3.49) give the stress distribution of the plastic region between  $r = a$  and  $r = c$  of a thick walled cylindrical vessel which was pressured on the inner wall (Jost, 1988).

Pressure  $P^*$ , that is applied on  $r = a$  and causes plastic yielding up to  $r = c$ , can be obtained from the expression in Eq.(3.47). In case of the application of pressure  $P^*$ , if we express the radial stress by  $\sigma_r^*$  at  $r = a$ ,  $P^* = -\sigma_r^*$  will be obtained (Jost, 1988).

$$P^* = \frac{\sigma_0}{2} \left( 1 - \frac{c^2}{b^2} - \ln \frac{a^2}{c^2} \right) \quad (3.50)$$

#### 3.4.1.2 The Stresses in the Elastic Region in Loading Condition

To obtain the governing equations of the elastic region, we can ignore the plastic region and consider the cylinder as an elastic one bounded by  $r = c$  and  $r = b$ . Then,  $-\sigma_{r_c}$  will express the  $P_c$  pressure that will start yielding at  $r = c$  in our imaginary cylinder whose inner radius is  $c$  and outer radius is  $b$  (Jost, 1988).

$$P_c = \frac{\sigma_0}{2} \left( 1 - \frac{c^2}{b^2} \right) \quad (3.51)$$

If  $P$  is substituted by the expression in Eq.(3.51) and the  $a$  radius substituted by  $b$  in Eq.(3.33), Eq.(3.34) and Eq.(3.35) which give the stress distribution in the elastic region of the cylinder which is subject to only internal pressure, the stresses in the elastic region of the cylindrical vessel is obtained in loading condition (Jost, 1988).

$$\sigma_r = \frac{\sigma_0}{2} \left( -\frac{c^2}{r^2} + \frac{c^2}{b^2} \right) \quad (3.52)$$

$$\sigma_\theta = \frac{\sigma_0}{2} \left( \frac{c^2}{r^2} + \frac{c^2}{b^2} \right) \quad (3.53)$$

$$\sigma_z = \nu \sigma_0 \frac{c^2}{b^2} \quad (3.54)$$

#### 3.4.1.3 Determination of the Elastic-Plastic Junction

In this section, the mathematical relation between interference and elastic-plastic junction will be established. The interference which is represented by the symbol  $I$  is defined by the difference between the outer radius of the mandrel and the inner radius of the cylinder (Chakrabarty, 1996).

$$I = r_m - a \quad (3.55)$$

During the swage autofrettage process, as the mandrel passes through the cylinder, a radial expansion on the hole surface and a radial reduction on the mandrel surface occur. The difference between the positive radial displacement on the cylinder's inner wall and the negative radial displacement on the mandrel's outer wall is equal to the interference value (Chakrabarty, 1996).

$$I = u_a - u_m = a(\varepsilon_{\theta_t})_a - a(\varepsilon_{\theta_m})_a \quad (3.56)$$

According to the Generalized Hook's Law, strains in the cylindrical coordinates are expressed as follows (Chakrabarty, 1996).

$$\varepsilon_r = \frac{1}{E} [\sigma_r - \nu(\sigma_\theta + \sigma_z)] \quad (3.57)$$

$$\varepsilon_\theta = \frac{1}{E} [\sigma_\theta - \nu(\sigma_r + \sigma_z)] \quad (3.58)$$

$$\varepsilon_z = \frac{1}{E} [\sigma_z - \nu(\sigma_r + \sigma_\theta)] \quad (3.59)$$

The following equation is obtained if the plane strain condition ( $\varepsilon_z = 0$ ) is applied for Eq.(3.59) (Chakrabarty, 1996).

$$\sigma_z = \nu(\sigma_r + \sigma_\theta) \quad (3.60)$$

If this equation is used in Eq.(3.57) and Eq.(3.58), strain components in the plane strain condition are obtained (Chakrabarty, 1996).

$$\varepsilon_r = \frac{1+\nu}{E} [(1 - \nu)\sigma_r - \nu\sigma_\theta] \quad (3.61)$$

$$\varepsilon_\theta = \frac{1+\nu}{E} [(1 - \nu)\sigma_\theta - \nu\sigma_r] \quad (3.62)$$

Since the above equations are valid only in the elastic limits, we can obtain the strain expressions in the elastic region by substituting Eq.(3.52) and Eq.(3.53) in Eq.(3.61) and Eq.(3.62) (Chakrabarty, 1996).

$$\varepsilon_r = (1 + \nu) \frac{\sigma_0 c^2}{2Eb^2} \left(1 - 2\nu - \frac{b^2}{r^2}\right) \quad (3.63)$$

$$\varepsilon_\theta = (1 + \nu) \frac{\sigma_0 c^2}{2Eb^2} \left(1 - 2\nu + \frac{b^2}{r^2}\right) \quad (3.64)$$

Previously, it was mentioned that the volume does not change during the plastic deformation and as a result of this condition, the sum of the plastic strain components should be zero. The following strain conditions are valid in the plane strain condition for the plastic region (Chakrabarty, 1996).

$$\varepsilon_r^p + \varepsilon_\theta^p = 0 \quad (3.65)$$

$$\varepsilon_r + \varepsilon_\theta = (\varepsilon_r^e + \varepsilon_\theta^e) + (\varepsilon_r^p + \varepsilon_\theta^p) \quad (3.66)$$

$$\varepsilon_r + \varepsilon_\theta = \frac{\partial u}{\partial r} + \frac{u}{r} = \varepsilon_r^e + \varepsilon_\theta^e = \frac{(1+\nu)(1-2\nu)}{E} (\sigma_r + \sigma_\theta) \quad (3.67)$$

The equilibrium equation in Eq.(3.4) can be expressed as follows as well (Chakrabarty, 1996).

$$(\sigma_r + \sigma_\theta) = \frac{1}{r} \frac{\partial}{\partial r} (r^2 \sigma_r) \quad (3.68)$$

If Eq.(3.68) is substituted in Eq.(3.67) and the equation is rewritten by using the following shear modulus and elasticity modulus relation, Eq.(3.70) is obtained (Chakrabarty, 1996).

$$G = \frac{E}{2(1+\nu)} \quad (3.69)$$

$$\frac{\partial u}{\partial r} + \frac{u}{r} = \frac{1-2\nu}{2Gr} \frac{\partial}{\partial r} (r^2 \sigma_r) \quad (3.70)$$

The differential equation above is valid both in the elastic and plastic regions of the cylinder. The following equation is obtained when Eq.(3.70) is solved (Chakrabarty, 1996).

$$\varepsilon_\theta = \frac{u}{r} = \frac{1-2\nu}{2G} \sigma_r + \frac{C_1}{r^2} \quad (3.71)$$

When we apply the boundary condition  $\sigma_r = 0$  for  $r = b$ , Eq.(3.72) is obtained (Chakrabarty, 1996).

$$(\varepsilon_\theta)_b = \frac{C_1}{b^2} \quad (3.72)$$

Eq.(3.64) gives the tangential strain in the elastic region. Then, the tangential strain equation for  $r = b$  will be as the following (Chakrabarty, 1996).



$$(\varepsilon_{\theta})_b = (1 - \nu^2) \frac{\sigma_0 c^2}{Eb^2} = (1 - \nu) \frac{\sigma_0 c^2}{2Gb^2} \quad (3.73)$$

When Eq.(3.72) and Eq.(3.73) are equalized, the integration constant  $c_1$  is obtained.

$$c_1 = (1 - \nu) \frac{\sigma_0 c^2}{2G} \quad (3.74)$$

When Eq.(3.74) is substituted in Eq.(3.71), the tangential strain equation of the cylinder is obtained (Chakrabarty, 1996).

$$\varepsilon_{\theta_t} = \frac{u}{r} = (1 - \nu) \frac{\sigma_0 c^2}{2Gr^2} + (1 - 2\nu) \frac{\sigma_r}{2G} \quad (3.75)$$

Mandrel that is used at the swage autofrettage process is manufactured from a material having high elasticity modulus. Therefore, the cylindrical tube is subject to plastic deformation but only the elastic deformation is observed on the mandrel. Stress equations of the cylindrical tube which is subject to only external pressure will be made use of to obtain the strain equations of the mandrel. While the equations that were derived for the externally pressurized cylindrical tube are rewritten for the mandrel, the radius  $a$  should be taken as zero in the equations Eq.(3.36)-(3.37)-(3.38). So, the stress equations for the mandrel will be as follows (Jost, 1988).

$$\sigma_r = \sigma_{\theta} = -P^* \quad (3.76)$$

$$\sigma_z = -2\nu_m P^* \quad (3.77)$$

If Eq.(3.76) is used in Eq.(3.62), the tangential strain equation of the mandrel is obtained (Jost, 1988).

$$\varepsilon_{\theta_m} = \frac{P^*}{E_m} (2\nu_m - 1)(\nu_m + 1) \quad (3.78)$$

When the expressions  $\varepsilon_{\theta_t}$  and  $\varepsilon_{\theta_m}$  given by Eq.(3.75) and Eq.(3.78) are substituted for  $r = a$  in Eq.(3.56), the following equation is obtained (Chakrabarty, 1996).

$$I = r_m - a$$

$$I = (1 - \nu) \frac{\sigma_0 c^2}{2Ga} - a(1 - 2\nu) \frac{P^*}{2G} - \frac{P^*}{E_m} a(2\nu_m - 1)(\nu_m + 1) \quad (3.79)$$

Elastic-plastic junction can be obtained with a simple iteration of the above equation.

#### 3.4.1.4 Residual Stresses

With the release of the pressure on the inner wall of the cylinder, an elastic recovery to the pre-loading geometry of the cylinder starts. Since a complete recovery can not be accomplished due to the plastic region surrounding the inner wall, residual stresses on the cylinder occur. During this recovery there are two cases. Since the compressive yielding stress at inner surface of the cylinder is not exceeded during the elastic recovery, a new plastic yielding does not occur in the first case but secondary plastic yielding occurs from the inner wall to the outer by exceeding the compressive yielding stress at the bore in the second case (Jost, 1988).

#### 3.4.1.5 Elastic Recovery without Re-yielding

The internal pressure that causes yielding from the cylinder's inner wall to the elastic-plastic junction in loading condition is zeroized during unloading. Residual stresses are obtained with the subtraction of the elastic stresses, which are raised by the autofrettage pressure that causes the cylinder to yield up to  $r = c$  radius, from the loading condition stresses.

##### 3.4.1.5.1 Residual Stresses in the Plastic Region

$$\sigma_r = \frac{\sigma_0}{2} \left( -1 + \frac{c^2}{b^2} + \ln \frac{r^2}{c^2} \right) - \left( \frac{P^* a^2}{b^2 - a^2} \right) \left( 1 - \frac{b^2}{r^2} \right) \quad (3.80)$$

$$\sigma_\theta = \frac{\sigma_0}{2} \left( 1 + \frac{c^2}{b^2} + \ln \frac{r^2}{c^2} \right) - \left( \frac{P^* a^2}{b^2 - a^2} \right) \left( 1 + \frac{b^2}{r^2} \right) \quad (3.81)$$

$$\sigma_z = \nu \sigma_0 \left( \frac{c^2}{b^2} + \ln \frac{r^2}{c^2} \right) - 2\nu \left( \frac{P^* a^2}{b^2 - a^2} \right) \quad (3.82)$$

##### 3.4.1.5.2 Residual Stresses in the Elastic Region

$$\sigma_r = \frac{\sigma_0}{2} \left( -\frac{c^2}{r^2} + \frac{c^2}{b^2} \right) - \left( \frac{P^* a^2}{b^2 - a^2} \right) \left( 1 - \frac{b^2}{r^2} \right) \quad (3.83)$$

$$\sigma_\theta = \frac{\sigma_0}{2} \left( \frac{c^2}{r^2} + \frac{c^2}{b^2} \right) - \left( \frac{P^* a^2}{b^2 - a^2} \right) \left( 1 + \frac{b^2}{r^2} \right) \quad (3.84)$$

$$\sigma_z = \nu\sigma_0 \frac{c^2}{b^2} - 2\nu \left( \frac{P^*a^2}{b^2-a^2} \right) \quad (3.85)$$

#### 3.4.1.6 Elastic Recovery with Re-yielding

The secondary plastic yielding which occurs during the elastic recovery starts from the inner wall and extends to the outer in a similar way with the first plastic yielding. To start a secondary yielding, it is necessary that the equivalent stress on the inner wall of the cylinder reaches to compressive yielding stress (Parker, 1997).

$$(\sigma_\theta - \sigma_r)_{r=a} \leq -\sigma_0 \quad (3.86)$$

When the inequality given by the Eq.(3.86) is obtained, the secondary yielding in the cylinder occurs. When the expressions  $\sigma_r$  and  $\sigma_\theta$  given by Eq.(3.80) and Eq.(3.81) are substituted for  $r = a$  in Eq.(3.86), the following expressions is obtained (Parker, 1997).

$$\frac{\sigma_0}{2} \left( 1 + \frac{c^2}{b^2} + \ln \frac{a^2}{c^2} \right) - \left( \frac{P^*a^2}{b^2-a^2} \right) \left( 1 + \frac{b^2}{a^2} \right) \leq -\sigma_0 \quad (3.87)$$

If the necessary editing and simplification are performed on these equations, Eq.(3.88) is obtained (Jost, 1988).

$$\left( \frac{b}{a} \right)^2 \leq \frac{\left( \frac{c}{a} \right)^2 - 2}{2 \ln \left( \frac{c}{a} \right) - 1} \quad (3.88)$$

Eq.(3.88) defines the necessary condition to start a secondary yielding in the cylindrical tube after the autofrettage. According to the results obtained from the solution of the above inequality, if b/a ratio is smaller than 2.22 or c/a ratio is smaller than 1.65, the secondary yielding does not occur for certain (Jost, 1988).

##### 3.4.1.6.1 Stresses in ( $a \leq r \leq d$ ) Region

In case of secondary yielding, when the load is released, a new plastic region is formed starting from the inner wall and extending to  $r = d$  point. The residual stress equations in this region are obtained in a similar way with the plastic yielding ones. However, this time, different boundary conditions are used. In the new condition, the yielding criterion is defined as follows (Parker, 1997).

$$\sigma_{\theta} - \sigma_r = -\sigma_0 \quad (3.89)$$

If Eq.(3.89) is substituted in Eq.(3.4) and integrated, the following equation is obtained (Parker, 1997).

$$\sigma_r = -\sigma_0 \ln r + c_1 \quad (3.90)$$

In  $r = a$ , the integration constant can be obtained by using  $\sigma_r = 0$  boundary condition (Parker, 1997).

$$c_1 = \sigma_0 \ln a \quad (3.91)$$

If the  $c_1$  constant that is given by Eq.(3.91) is substituted in Eq.(3.90),  $\sigma_r$  expression of the secondary plastic region is obtained (Parker, 1997).

$$\sigma_r = -\sigma_0 \ln \frac{r}{a} \quad (3.92)$$

If Eq.(3.92) is substituted in Eq.(3.89), the tangential stress expression for the plastic region is obtained (Parker, 1997).

$$\sigma_{\theta} = -\sigma_0 \left( 1 + \ln \frac{r}{a} \right) \quad (3.93)$$

When Eq.(3.92) and Eq.(3.93) are substituted in Eq.(3.40),  $\sigma_z$  expression for the secondary plastic region is obtained (Parker, 1997).

$$\sigma_z = -v\sigma_0 \left( 2 \ln \frac{r}{a} + 1 \right) \quad (3.94)$$

#### 3.4.1.6.2 Stresses in ( $d \leq r \leq c$ ) Region

When the pressure expression at the  $r = d$ , radius of the secondary plastic region, is subtracted from the pressure expression at the radius  $d$  at the autofrettage loading level, the pressure change on the elastic-plastic junction from the start of the autofrettage process to the end of the secondary yielding is obtained. This pressure difference is a positive value and will be expressed by  $\Delta P$ . Elastic stresses that  $\Delta P$  pressure produced in  $d \leq r \leq b$  region are obtained by substituting  $a$  with  $d$  and  $P$  with  $\Delta P$  in the elastic stress equations expressed by Eq.(3.33)-(3.34)-(3.35) (Parker, 1997).

$$\Delta P = \frac{\sigma_0}{2} \left( 1 - \frac{c^2}{b^2} - \ln \frac{d^2}{c^2} - \ln \frac{d^2}{a^2} \right) \quad (3.95)$$

$$\sigma_r = \left( \frac{(\Delta P)d^2}{b^2-d^2} \right) \left( 1 - \frac{b^2}{r^2} \right) \quad (3.96)$$

$$\sigma_\theta = \left( \frac{(\Delta P)d^2}{b^2-d^2} \right) \left( 1 + \frac{b^2}{r^2} \right) \quad (3.97)$$

$$\sigma_z = 2\nu \left( \frac{(\Delta P)d^2}{b^2-d^2} \right) \quad (3.98)$$

The following residual stresses are obtained with the subtraction of the elastic stresses expressed by Eq.(3.96)-(3.97)-(3.98) from the governing equations in the plastic region and expressed by Eq.(3.47)-(3.48)-(3.49) (Parker, 1997).

$$\sigma_r = \frac{\sigma_0}{2} \left( -1 + \frac{c^2}{b^2} + \ln \frac{r^2}{c^2} \right) - \left( \frac{(\Delta P)d^2}{b^2-d^2} \right) \left( 1 - \frac{b^2}{r^2} \right) \quad (3.99)$$

$$\sigma_\theta = \frac{\sigma_0}{2} \left( 1 + \frac{c^2}{b^2} + \ln \frac{r^2}{c^2} \right) - \left( \frac{(\Delta P)d^2}{b^2-d^2} \right) \left( 1 + \frac{b^2}{r^2} \right) \quad (3.100)$$

$$\sigma_z = \nu\sigma_0 \left( \frac{c^2}{b^2} + \ln \frac{r^2}{c^2} \right) - 2\nu \left( \frac{(\Delta P)d^2}{b^2-d^2} \right) \quad (3.101)$$

#### 3.4.1.6.3 Stresses in ( $c \leq r \leq b$ ) Region

The following residual stresses are obtained with the subtraction of the elastic stresses expressed by Eq.(3.96)-(3.97)-(3.98) from the governing equations in the loaded plastic region and expressed by Eq.(3.52)-(3.53)-(3.54) (Parker, 1997).

$$\sigma_r = \frac{\sigma_0}{2} \left( -\frac{c^2}{r^2} + \frac{c^2}{b^2} \right) - \left( \frac{(\Delta P)d^2}{b^2-d^2} \right) \left( 1 - \frac{b^2}{r^2} \right) \quad (3.102)$$

$$\sigma_\theta = \frac{\sigma_0}{2} \left( \frac{c^2}{r^2} + \frac{c^2}{b^2} \right) - \left( \frac{(\Delta P)d^2}{b^2-d^2} \right) \left( 1 + \frac{b^2}{r^2} \right) \quad (3.103)$$

$$\sigma_z = \nu\sigma_0 \frac{c^2}{b^2} - 2\nu \left( \frac{(\Delta P)d^2}{b^2-d^2} \right) \quad (3.104)$$

#### 3.4.1.7 Bauschinger Effect in Autofrettage Process

A decrease takes place in the compressive yielding strength of the cylinder which is subject to plastic deformation in autofrettage process. This decrease in the compressive yielding strength is closely related with the plastic strain amount. The analytical approaches in the previous sections realized ignoring Bauschinger effect. However, in practice, Bauschinger effect is observed in many metals and it affects the stress distribution of the autofrettage cylinders considerably. In the previous

sections, it was introduced that the secondary yielding is related with the applied pressure and the geometry of the tube. Additionally, it was deduced that the secondary yielding will certainly not happen if the  $b/a$  ratio is smaller than 2.22 or the  $c/a$  ratio is smaller than 1.65. However, this deduction loses its validity when Bauschinger effect is taken into consideration. Even if the  $b/a$  ratio is smaller than 2.22, the decrease in the compressive yielding strength due to Bauschinger effect can cause the secondary yielding to happen (Parker, 1997).

#### 3.4.1.7.1 Secondary Yielding Resulting from Bauschinger Effect

It is necessary that the residual stresses on the cylinder's inner wall fulfill the yielding condition to happen the secondary yielding under the effect of Bauschinger (Parker, 1997).

$$(\sigma_{\theta} - \sigma_r)_{r=a} \leq -f\sigma_0 \quad (3.105)$$

The  $f$  term, that is multiplied with the compressive yielding stress on the right side of the equation, is Bauschinger Effect Factor. Bauschinger Effect Factor is the ratio of compressive yielding strength to tensile yielding strength and it takes the values between 0-1 (Parker, 1997).

When the inequality expressed by Eq.(3.105) is realized, the secondary yielding occurs. When the expressions  $\sigma_r$  and  $\sigma_{\theta}$  given by Eq.(3.80) and Eq.(3.81) are substituted for  $r = a$  in Eq.(3.105), the following expressions is obtained (Parker, 1997).

$$\frac{\sigma_0}{2} \left( 1 + \frac{c^2}{b^2} + \ln \frac{a^2}{c^2} \right) - \left( \frac{P^*a^2}{b^2-a^2} \right) \left( 1 + \frac{b^2}{a^2} \right) \leq -f\sigma_0 \quad (3.106)$$

If the necessary editing and simplification are performed on these equations, Eq.(3.107) is obtained (Parker, 1997).

$$\left( \frac{b}{a} \right)^2 \leq \frac{\left( \frac{c}{a} \right)^2 - (1+f)}{2 \ln \left( \frac{c}{a} \right) - f} \quad (3.107)$$

### 3.4.1.7.2 Stresses in $(a \leq r \leq d)$ Region

$$\sigma_r = -f\sigma_0 \ln \frac{r}{a} \quad (3.108)$$

$$\sigma_\theta = -f\sigma_0 \left(1 + \ln \frac{r}{a}\right) \quad (3.109)$$

$$\sigma_z = -fv\sigma_0 \left(2 \ln \frac{r}{a} + 1\right) \quad (3.110)$$

### 3.4.1.7.3 Stresses in $(d \leq r \leq c)$ Region

$$\Delta P^* = \frac{\sigma_0}{2} \left(1 - \frac{c^2}{b^2} - \ln \frac{d^2}{c^2}\right) - \frac{f\sigma_0}{2} \left(\ln \frac{d^2}{a^2}\right) \quad (3.111)$$

$$\sigma_r = \frac{\sigma_0}{2} \left(-1 + \frac{c^2}{b^2} + \ln \frac{r^2}{c^2}\right) - \left(\frac{(\Delta P^*)d^2}{b^2-d^2}\right) \left(1 - \frac{b^2}{r^2}\right) \quad (3.112)$$

$$\sigma_\theta = \frac{\sigma_0}{2} \left(1 + \frac{c^2}{b^2} + \ln \frac{r^2}{c^2}\right) - \left(\frac{(\Delta P^*)d^2}{b^2-d^2}\right) \left(1 + \frac{b^2}{r^2}\right) \quad (3.113)$$

$$\sigma_z = v\sigma_0 \left(\frac{c^2}{b^2} + \ln \frac{r^2}{c^2}\right) - 2v \left(\frac{(\Delta P^*)d^2}{b^2-d^2}\right) \quad (3.114)$$

### 3.4.1.7.4 Stresses in $(c \leq r \leq b)$ Region

$$\sigma_r = \frac{\sigma_0}{2} \left(-\frac{c^2}{r^2} + \frac{c^2}{b^2}\right) - \left(\frac{(\Delta P^*)d^2}{b^2-d^2}\right) \left(1 - \frac{b^2}{r^2}\right) \quad (3.115)$$

$$\sigma_\theta = \frac{\sigma_0}{2} \left(\frac{c^2}{r^2} + \frac{c^2}{b^2}\right) - \left(\frac{(\Delta P^*)d^2}{b^2-d^2}\right) \left(1 + \frac{b^2}{r^2}\right) \quad (3.116)$$

$$\sigma_z = v\sigma_0 \frac{c^2}{b^2} - 2v \left(\frac{(\Delta P^*)d^2}{b^2-d^2}\right) \quad (3.117)$$

## 3.4.2 Bilinear Hardening Model

Tresca yielding criterion for the materials that have strain hardening is expressed as the following (Chakrabarty, 1996).

$$\sigma_\theta - \sigma_r = \sigma \quad (3.118)$$

$\sigma$  in Eq.(3.118) is the yielding stress at any point of the plastic deformation. Yielding stress in the bilinear hardening model changes linearly with respect to plastic strain. Eq.(3.118) is expressed for bilinear hardening model in uniaxial stress state as follows (Chakrabarty, 1996).

$$\sigma = \sigma_0 + E_t \varepsilon^p \quad (3.119)$$

The  $E_t$  here is related with the slope of the plastic region and named as tangent modulus.  $\varepsilon^p$  defines the plastic strain. There is multi-axial stress in autofrettage process. Eq.(3.119) is defined as the following in terms of effective strain for multi-axial stress state (Chakrabarty, 1996).

$$\sigma = \sigma_0 + E_t \bar{\varepsilon}^p \quad (3.120)$$

It is considered that  $\sigma$  depends only on the total plastic work per any element's unit volume. The plastic work done per unit volume is expressed by the following equation in the cylindrical coordinates (Chakrabarty, 1996).

$$dW^p = \sigma_r d\varepsilon_r^p + \sigma_\theta d\varepsilon_\theta^p + \sigma_z d\varepsilon_z^p \quad (3.121)$$

If we equalize the plastic work done per unit volume in multi-axial stress to the plastic work done per unit volume in uniaxial stress, we obtain the following equation (Chakrabarty, 1996).

$$\sigma_r d\varepsilon_r^p + \sigma_\theta d\varepsilon_\theta^p + \sigma_z d\varepsilon_z^p = \sigma d\bar{\varepsilon}^p \quad (3.122)$$

The principle of constant volume during the plastic deformation is expressed as follows in terms of strains (Chakrabarty, 1996).

$$(d\varepsilon_r^p + d\varepsilon_\theta^p + d\varepsilon_z^p) = 0 \quad (3.123)$$

Since  $d\varepsilon_z^p = 0$  in the above equation for the plane strain condition, Eq.(3.123) can be written as follows (Chakrabarty, 1996).

$$d\varepsilon_r^p = -d\varepsilon_\theta^p \quad (3.124)$$

When Eq.(3.124) is substituted in Eq.(3.122), the following equation is obtained (Chakrabarty, 1996).

$$(\sigma_\theta - \sigma_r)d\varepsilon_\theta^p = \sigma d\bar{\varepsilon}^p \quad (3.125)$$

Since  $(\sigma_\theta - \sigma_r) = \sigma$ , the following result is obtained from the above equation (Chakrabarty, 1996).

$$d\bar{\varepsilon}^p = d\varepsilon_\theta^p \quad (3.126)$$



Eq.(3.126) can be written as follows for the bilinear hardening model (Chakrabarty, 1996).

$$\bar{\varepsilon}^p = \varepsilon_{\theta}^p \quad (3.127)$$

Eq.(3.127) states that the effective plastic strain for the bilinear hardening model is equal to the tangential plastic strain. If Eq.(3.127) is substituted in Eq.(3.120), the stress-strain equation for the bilinear hardening model is obtained (Chakrabarty, 1996).

$$\sigma = \sigma_0 + E_t \varepsilon_{\theta}^p \quad (3.128)$$

#### 3.4.2.1 Stresses in the Plastic Region

The total tangential strain in a thick walled cylinder is given by Eq.(3.75). Eq.(3.62) gives the tangential strain in a thick walled cylinder as stated before. When Eq.(3.62) is subtracted from Eq.(3.75), the plastic tangential strain expression is obtained for the thick walled cylinder.

$$\varepsilon_{\theta}^p = \varepsilon_{\theta} - \varepsilon_{\theta}^e = (1 - \nu^2) \left[ \frac{\sigma_0 c^2}{Er^2} - \frac{\sigma}{E} \right] \quad (3.129)$$

When the plastic tangential strain expression given by Eq.(3.129) is substituted in Eq.(3.128), Eq.(3.130) is obtained.

$$\sigma = \sigma_{\theta} - \sigma_r = \frac{\sigma_0 \left[ 1 + (1 - \nu^2) \frac{E_t c^2}{Er^2} \right]}{\left[ 1 + (1 - \nu^2) \frac{E_t}{E} \right]} \quad (3.130)$$

If the above expression is substituted by  $\sigma_{\theta} - \sigma_r$  in the equilibrium equation given by Eq.(3.4) and the obtained equation is integrated, Eq.(3.131) is obtained.

$$\sigma_r = \frac{\sigma_0 \ln r - \frac{\sigma_0}{2} (1 - \nu^2) \frac{E_t c^2}{Er^2}}{1 + (1 - \nu^2) \frac{E_t}{E}} + \frac{C_1}{1 + (1 - \nu^2) \frac{E_t}{E}} \quad (3.131)$$

The radial stress  $\sigma_{r_c}$  that is generated by the autofrettage pressure on the inner wall was given by Eq.(3.45). Then, when  $r$  is substituted by  $c$  in Eq.(3.131) and  $\sigma_r$  is substituted by  $\sigma_{r_c}$  which is given in Eq.(3.45), integration constant is obtained.

$$\frac{\sigma_0 \ln c - \frac{\sigma_0 (1-v^2) E_t}{E}}{1+(1-v^2) \frac{E_t}{E}} + \frac{c_1}{1+(1-v^2) \frac{E_t}{E}} = \frac{\sigma_0}{2} \left( -1 + \frac{c^2}{b^2} \right) \quad (3.132)$$

$$c_1 = \frac{\sigma_0}{2} \left( -1 + \frac{c^2}{b^2} \right) \left( 1 + (1-v^2) \frac{E_t}{E} \right) - \left( \sigma_0 \ln c - \frac{\sigma_0 (1-v^2) E_t}{E} \right) \quad (3.133)$$

If Eq.(3.133) is substituted in Eq.(3.131), the radial stress expression for plastic region is obtained.

$$\sigma_r = \frac{-\frac{\sigma_0}{2} \left[ 1 - \frac{c^2}{b^2} + \ln \frac{c^2}{r^2} + (1-v^2) \frac{E_t}{E} \left( \frac{c^2}{r^2} - \frac{c^2}{b^2} \right) \right]}{1+(1-v^2) \frac{E_t}{E}} \quad (3.134)$$

If the radial stress expression in Eq.(3.134) is substituted in Eq.(3.118), the tangential stress equation in the plastic region is obtained.

$$\sigma_\theta = \frac{\frac{\sigma_0}{2} \left[ 1 + \frac{c^2}{b^2} - \ln \frac{c^2}{r^2} + (1-v^2) \frac{E_t}{E} \left( \frac{c^2}{r^2} + \frac{c^2}{b^2} \right) \right]}{1+(1-v^2) \frac{E_t}{E}} \quad (3.135)$$

When the radial and tangential stress expressions that are valid in the plastic region are substituted in Eq.(3.40),  $\sigma_z$  expression for the plastic region is obtained.

$$\sigma_z = \frac{v \sigma_0 \left[ \frac{c^2}{b^2} - \ln \frac{c^2}{r^2} + (1-v^2) \frac{E_t}{E} \frac{c^2}{b^2} \right]}{1+(1-v^2) \frac{E_t}{E}} \quad (3.136)$$

Eq.(3.134) is made use of to obtain the autofrettage pressure  $\dot{P}$ . In case of the application of pressure  $\dot{P}$ , if we express the radial stress at  $r = a$  with  $\sigma_r$ , then we will have  $\dot{P} = -\sigma_r$ .

$$\dot{P} = \frac{\frac{\sigma_0}{2} \left[ 1 - \frac{c^2}{b^2} + \ln \frac{c^2}{a^2} + (1-v^2) \frac{E_t}{E} \left( \frac{c^2}{a^2} - \frac{c^2}{b^2} \right) \right]}{1+(1-v^2) \frac{E_t}{E}} \quad (3.137)$$

### 3.4.2.2 Stresses in the Elastic Region

The bilinear hardening model stress equations that are prevalent in the elastic region of the cylinder are same with the elastic perfectly plastic model's elastic region equations.

$$\sigma_r = \frac{\sigma_0}{2} \left( -\frac{c^2}{r^2} + \frac{c^2}{b^2} \right) \quad (3.138)$$

$$\sigma_{\theta} = \frac{\sigma_0}{2} \left( \frac{c^2}{r^2} + \frac{c^2}{b^2} \right) \quad (3.139)$$

$$\sigma_z = \nu \sigma_0 \frac{c^2}{b^2} \quad (3.140)$$

### 3.4.2.3 Determination of Elastic-Plastic Junction

The equation that describes the relation between the elastic-plastic junction and the interference in the bilinear hardening model is obtained in a similar way with the one in elastic perfectly plastic model. The autofrettage pressure  $\dot{P}$  in the bilinear hardening model is calculated with the equation Eq.(3.137).

$$\begin{aligned} I &= r_m - a \\ &= (1 - \nu) \frac{\sigma_0 c^2}{2Ga} - a(1 - 2\nu) \frac{\dot{P}}{2G} - \frac{\dot{P}}{E} a(2\nu_m - 1)(\nu_m + 1) \end{aligned} \quad (3.141)$$

Elastic-plastic junction can be obtained with a simple iteration in the above equation.

### 3.4.2.4 Residual Stresses in the Plastic Region

$$\sigma_r = \frac{-\frac{\sigma_0}{2} \left[ 1 - \frac{c^2}{b^2} + \ln \frac{c^2}{r^2} + (1 - \nu^2) \frac{E_t}{E} \left( \frac{c^2}{r^2} - \frac{c^2}{b^2} \right) \right]}{1 + (1 - \nu^2) \frac{E_t}{E}} - \left( \frac{\dot{P} a^2}{b^2 - a^2} \right) \left( 1 - \frac{b^2}{r^2} \right) \quad (3.142)$$

$$\sigma_{\theta} = \frac{\frac{\sigma_0}{2} \left[ 1 + \frac{c^2}{b^2} - \ln \frac{c^2}{r^2} + (1 - \nu^2) \frac{E_t}{E} \left( \frac{c^2}{r^2} + \frac{c^2}{b^2} \right) \right]}{1 + (1 - \nu^2) \frac{E_t}{E}} - \left( \frac{\dot{P} a^2}{b^2 - a^2} \right) \left( 1 + \frac{b^2}{r^2} \right) \quad (3.143)$$

$$\sigma_z = \frac{\nu \sigma_0 \left[ \frac{c^2}{b^2} - \ln \frac{c^2}{r^2} + (1 - \nu^2) \frac{E_t c^2}{E b^2} \right]}{1 + (1 - \nu^2) \frac{E_t}{E}} - 2\nu \left( \frac{\dot{P} a^2}{b^2 - a^2} \right) \quad (3.144)$$

### 3.4.2.5 Residual Stresses in the Elastic Region

$$\sigma_r = \frac{\sigma_0}{2} \left( -\frac{c^2}{r^2} + \frac{c^2}{b^2} \right) - \left( \frac{\dot{P} a^2}{b^2 - a^2} \right) \left( 1 - \frac{b^2}{r^2} \right) \quad (3.145)$$

$$\sigma_{\theta} = \frac{\sigma_0}{2} \left( \frac{c^2}{r^2} + \frac{c^2}{b^2} \right) - \left( \frac{\dot{P} a^2}{b^2 - a^2} \right) \left( 1 + \frac{b^2}{r^2} \right) \quad (3.146)$$

$$\sigma_z = \nu \sigma_0 \frac{c^2}{b^2} - 2\nu \left( \frac{\dot{P} a^2}{b^2 - a^2} \right) \quad (3.147)$$

### 3.4.2.6 Secondary Yielding Resulting from Bauschinger Effect

#### 3.4.2.6.1 Stresses in ( $a \leq r \leq d$ ) Region

$$\sigma_r = \frac{\frac{f\sigma_0}{2} \left[ \ln \frac{a^2}{r^2} + (1-\nu^2) \frac{E_t}{E} \left( \frac{c^2}{r^2} - \frac{c^2}{a^2} \right) \right]}{\left[ 1 + (1-\nu^2) \frac{E_t}{E} \right]} \quad (3.148)$$

$$\sigma_\theta = \frac{\frac{f\sigma_0}{2} \left[ \ln \frac{a^2}{r^2} - (1-\nu^2) \frac{E_t}{E} \left( \frac{c^2}{r^2} + \frac{c^2}{a^2} \right) - 2 \right]}{\left[ 1 + (1-\nu^2) \frac{E_t}{E} \right]} \quad (3.149)$$

$$\sigma_z = \frac{fv\sigma_0 \left[ \ln \frac{a^2}{r^2} - (1-\nu^2) \frac{E_t}{E} \frac{c^2}{a^2} - 1 \right]}{\left[ 1 + (1-\nu^2) \frac{E_t}{E} \right]} \quad (3.150)$$

#### 3.4.2.6.2 Stresses in ( $d \leq r \leq c$ ) Region

$$\widehat{\Delta P} = \frac{\frac{\sigma_0}{2} \left[ 1 - \frac{c^2}{b^2} + \ln \frac{c^2}{d^2} + (1-\nu^2) \frac{E_t}{E} \left( \frac{c^2}{d^2} - \frac{c^2}{b^2} \right) \right]}{\left[ 1 + (1-\nu^2) \frac{E_t}{E} \right]} + \frac{\frac{f\sigma_0}{2} \left[ \ln \frac{a^2}{d^2} + (1-\nu^2) \frac{E_t}{E} \left( \frac{c^2}{d^2} - \frac{c^2}{a^2} \right) \right]}{\left[ 1 + (1-\nu^2) \frac{E_t}{E} \right]} \quad (3.151)$$

$$\sigma_r = \frac{-\frac{\sigma_0}{2} \left[ 1 - \frac{c^2}{b^2} + \ln \frac{c^2}{r^2} + (1-\nu^2) \frac{E_t}{E} \left( \frac{c^2}{r^2} - \frac{c^2}{b^2} \right) \right]}{1 + (1-\nu^2) \frac{E_t}{E}} - \left( \frac{\widehat{\Delta P}}{b^2 - d^2} \right) \left( 1 - \frac{b^2}{r^2} \right) \quad (3.152)$$

$$\sigma_\theta = \frac{\frac{\sigma_0}{2} \left[ 1 + \frac{c^2}{b^2} - \ln \frac{c^2}{r^2} + (1-\nu^2) \frac{E_t}{E} \left( \frac{c^2}{r^2} + \frac{c^2}{b^2} \right) \right]}{1 + (1-\nu^2) \frac{E_t}{E}} - \left( \frac{\widehat{\Delta P}}{b^2 - d^2} \right) \left( 1 + \frac{b^2}{r^2} \right) \quad (3.153)$$

$$\sigma_z = \frac{v\sigma_0 \left[ \frac{c^2}{b^2} - \ln \frac{c^2}{r^2} + (1-\nu^2) \frac{E_t}{E} \frac{c^2}{b^2} \right]}{1 + (1-\nu^2) \frac{E_t}{E}} - 2\nu \left( \frac{\widehat{\Delta P}}{b^2 - d^2} \right) \quad (3.154)$$

#### 3.4.2.6.3 Stresses in ( $c \leq r \leq b$ ) Region

$$\sigma_r = \frac{\sigma_0}{2} \left( -\frac{c^2}{r^2} + \frac{c^2}{b^2} \right) - \left( \frac{\widehat{\Delta P}}{b^2 - d^2} \right) \left( 1 - \frac{b^2}{r^2} \right) \quad (3.155)$$

$$\sigma_\theta = \frac{\sigma_0}{2} \left( \frac{c^2}{r^2} + \frac{c^2}{b^2} \right) - \left( \frac{\widehat{\Delta P}}{b^2 - d^2} \right) \left( 1 + \frac{b^2}{r^2} \right) \quad (3.156)$$

$$\sigma_z = v\sigma_0 \frac{c^2}{b^2} - 2\nu \left( \frac{\widehat{\Delta P}}{b^2 - d^2} \right) \quad (3.157)$$

### 3.4.2.7 Determination of Bauschinger Effect Factor for Bilinear Kinematic Hardening Model

Bauschinger Effect Factor in the kinematic hardening model changes with respect to the plastic strain amount in the  $\sigma - \varepsilon$  graphic. In the bilinear kinematic hardening model, if the increase in plastic stress starting from the initial plastic yielding is

expressed by  $\sigma_h$  , the compressive yielding strength in case of reversal of loading is  $-\sigma_0 + \sigma_h$  . Then, Bauschinger Effect Factor for kinematics hardening model can be expressed as follows.

$$f = 1 - \frac{\sigma_h}{\sigma_0} \quad (3.158)$$

$$\sigma_h = E^t \varepsilon_\theta^p = E^t (1 - \nu^2) \left[ \frac{\sigma_0 c^2}{Er^2} - \frac{\sigma}{E} \right] \quad (3.159)$$

$$f = 1 - \frac{E^t(1-\nu^2)}{\sigma_0} \left[ \frac{\sigma_0 c^2}{Er^2} - \frac{\sigma}{E} \right] \quad (3.160)$$

### 3.4.3 Effect of Turning Process on the Residual Stresses

After the autofrettage process, most of the time an amount of material is removed from the inner or outer surface of the cylinder by external or internal turning. To implement the wire winding method, which is generally used for the production of heavy armor barrel, material on the external surface is removed; whereas there is material loss on the inner surface of the cylinder during rifling process. This process changes the residual stress distribution on the cylinder. In this section, the effect of material removal from either inner or outer surface of the cylinder will be discussed.

#### 3.4.3.1 The Stresses Due to Only Internal Turning

If we consider the negative expression of the residual radial stress at  $r = \acute{a}$  as the hydrostatic pressure at  $r = \acute{a}$ , we can express the pressure change on this surface after turning process as follows.

$$\Delta\ddot{P} = P_{\acute{a}_2} - P_{\acute{a}_1} \quad (3.161)$$

$P_{\acute{a}_1}$  is the pressure prior to turning and the negative expression of the residual radial stress at  $r = \acute{a}$  .  $P_{\acute{a}_2}$  is the pressure after turning at  $\acute{a}$ , which is new inner radius of the cylinder, and this value is equal to zero. The elastic stresses that the  $\Delta\ddot{P}$  pressure change produces can be expressed as follows.

$$\sigma_r = \left( \frac{\Delta\ddot{P}\acute{a}^2}{b^2 - \acute{a}^2} \right) \left( 1 - \frac{b^2}{r^2} \right) \quad (3.162)$$

$$\sigma_\theta = \left( \frac{\Delta\ddot{P}\acute{a}^2}{b^2 - \acute{a}^2} \right) \left( 1 + \frac{b^2}{r^2} \right) \quad (3.163)$$

$$\sigma_z = 2\nu \left( \frac{\Delta\ddot{P}a^2}{b^2-a^2} \right) \quad (3.164)$$

As the result of the superposition of the elastic stresses that are produced by the  $\Delta\ddot{P}$  pressure and the residual stresses, the new stress distribution is obtained.

#### 3.4.3.2 The Stresses Due to Only External Turning

If we consider the negative expression of the pre-turning residual radial stress at outer radius  $\hat{b}$  as the hydrostatic pressure at  $r = \hat{b}$ , we can express the pressure change on this surface after turning process as follows.

$$\Delta\ddot{P} = P_{\hat{b}_2} - P_{\hat{b}_1} \quad (3.165)$$

$P_{\hat{b}_1}$  is the pressure prior to turning and the negative expression of the residual radial stress at  $r = \hat{b}$ .  $P_{\hat{b}_2}$  is the pressure after turning at  $\hat{b}$ , which is new outer radius of the cylinder, and this value is equal to zero. The elastic stresses that the  $\Delta\ddot{P}$  pressure change produce can be expressed as follows.

$$\sigma_r = \left( \frac{-\Delta\ddot{P}\hat{b}^2}{\hat{b}^2-a^2} \right) \left( 1 - \frac{a^2}{r^2} \right) \quad (3.166)$$

$$\sigma_\theta = \left( \frac{-\Delta\ddot{P}\hat{b}^2}{\hat{b}^2-a^2} \right) \left( 1 + \frac{a^2}{r^2} \right) \quad (3.167)$$

$$\sigma_z = 2\nu \left( \frac{-\Delta\ddot{P}\hat{b}^2}{\hat{b}^2-a^2} \right) \quad (3.168)$$

As the result of the superposition of the elastic stresses that are produced by the  $\Delta\ddot{P}$  pressure and the residual stresses, the new stress distribution is obtained.

#### 3.4.4 Stresses Occurring at Service Pressure

Autofrettaged thick walled cylinders are subject to different operating pressures with respect to their usage areas. In order that the cylindrical vessel works safely, the pressure applied on the inner wall of the cylinder should not cause plastic deformation. To design a proper pressure vessel, the stress distribution of the cylindrical container, that is subject to operating pressure after autofrettage, should be known.

The stresses in the thick walled cylindrical containers that are subject to operating pressure is obtained by the superposition of the elastic stresses that are produced by the service pressure and residual stresses that are produced by autofrettage process.

$$\sigma_{total} = \sigma_{ser} + \sigma_{res} \quad (3.169)$$

$$(\sigma_r)_{ser} = \left( \frac{P_{ser} a^2}{b^2 - a^2} \right) \left( 1 - \frac{b^2}{r^2} \right) \quad (3.170)$$

$$(\sigma_\theta)_{ser} = \left( \frac{P_{ser} a^2}{b^2 - a^2} \right) \left( 1 + \frac{b^2}{r^2} \right) \quad (3.171)$$

$$(\sigma_z)_{ser} = 0 \quad (3.172)$$

### ***3.4.5 Derivation of the Equations in Accordance with Von Mises Criterion***

All the equations that are derived up to now are derived with respect to Tresca yielding criterion. Due to the complex structure of mathematical expression of Von Mises criterion, it is pretty difficult to derive the equations with respect to von Mises criterion. To make it convenient, Von Mises criterion can be expressed in the following form.

$$\sigma_\theta - \sigma_r = \frac{2}{\sqrt{3}} \sigma_0 \quad (3.173)$$

## CHAPTER 4

### 4. RESULTS AND DISCUSSIONS

#### 4.1 Results of Analytical Model

Matlab program will be made use of to solve the equations derived in the previous section and to obtain the regarding graphics. Matlab program is a developed program that provides the opportunity to realize the engineering applications, calculations and simulations.

##### 4.1.1 Autofrettage and Steel Barrel Draft

A hole is drilled into the cylindrical steel rod that is prepared for the production of the barrel. It is brought to the autofrettage dimensions with machining (blue colored condition). After that, a mandrel is passed through this draft and autofrettage process is realized. After this process, steel barrel draft is built with rifling and setting the final dimensions of the outer part.

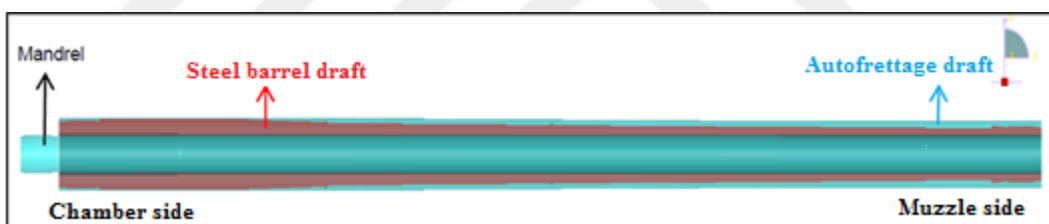


Figure 4.1 Representation of autofrettage and steel barrel draft

Table 4.1 Geometrical data of Autofrettage draft

Length of Autofrettage Draft	Outer Radius of Autofrettage Draft
3150 mm	96 mm

Barrel material is 35NiCrMoV12.5 quality steel. Its uniaxial tensile test graphic is given in the following figure.



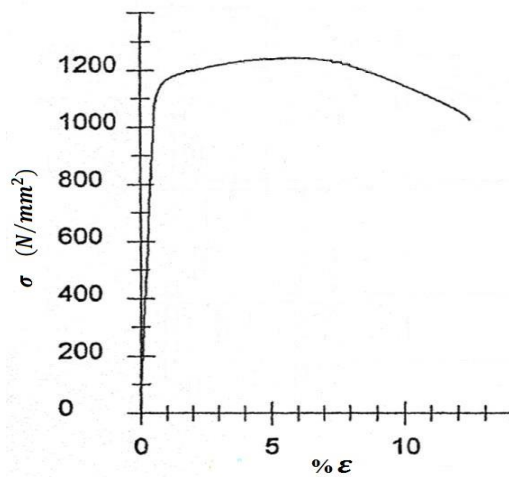


Figure 4.2 35NiCrMoV12.5 Stress-strain diagram

Yielding value of the barrel material is calculated as  $\sigma_0=1142.46$  MPa from the curve in Fig. 4.2.

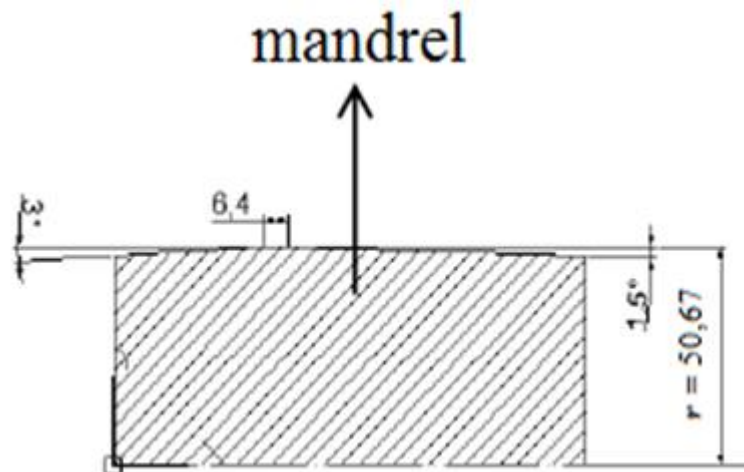


Figure 4.3 Mandrel cross section picture

The width of the flat section where the mandrel has the widest diameter is set to 6.4 mm and this region's radius is 50.67 mm. The angle of the frontal conical part is extended to 1.5° and it is smaller than the bore of the barrel. The back part is also set up to the same diameter conically with 3°. The material of the mandrel is WC. The material properties of mandrel and barrel are given in the following table.

**Table 4.2 Material properties of cylinder and mandrel**

Property	35NiCrMoV12.5	WC
E (GPa)	195.7	450
v	0.28	0.285
$\sigma_0$ (MPa)	1142.46	-----
$E^t$ (GPa)	2.8324	-----

#### 4.1.2 Determination of the Elastic-Plastic Junctions at Different Interference Values

Inner radius and elastic-plastic radius values with respect to the percent interference values of the cylinder and mandrel are given in Table-3. The values in the table are for the cylinder having the outer diameter as 96 mm. The radius of the hole that will be drilled into the cylinder with different % interference values is obtained with the help of the formula below.  $i$  in the formula represents the % interference value.

$$a = \frac{b*i-100*r_m}{i-100} \quad (4.1)$$

Bilinear hardening material model will be used in all the calculations since it represents the real stress-strain curve of the material better.

**Table 4.3 Elastic-plastic radius values corresponding to various interference ratios**

% Interference	Inner Radius (mm)	Tresca Elastic-Plastic Radius (mm)	Von Mises Elastic-Plastic Radius (mm)
0.75 %	50.3275	60.1925	56.1795
1 %	50.2121	68.9921	64.4771
1.25 %	50.0962	76.6132	71.6272
1.5 %	49.9797	83.4477	78.0227
1.75 %	49.8626	89.7026	83.8676
2 %	49.7449	95.5099	89.2869
2.25 %	49.6266	-----	94.3656

#### 4.1.3 Investigation of Bauschinger Effect for Different Interference Values

In this section, Bauschinger Effect Factors on the cylinder's inner wall will be determined regarding bilinear kinematic hardening model for different interference values. After Bauschinger Effect Factors are determined, it will be controlled if there will be a secondary plastic yielding on the inner wall of the cylinder.

**Table 4.4 Bauschinger effect factors corresponding to various interference ratios**

<b>% Interference</b>	<b>Inner Radius (mm)</b>	<b>(Tresca) Bauschinger Effect Factor</b>	<b>(Von Mises) Bauschinger Effect Factor</b>
0.75 %	50.3275	0.9766	0.9802
1 %	50.2121	0.9677	0.9713
1.25 %	50.0962	0.9600	0.9638
1.5 %	49.9797	0.9531	0.9571
1.75 %	49.8626	0.9465	0.9509
2 %	49.7449	0.9403	0.9451
2.25 %	49.6266	-----	0.9396

In order that Bauschinger effect can start the secondary plastic yielding, the following inequality should be satisfied in accordance with Tresca yielding criterion.

$$(\sigma_{\theta} - \sigma_r)_{r=a} \leq -f\sigma_0$$

The residual stresses  $\sigma_{\theta}$  and  $\sigma_r$  in the above inequality are calculated in accordance with Tresca and Von Mises criteria and tabularized.

**Table 4.5 The effect of BEF on secondary yielding in various interference ratios according to Tresca criteria**

<b>% Interference</b>	<b>(Tresca) Bauschinger Effect Factor</b>	$(\sigma_{\theta} - \sigma_r)_{r=a}$	$-f\sigma_0$
0.75 %	0.9766	-372.6463	-1115.7
1 %	0.9677	-609.2612	-1105.6
1.25 %	0.9600	-751.5294	-1096.8
1.5 %	0.9531	-836.2073	-1088.8
1.75 %	0.9465	-881.7908	-1081.4
2 %	0.9403	-899.0705	-1074.3

**Table 4.6 The effect of BEF on secondary yielding in various section values according to Von Mises criteria**

<b>% Interference</b>	<b>(Von Mises) Bauschinger Effect Factor</b>	$(\sigma_{\theta} - \sigma_r)_{r=a}$	$-f\sigma_0$
0.75 %	0.9802	-272.9825	-1119.8
1 %	0.9713	-576.9348	-1109.6
1.25 %	0.9638	-768.9243	-1101.1
1.5 %	0.9571	-893.4015	-1093.4
1.75 %	0.9509	-972.3197	-1086.4
2 %	0.9451	-1018.3	-1079.8
2.25 %	0.9396	-1039.5	-1073.5

In the above tables, it is seen that Bauschinger effect is not at a level to start the secondary yielding with respect to both yielding criteria even at the biggest interference value. Therefore, in accordance with the calculations, Bauschinger effect does not have an effect on the stress distributions on the cylinder.

#### 4.1.4 Stress Distributions at Different Stages of Autofrettage

##### 4.1.4.1 Stresses in Loading Condition

Radial stress distributions in loading condition are obtained separately for Von Mises and Tresca criteria by using the equations derived for bilinear model. Stress distributions obtained for different interference ratios.

##### 4.1.4.1.1 Radial Stresses

When the curves in Fig. 4.4, Fig. 4.5, Fig. 4.6 are examined, it is seen that the compressive radial stresses increase with the increasing interference ratio. It was identified that the compressive radial stress calculation results with respect to Von Mises criteria was higher than the ones with respect to Tresca criteria. It is seen that this difference more significant in plastic region.

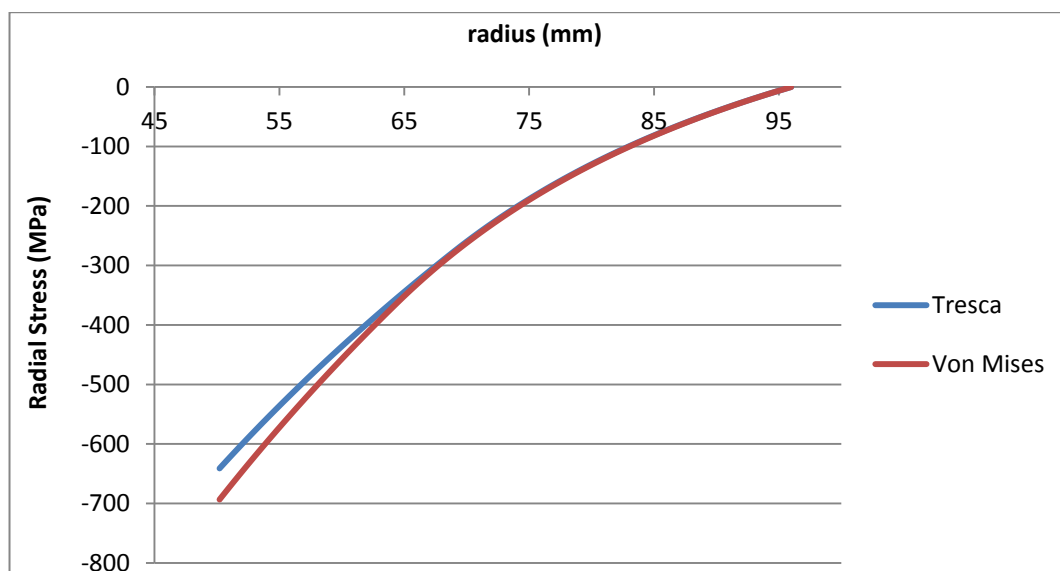
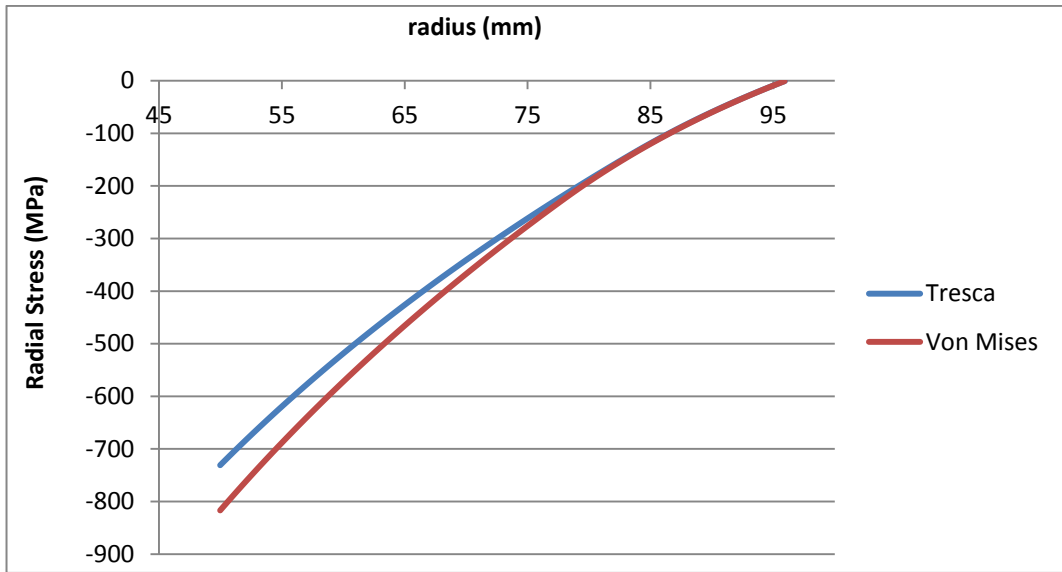
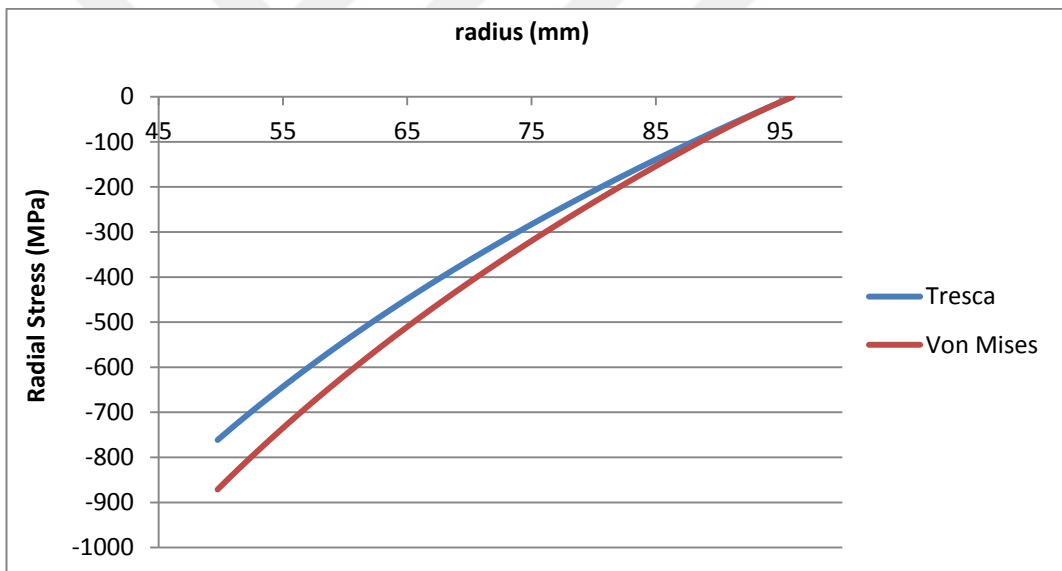


Figure 4.4 Radial stresses for 1% interference ratio



**Figure 4.5 Radial stresses for 1.5% interference ratio**



**Figure 4.6 Radial stresses for 2% interference ratio**

#### 4.1.4.1.2 Hoop Stresses

As it is seen in Fig. 4.7, Fig. 4.8, Fig. 4.9, the tangential stresses in loading condition are tensile throughout the wall. Tangential stresses have their largest value on the plastic junction. Tensions in the elastic region reach to the outer surface in a decreasing way. The calculations with respect to Von Mises criteria give higher values than the ones done with respect to Tresca criteria.

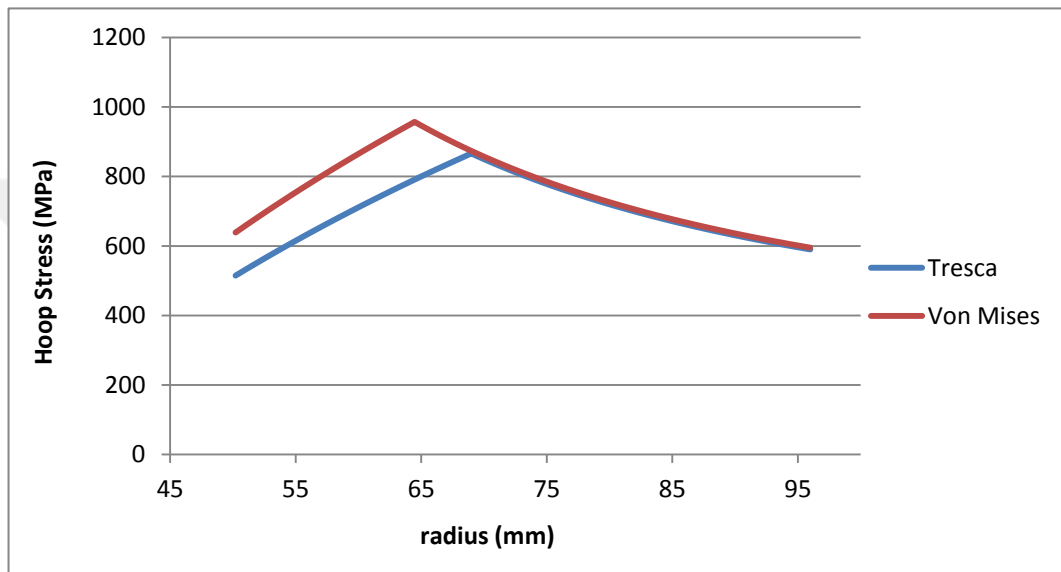


Figure 4.7 Hoop stresses for 1% interference ratio

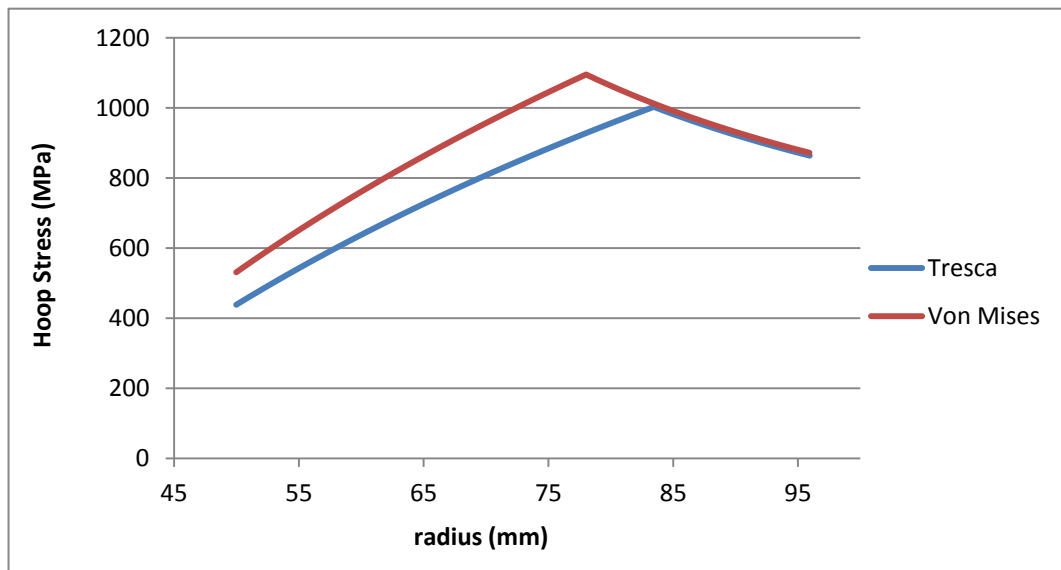
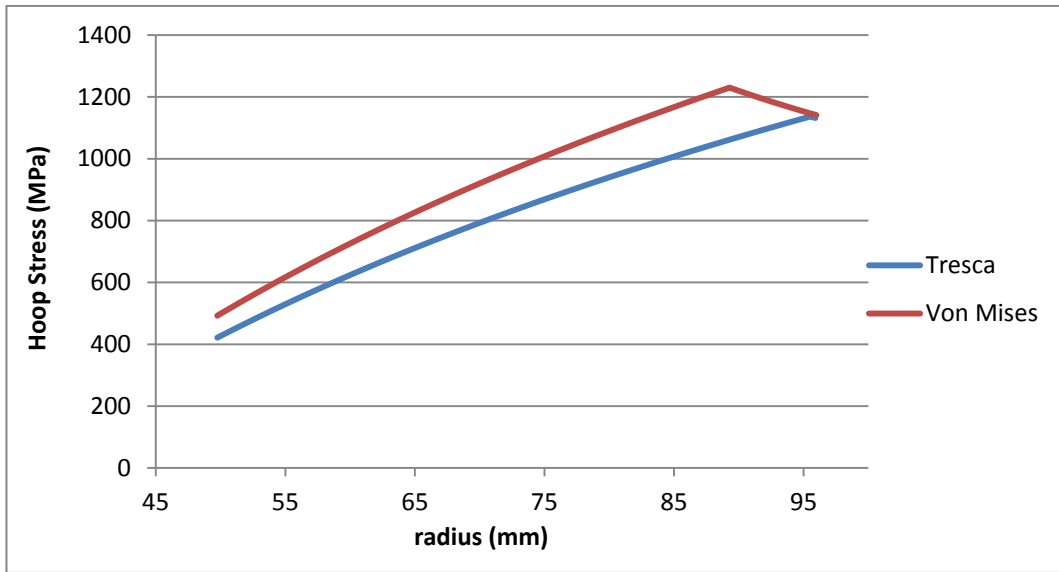


Figure 4.8 Hoop stresses for 1.5% interference ratio



**Figure 4.9 Hoop stresses for 2% interference ratio**

#### 4.1.4.1.3 Axial Stresses

As it is seen in Fig. 4.10, Fig. 4.11, Fig. 4.12, the axial stresses in loading condition have negative values in the vicinity of the inner wall namely, the stresses are compressive in this region. The compressive stresses decrease up to zero and then become tensile in this region. They increase up to the plastic junction and no change is met in the elastic region stresses. The results of Von Mises criteria are somewhat bigger than Tresca's.

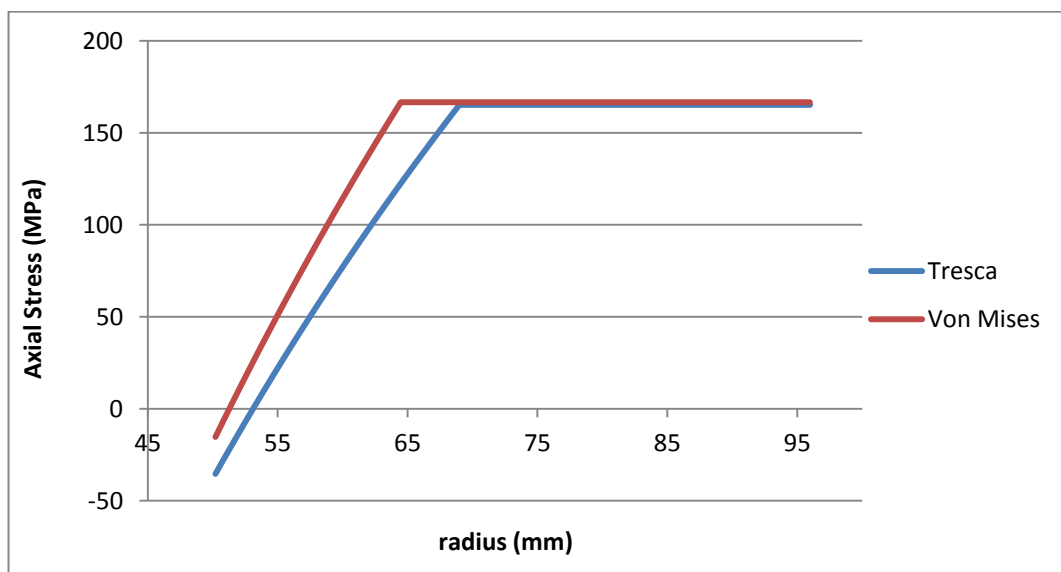


**Figure 4.10 Axial stresses for 1% interference ratio**



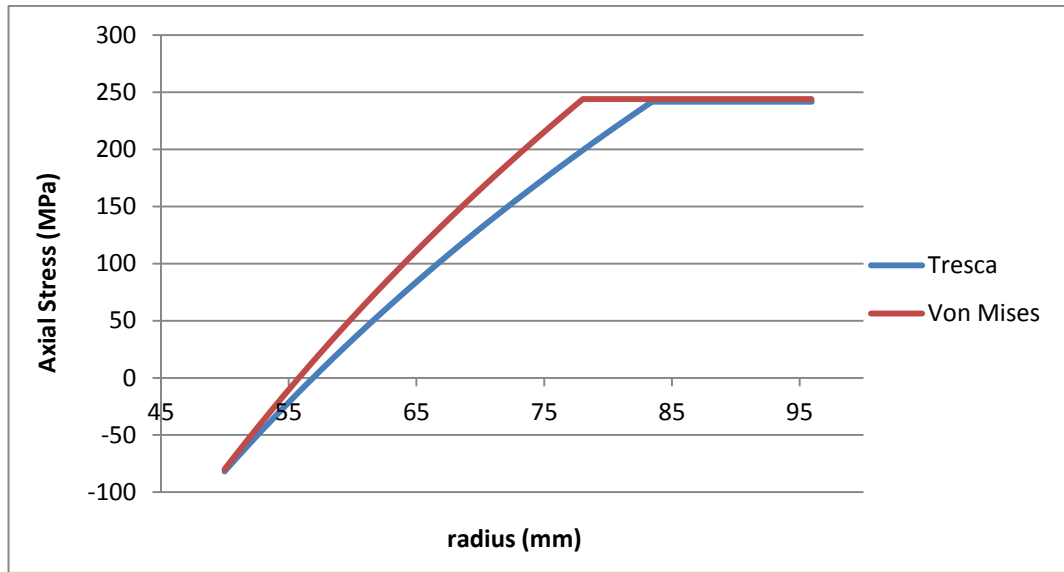


**Figure 4.11 Axial stresses for 1.5% interference ratio**

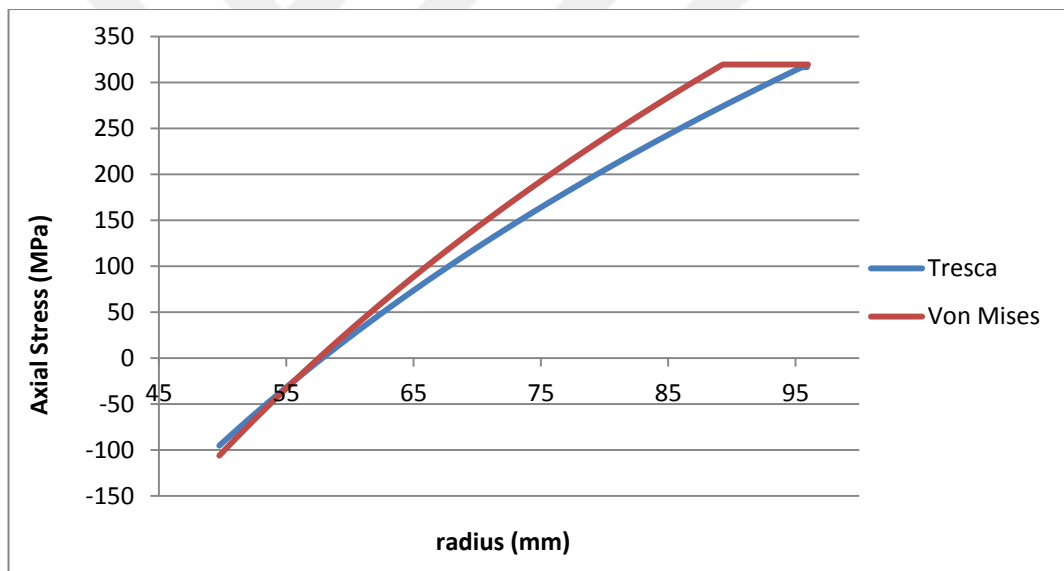


**Figure 4.12 Axial stresses for 2% interference ratio**

#### 4.1.4.2 Residual Stresses

##### 4.1.4.2.1 Radial Stresses

When Fig. 4.13, Fig. 4.14, Fig. 4.15 are examined, it is seen that the compressive radial stresses increase as the interference ratio increase. It is seen that there are slight differences between the graphics obtained with Von Mises and Tresca criteria. However, it can not be estimated how these two yielding criteria affect the results related to residual radial stresses.

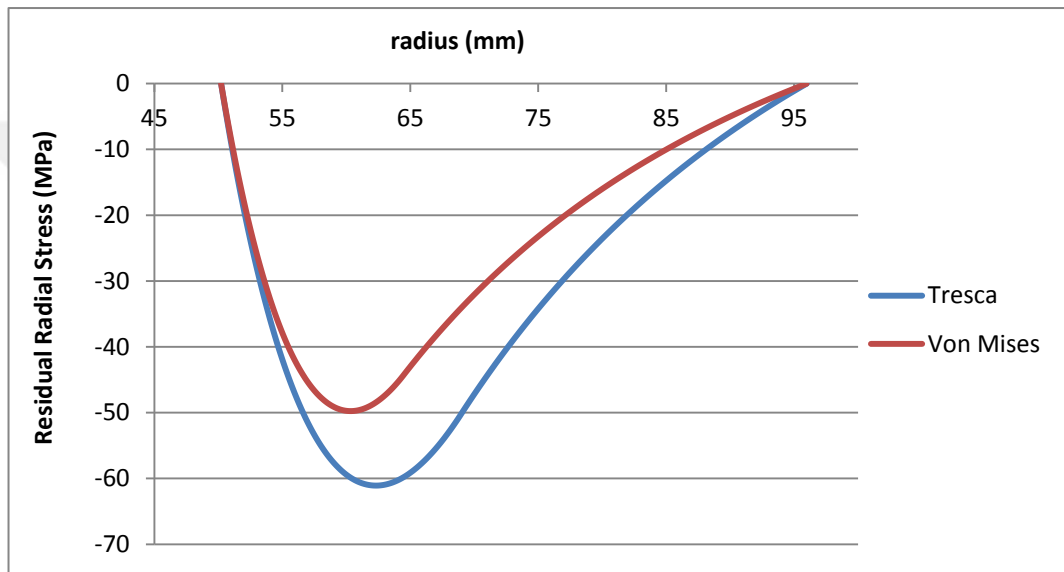


Figure 4.13 Residual radial stresses for 1% interference ratio

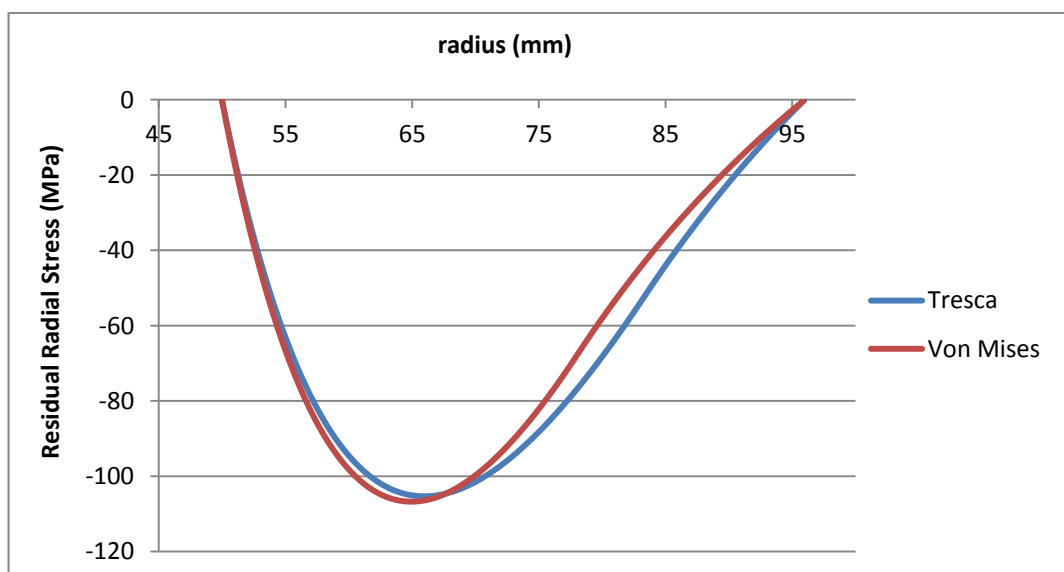
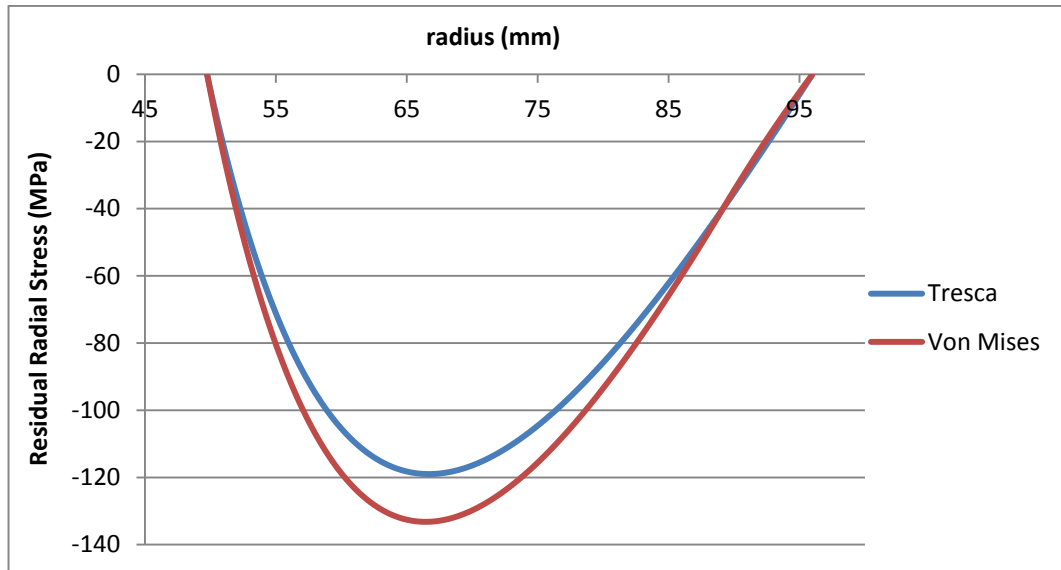


Figure 4.14 Residual radial stresses for 1.5% interference ratio



**Figure 4.15 Residual radial stresses for 2% interference ratio**

#### 4.1.4.2.2 Hoop Stresses

When Fig. 4.16, Fig. 4.17, Fig. 4.18 are examined, it is seen that the residual tangential stresses close to the hole surface are compressive and the stresses close to the cylinder's outer surface are tensile. Tensile stresses reach to maximum value on the elastic-plastic junction and the stresses in the plastic region decreases slightly as it is moved to the outer surface. Elastic stresses in Tresca criterion are somewhat bigger than the ones in Von Mises criterion.

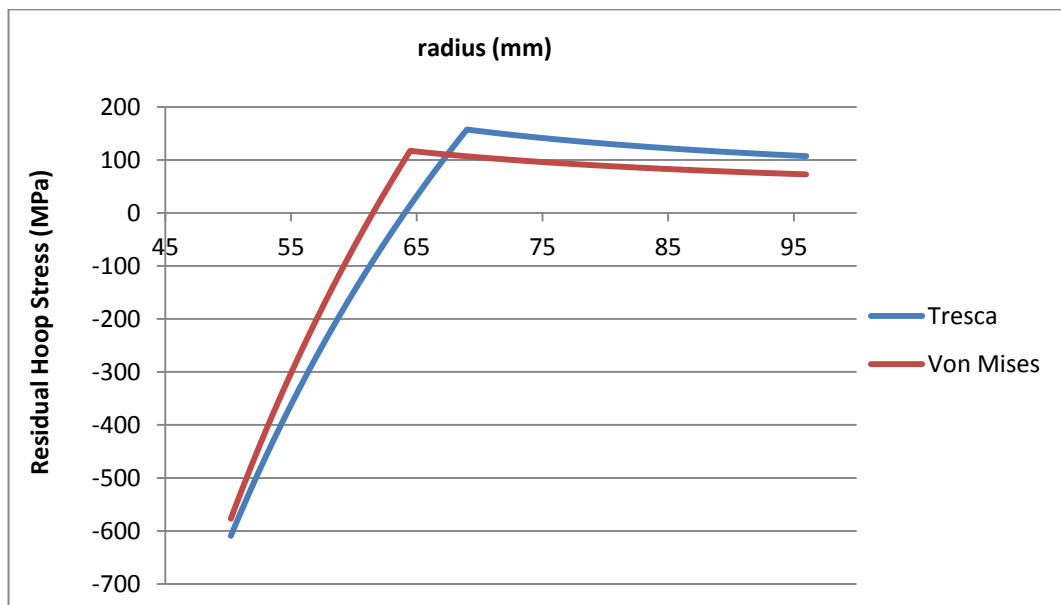


**Figure 4.16 Residual hoop stresses for 1% interference ratio**

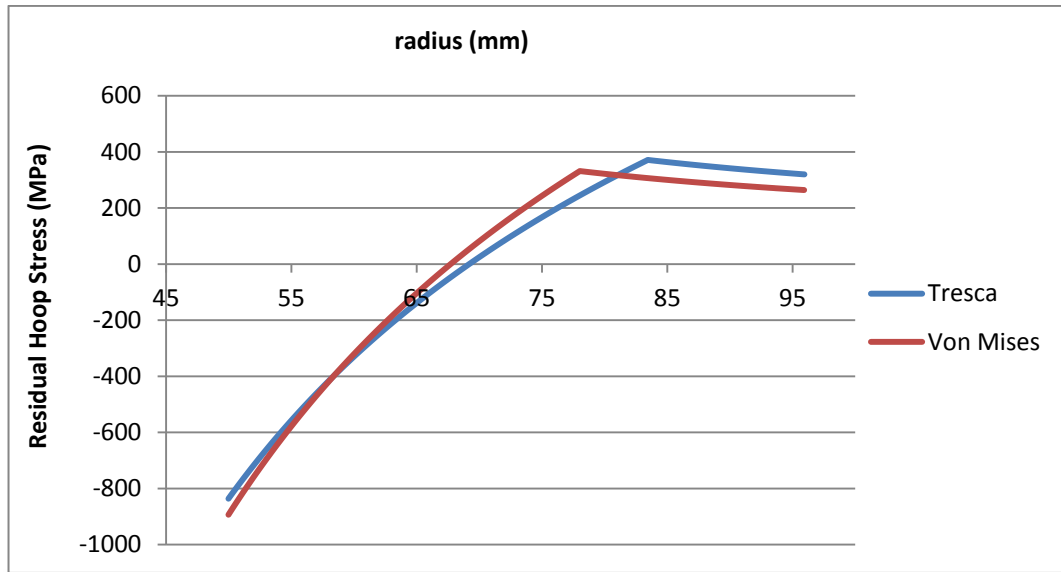


**Figure 4.17 Residual hoop stresses for 1.5% interference ratio**

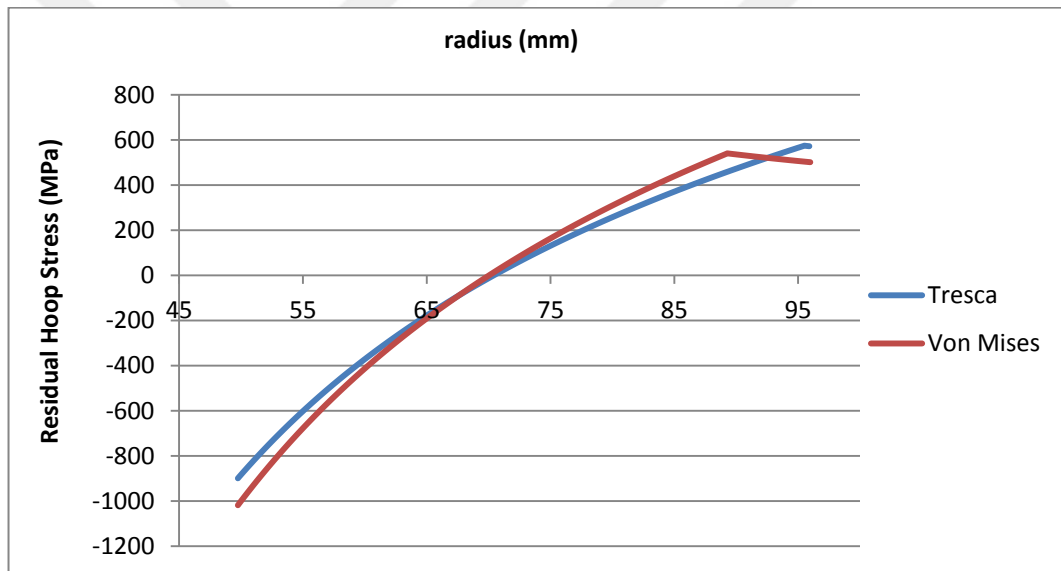


**Figure 4.18 Residual hoop stresses for 2% interference ratio**

#### 4.1.4.2.3 Axial Stresses

When Fig. 4.19, Fig. 4.20, Fig. 4.21 are examined, it is seen that although the residual axial stresses are compressive in a major part of the plastic region, they become tensile starting from a close point to the elastic-plastic junction. Compressive stresses increase up to elastic plastic junction and remain constant in the elastic region.

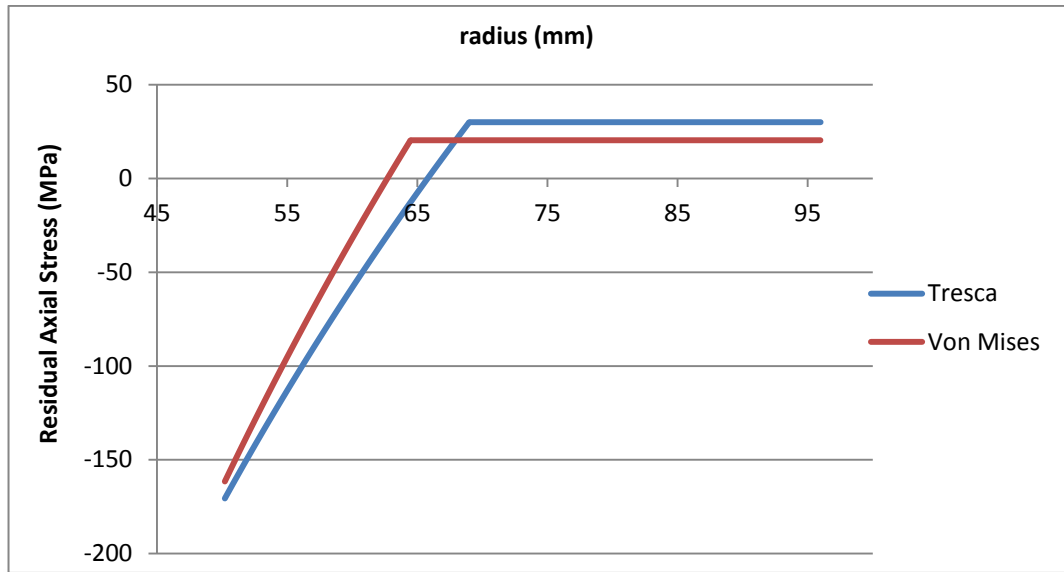


Figure 4.19 Residual axial stresses for 1% interference ratio

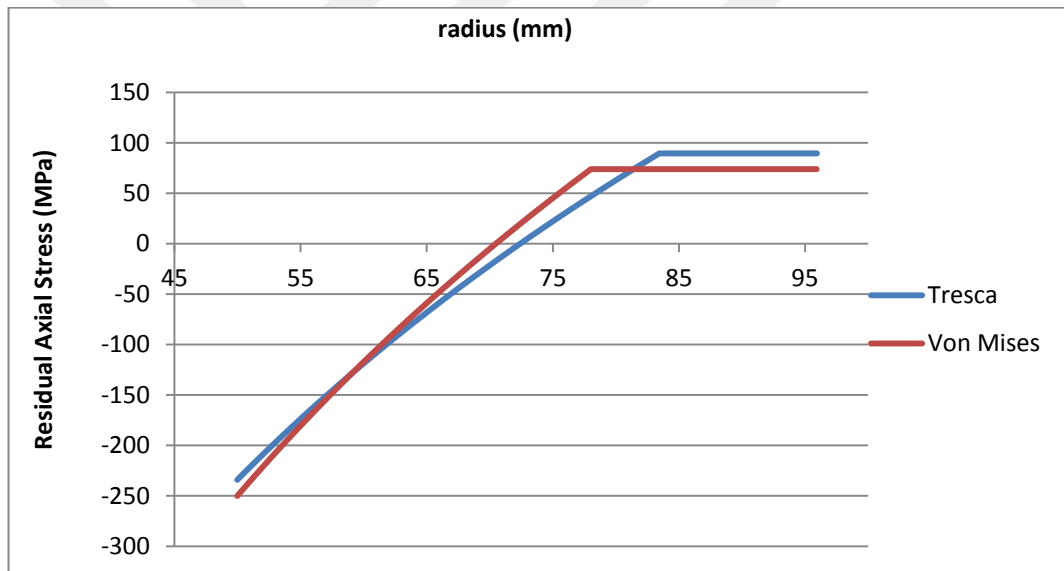
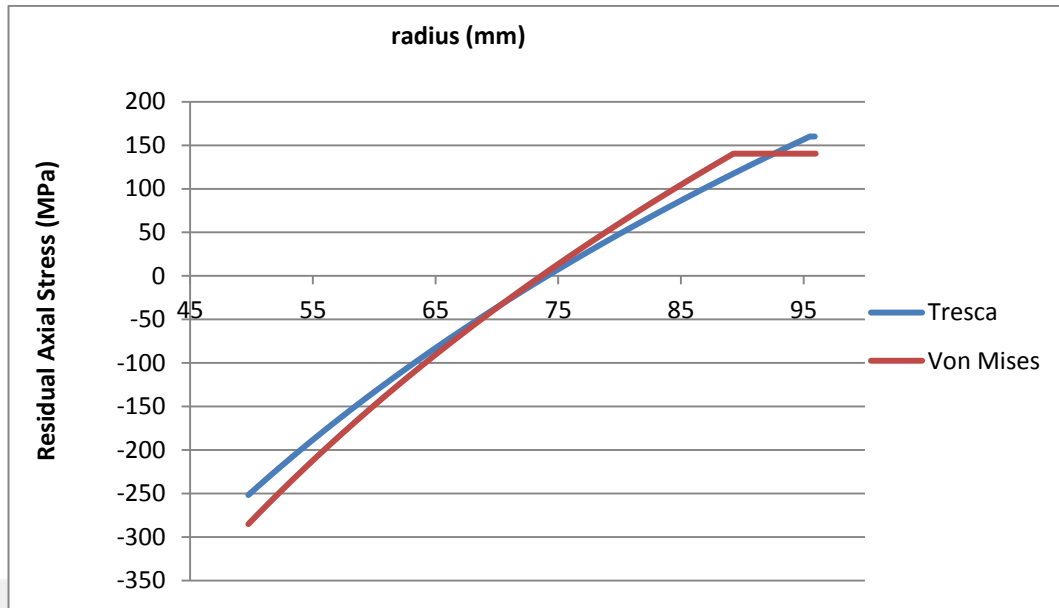


Figure 4.20 Residual axial stresses for 1.5% interference ratio



**Figure 4.21 Residual axial stresses for 2% interference ratio**

#### 4.1.4.3 Optimization of Interference

In this section, equivalent stress distributions that will occur for different interference values at operating pressure will be obtained analytically. It is assumed that the maximum pressure value in the barrel is 400 MPa at the bursting instant and it is also assumed that this pressure has an effect all through the barrel. The equivalent stress distributions that occur at operating pressure will be obtained separately with respect to Tresca and Von Mises. The stress distributions at operating pressure are obtained for each interference value in Table 4.3 by using bilinear hardening model.

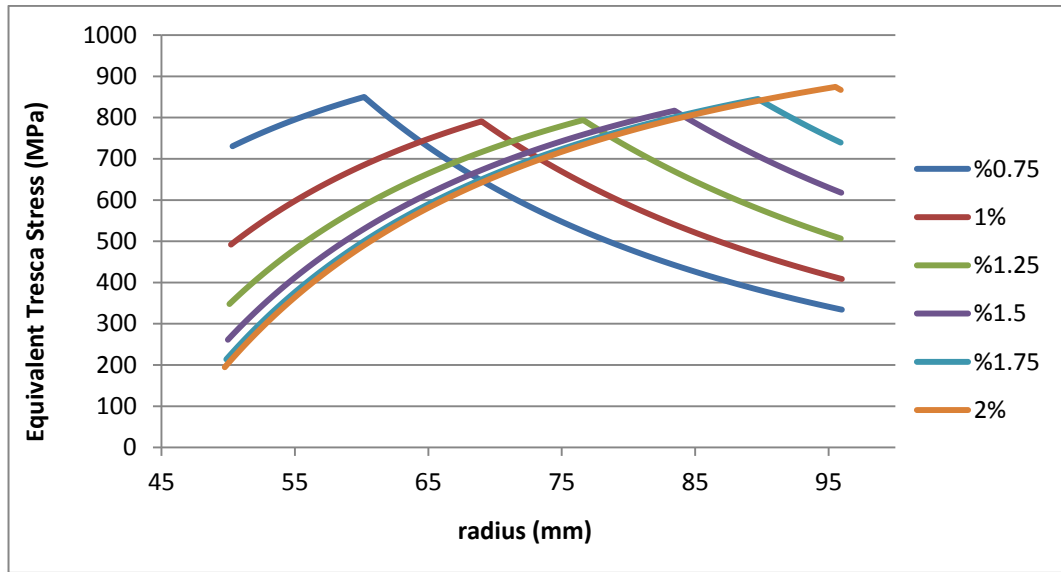


Figure 4.22 Tresca equivalent stresses in operating pressure

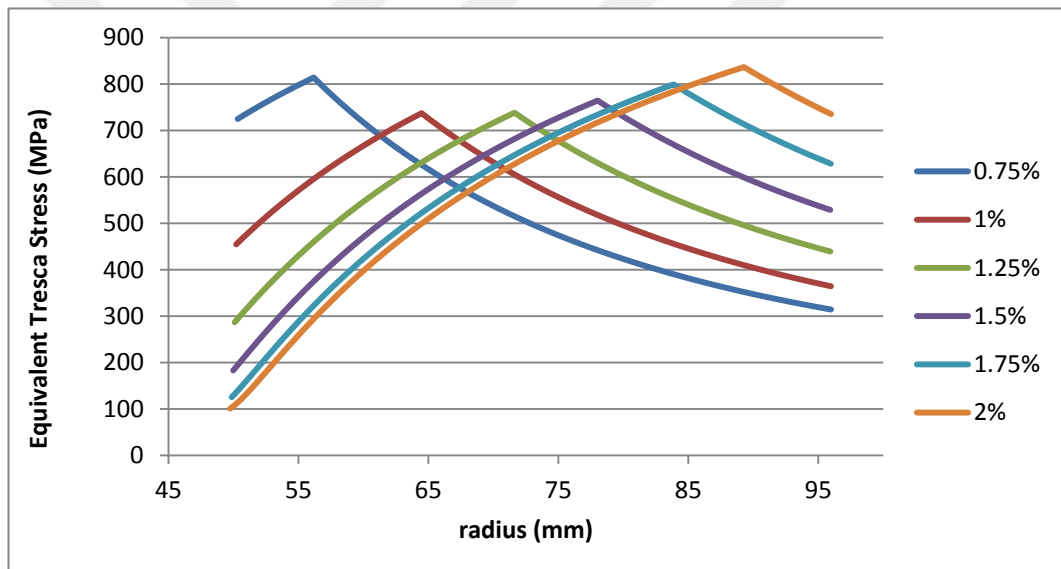


Figure 4.23 Von Mises equivalent stresses in operating pressure

In the above graphics, it is seen that the maximum stress values occur at the elastic-plastic junction. Therefore, the elastic-plastic junction is the most probable region for the plastic yielding. To determine the mandrel's optimum interference value with autofrettage draft, equivalent stresses for different interference values should be examined in the critical region and the interference value that has the least equivalent stress in this region should be chosen. When we examine the graphics, it is seen that the lowest Tresca and Von Mises equivalent stresses on the elastic plastic

junction occur on the 1% interference value. According to results of analytical model, the optimum interference is 1%.

#### 4.1.4.4 Investigation of the Stress Distributions in Case of Secondary Yielding Due to Bauschinger Effect

Previously, it was determined that autofrettage draft will not be subject to a secondary yielding due to Bauschinger effect. However, in this section, a hypothetical Bauschinger Effect Factor will be used to see the effect of the secondary yielding due to Bauschinger Effect on the stress behavior.

Previously, Bauschinger Effect Factors were determined for different interference values. Table 4.5 shows Bauschinger Effect Factors corresponding to different interference values according to Tresca yielding criterion. In Table 4.5, it is seen that BEF value corresponding to 1.5% interference ratio is 0.9531 for  $r = a$ . When the current BEF value changed to 0.5, it was seen that a secondary plastic yielding occurs in the autofrettage draft. It was assumed that the new BEF value does not depend on strain, i.e. it is constant. The stress distributions that are obtained for the new and previous BEF values are given below comparatively.

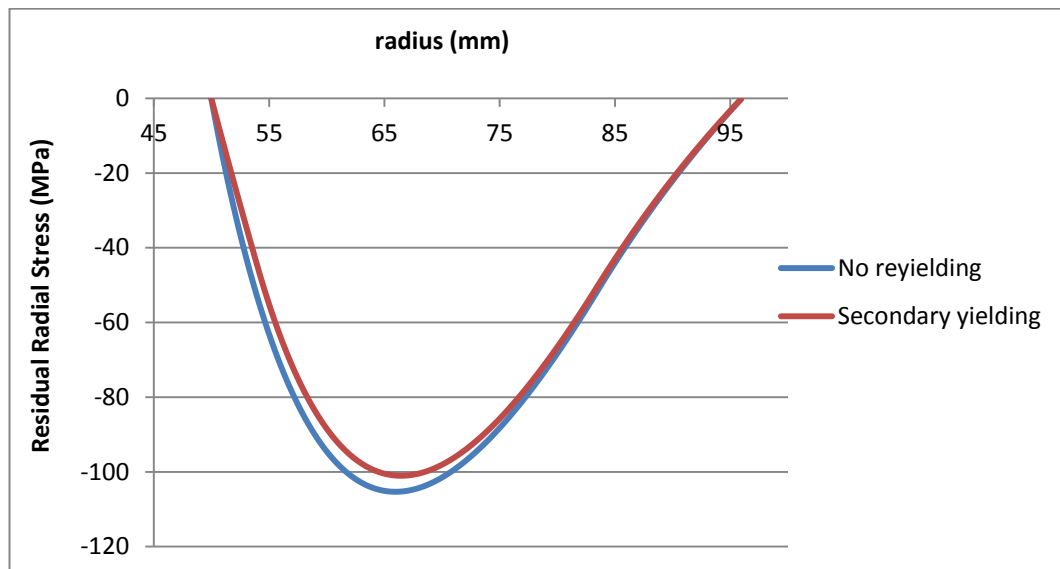


Figure 4.24 Residual radial stresses in case of secondary yielding



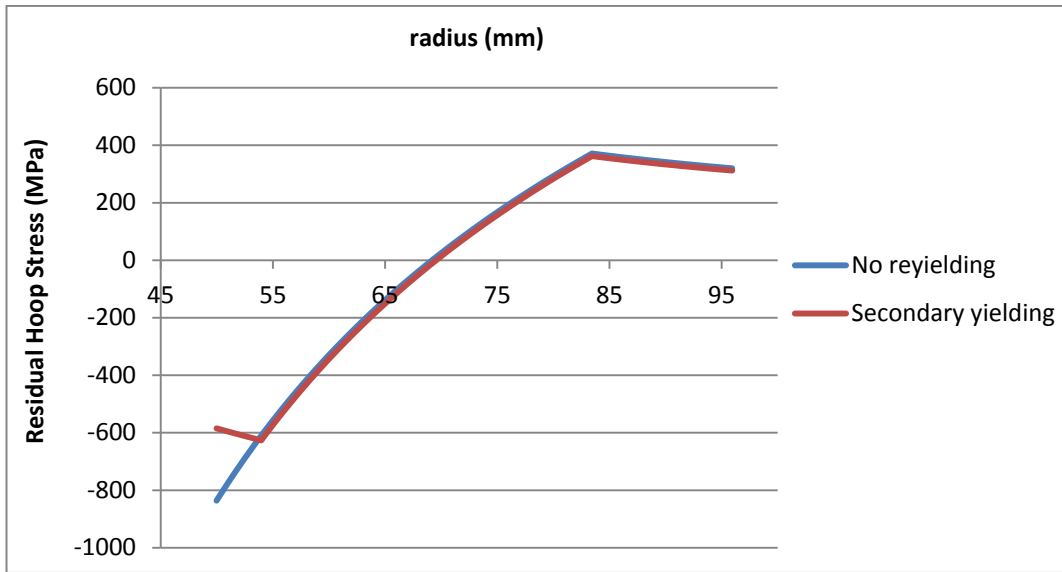


Figure 4.25 Residual hoop stresses in case of secondary yielding

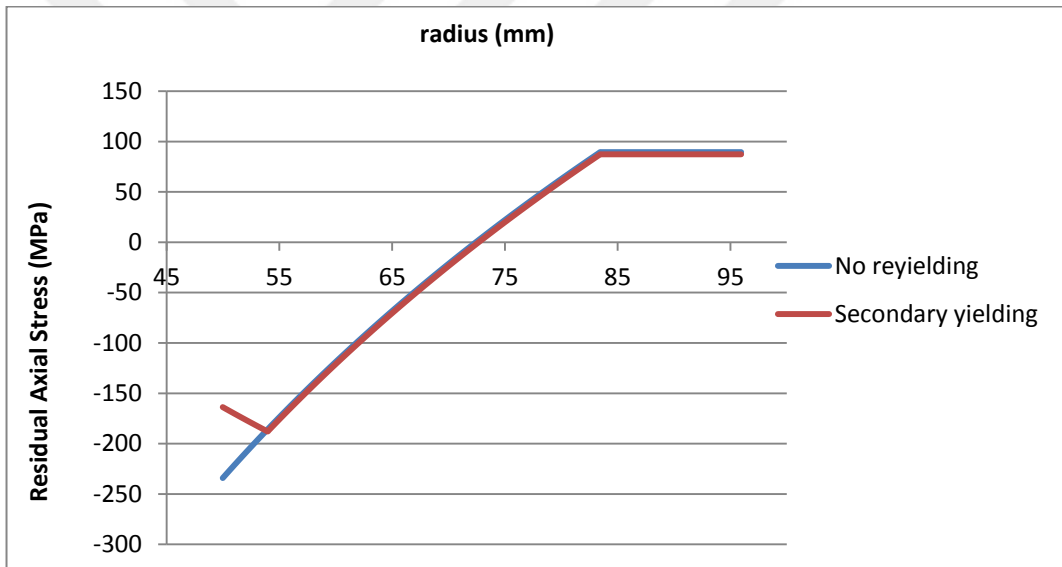
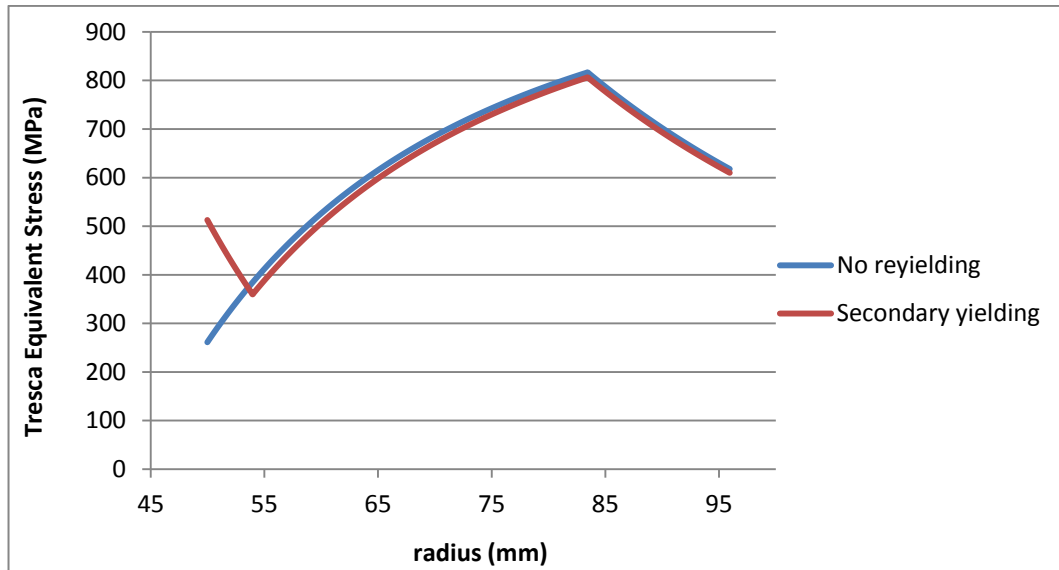


Figure 4.26 Residual axial stresses in case of secondary yielding



**Figure 4.27 Tresca equivalent stresses in service pressure in case of secondary yielding**

#### 4.1.4.5 Investigation of the Benefit of Autofrettage

In this section, the maximum pressure amount that the cylinder can withstand before the autofrettage process that is applied with 1% interference ratio and the maximum pressure amount that the cylinder can hold after the autofrettage process are compared.

**Table 4.7 Maximum pressure bearing capacity before and after autofrettage**

Before Autofrettage	After Autofrettage (Tresca)	After Autofrettage (Von Mises)
$P_{max}=414.956$ (MPa)	$P_{max}=641.099$ (MPa)	$P_{max}=688.281$ (MPa)

In Table 4.7, the maximum service pressures that can be applied up to the plastic yielding limit, before and after the autofrettage process that is applied with 1% interference ratio, are described. According to Tresca criterion, a 54% increase in the cylinder's pressure holding capacity is observed after the autofrettage whereas this increase is about 65% according to Von Mises criterion.

#### 4.1.4.6 Lightening the Barrel by External Turning

When the data in Table 4.7 are examined, it is seen that the pressure value that the barrel can hold within the safety limits is considerably higher than 400 MPa service

pressure. Therefore, it seems possible that the barrel can be lightened up to a certain amount by external turning without breaking the safety conditions of the barrel. In Table 4.8, the new outer radii that were obtained by external turning and the corresponding maximum pressure values are shown.

**Table 4.8 Tolerable maximum pressure values after removing material**

<b>Thickness of material removed from the outer surface (mm)</b>	<b>New outer radius (mm)</b>	<b>Pmax (MPa) according to Tresca criterion</b>	<b>Pmax (MPa) according to Von Mises criterion</b>
5	91	607.787	653.744
7.5	88.5	588.974	634.235
10	86	568.498	613
12.5	83.5	546.154	589.834
15	81	521.71	564.502
17.5	78.5	494.894	536.734
20	76	465.388	506.216
22.5	73.5	432.82	472.59
25	71	396.751	435.439
27.5	68.5	356.662	394.279
30	66	311.932	348.551

When the maximum material to be removed from the outer surface is being determined, the operation conditions of the barrel should be taken into consideration. It was stated previously that the operating pressure of the barrel is 400 MPa. Therefore, the pressure value that will start the plastic yielding after thinning the outer surface should be greater than 400 MPa. In the table above, it is seen that 22,5 mm thickness value provides higher values than the operating pressure for both two yielding criteria. Therefore, it is possible to reduce the outer radius from 96 mm to

73.5 mm. In the graphic below, the equivalent pre- and post-turning stress distributions of a cylinder that was autofrettaged with a 1% interference ratio are seen.

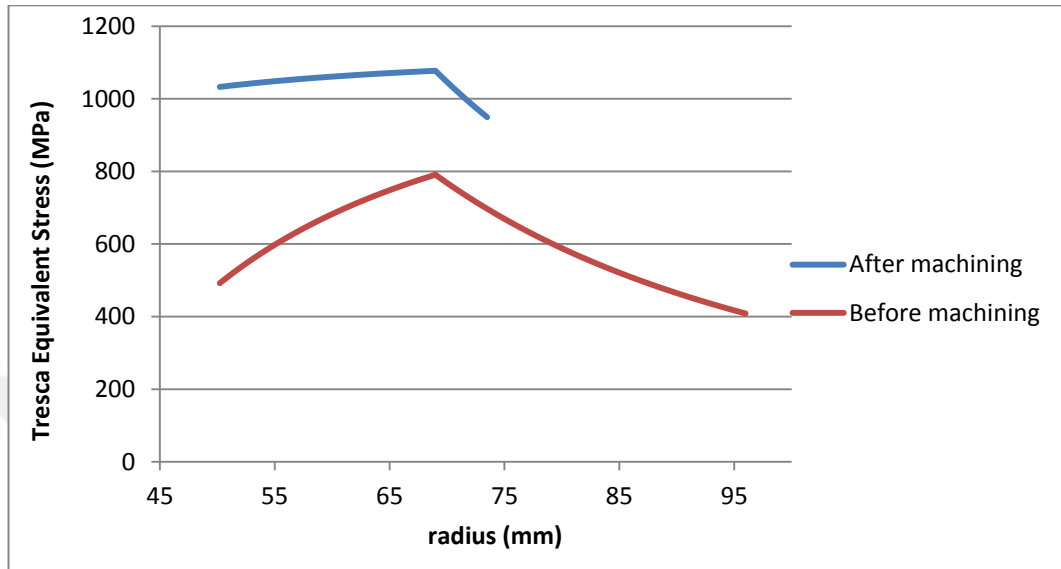


**Figure 4.28 Tresca equivalent stress distribution of 1% interference autofrettaged cylinder after 22.5 (mm) material is removed**

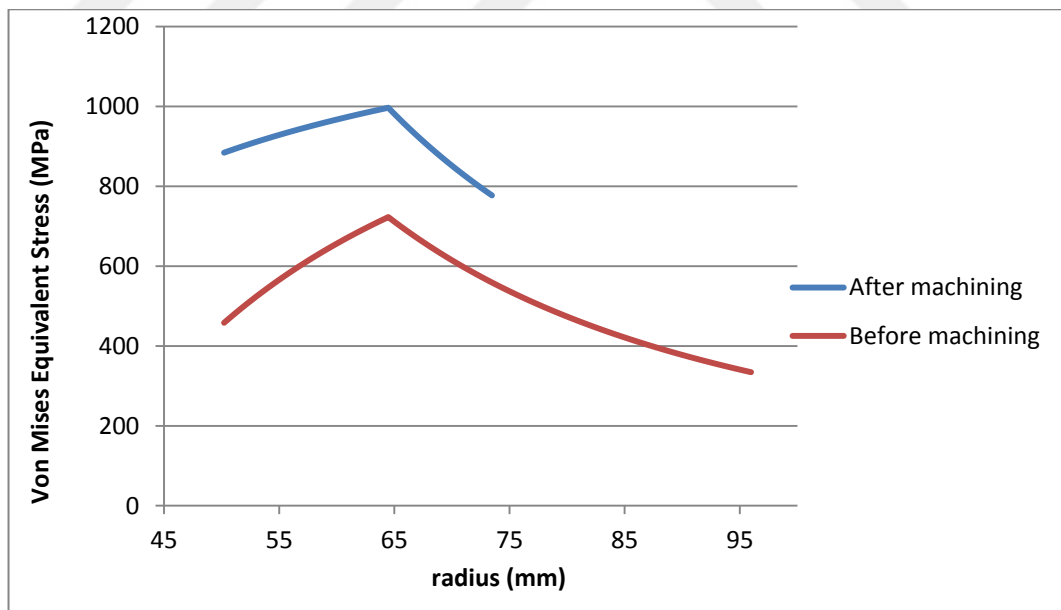


**Figure 4.29 Von Mises equivalent stress distribution of 1% interference autofrettaged cylinder after 22.5 mm material is removed**

## 4.2 Results of Finite Element Model

In this section, a three dimensional 1/4 cross-section calculation model will be constituted in Abaqus finite element program. Bilinear kinematic hardening model is used as the material model. The elastic-plastic material data are given for this model in Table 4.2. Autofrettage draft is fixed on one end to be subject to the tensile forces during the mandrel's movement. Mandrel was relocated and it was contacted to the draft all the way long. Friction coefficient is taken as 0.01.

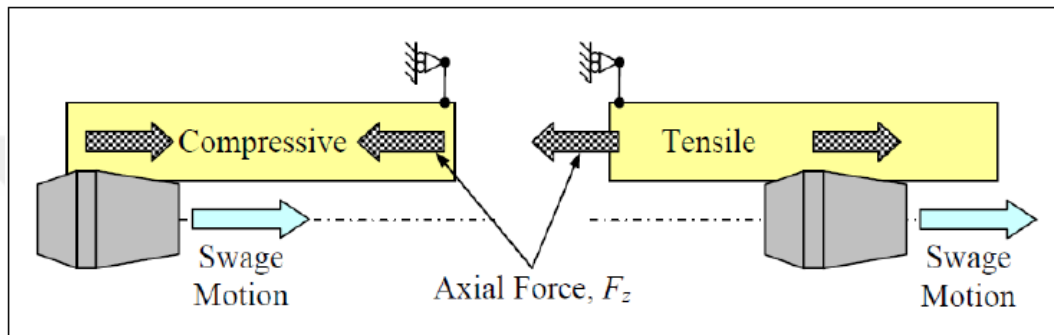


Figure 4.30 Movement of mandrel and tube constraints during swage autofrettage

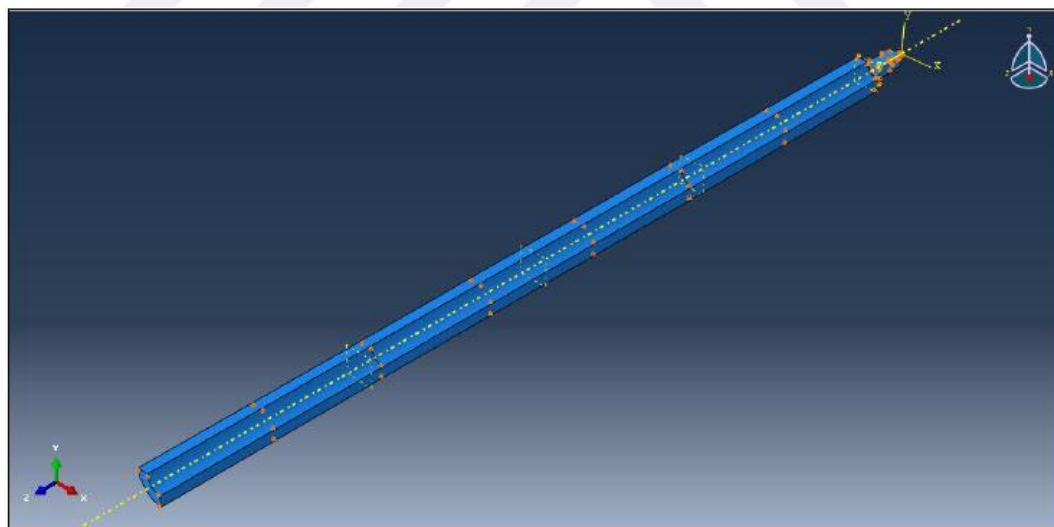


Figure 4.31 Abaqus 1/4 cross-sectioned calculation model

Both parts are modeled as transformable and the structure was formed by C3D8R (three dimensional 8 noded reduced integration element).

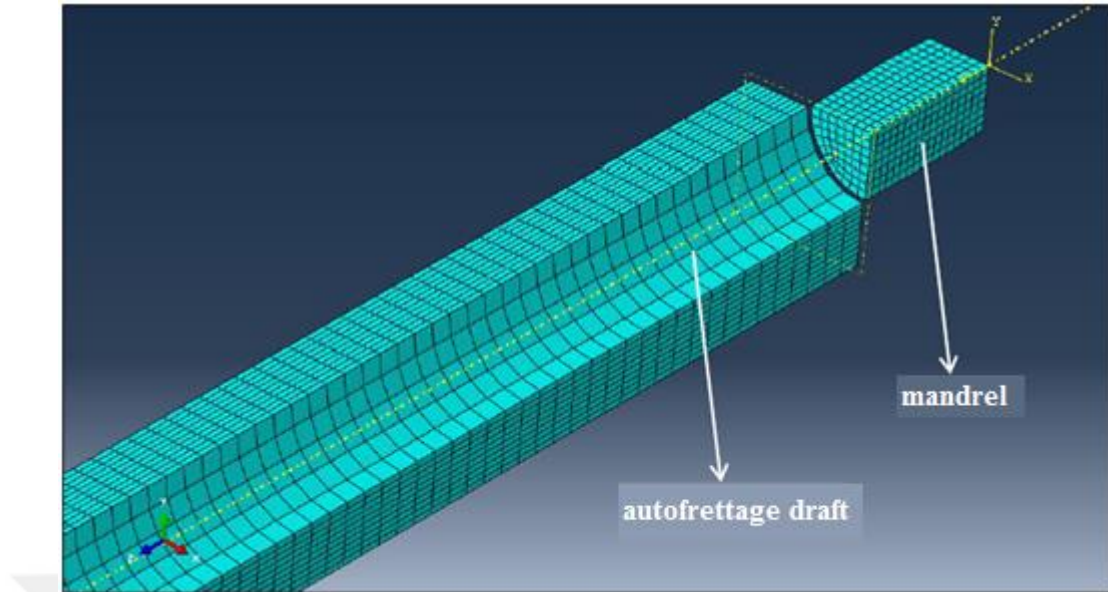


Figure 4.32 Mesh model

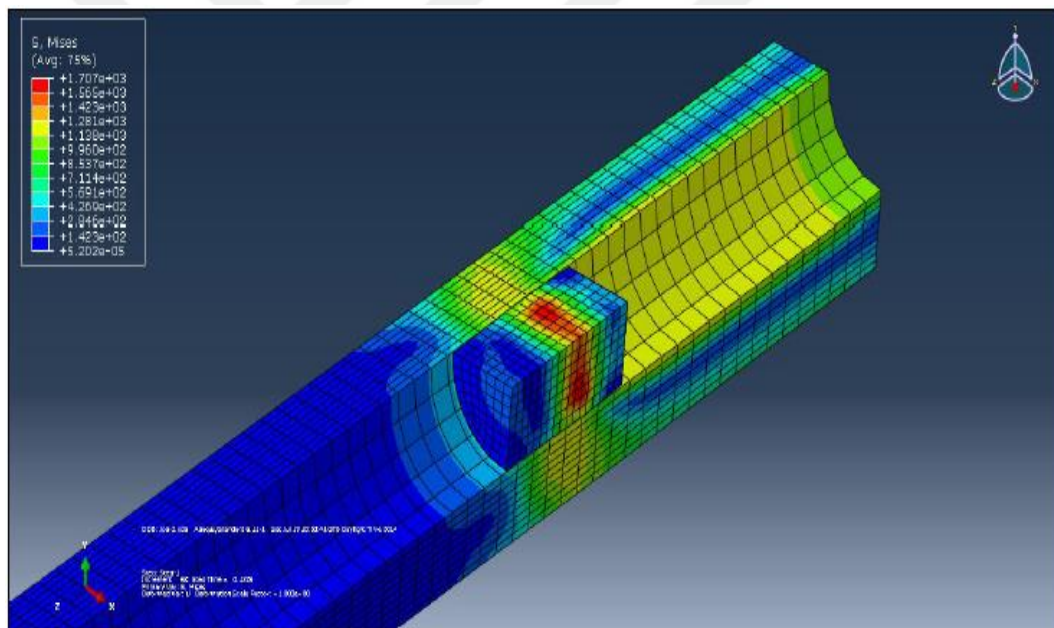


Figure 4.33 Representation of stresses during calculations

## 4.2.1 Residual Stresses

### 4.2.1.1 Radial Stresses

Figure 4.34 shows residual radial stress distributions that happen with different interference ratios. When the graphics are examined, it is seen that the radial stresses take negative values through the cylinder wall. Negative values describe that the residual radial stresses are compressive. Since there is no pressure force on the inner

and the outer surface of the cylinder, the residual radial stresses are zero on these surfaces. With the increase in the interference ratio, the bigger compressive stresses occur.

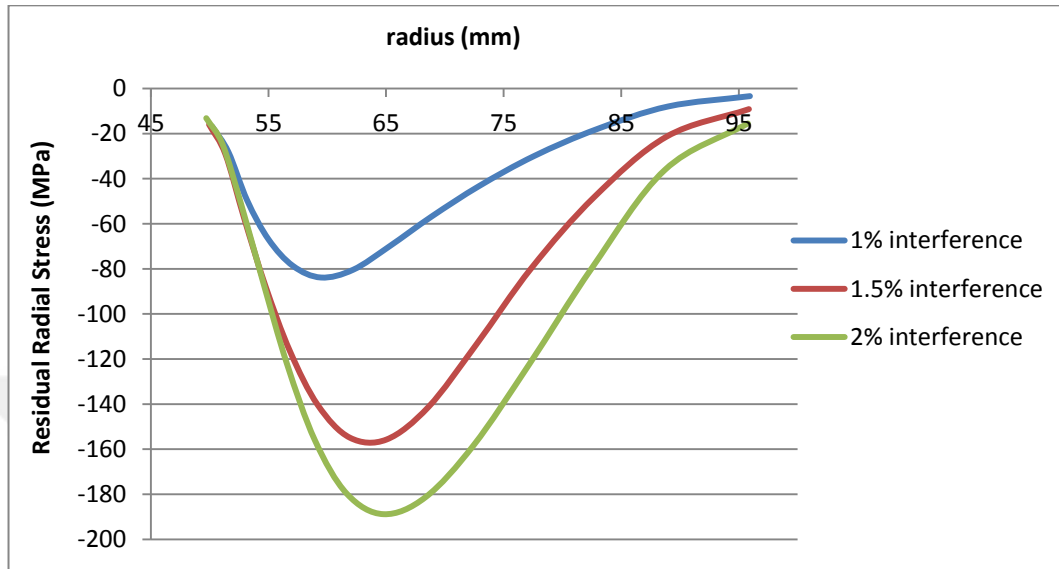


**Figure 4.34 Residual radial stresses for 1%, 1.5%, and 2% interference ratios**

#### 4.2.1.2 Hoop Stresses

Figure 4.35 shows residual tangential stress distributions that happen with different interference ratios. When the graphics are examined, it is seen that the residual tangential stresses take negative values on the cylinder's bore surface and in the region close to the inner surface. However, the tangential stresses are zeroized at a radius value close to the elastic region and have positive values after that point. Maximum tensile stresses are on the elastic plastic junction. In the graphic, there is a curvature in the region that is close to the inner hole surface. This curvature shows that a secondary plastic yielding happened in the cylinder.

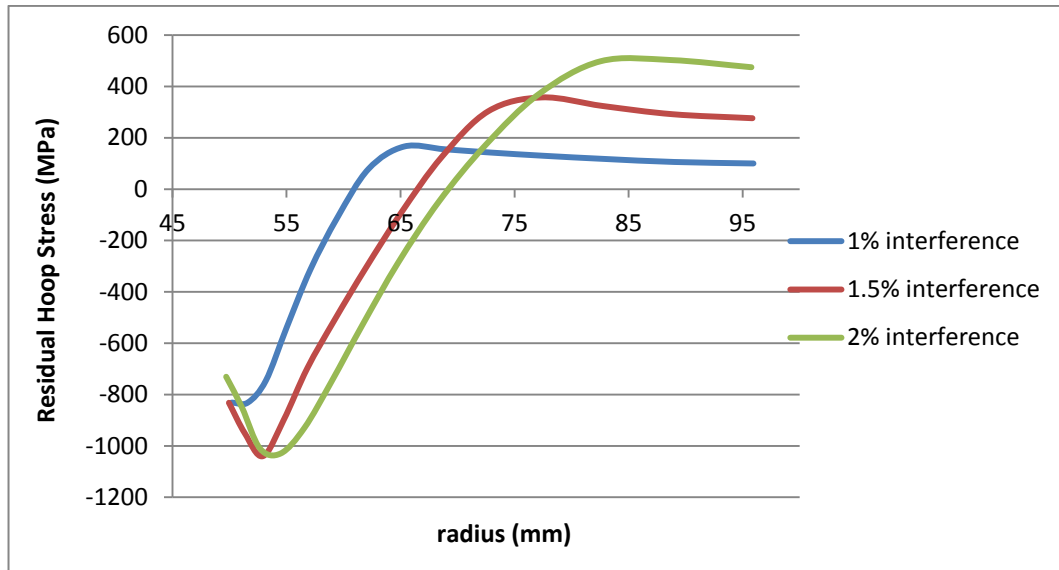


Figure 4.35 Residual hoop stresses for 1%, 1.5%, and 2% interference ratios

#### 4.2.1.3 Axial Stresses

As seen in Figure 4.36, the residual axial stresses exhibit a pretty wavy behavior. The residual axial stresses are compressive in two different region of the cylinder wall and tensile in two other different region.

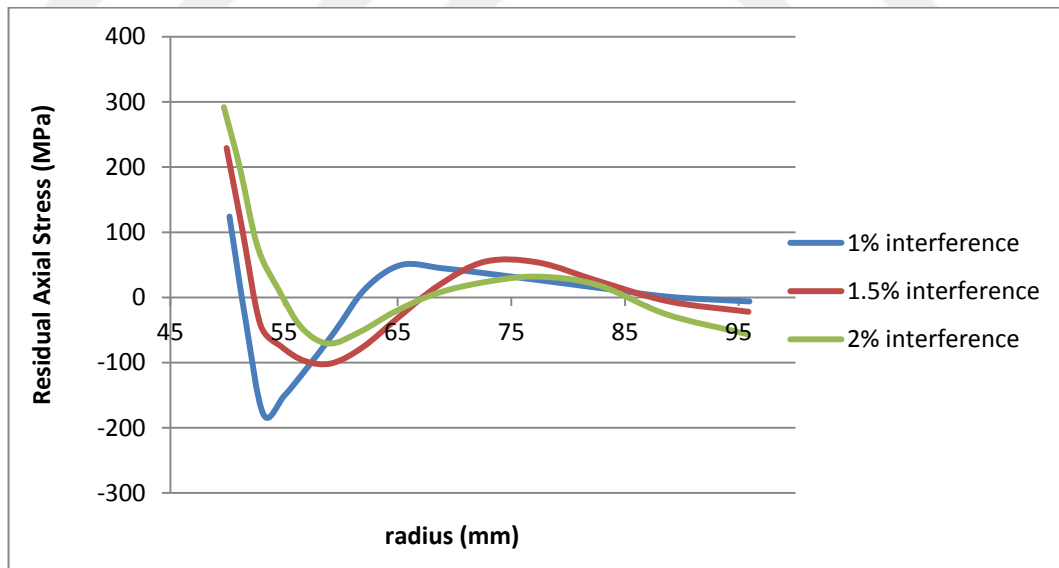


Figure 4.36 Residual axial stresses for 1%, 1.5%, and 2% interference ratios

#### 4.2.2 Equivalent Stresses at Operating Pressure

In Figure 4.37, Tresca equivalent stresses that occur due to operating pressure 400 MPa for different interference ratios are given. When the graphics are observed, it is



seen that the maximum stresses occur on the elastic plastic junction. The interference ratio at which the maximum stress has its minimum value is 1%. This interference ratio can be assumed to be the optimum interference ratio.

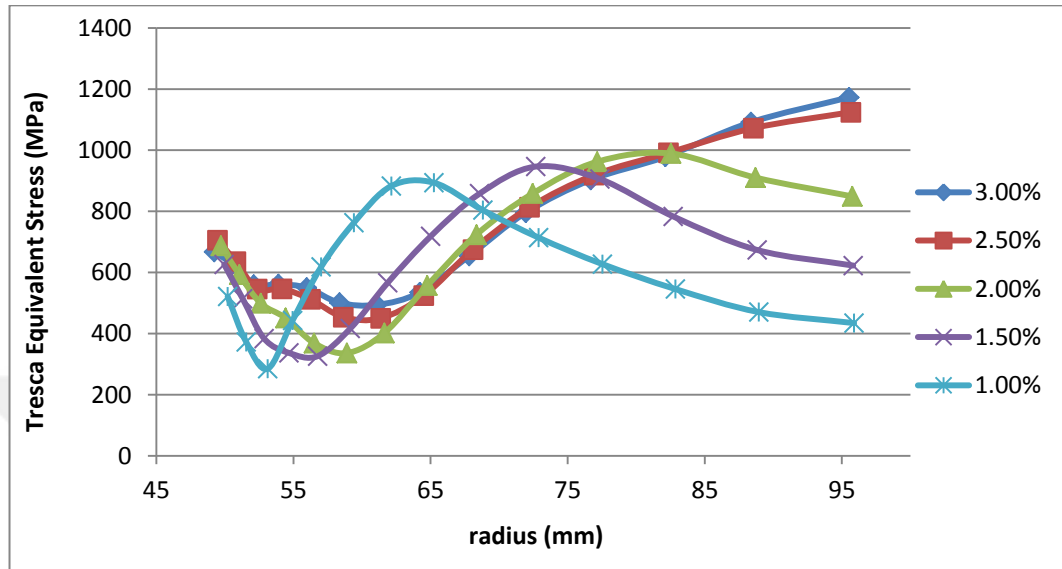


Figure 4.37 Tresca equivalent stresses occurring in the service pressure

In Figure 4.38, Von Mises equivalent stresses that occur due to operating pressure 400 MPa for different interference ratios are given. When the graphics are observed, it is seen that Von Mises equivalent stresses have a slight difference in behavior compared to Tresca equivalent stresses. Optimum interference ratio is 1.5% with respect to Von Mises criterion.

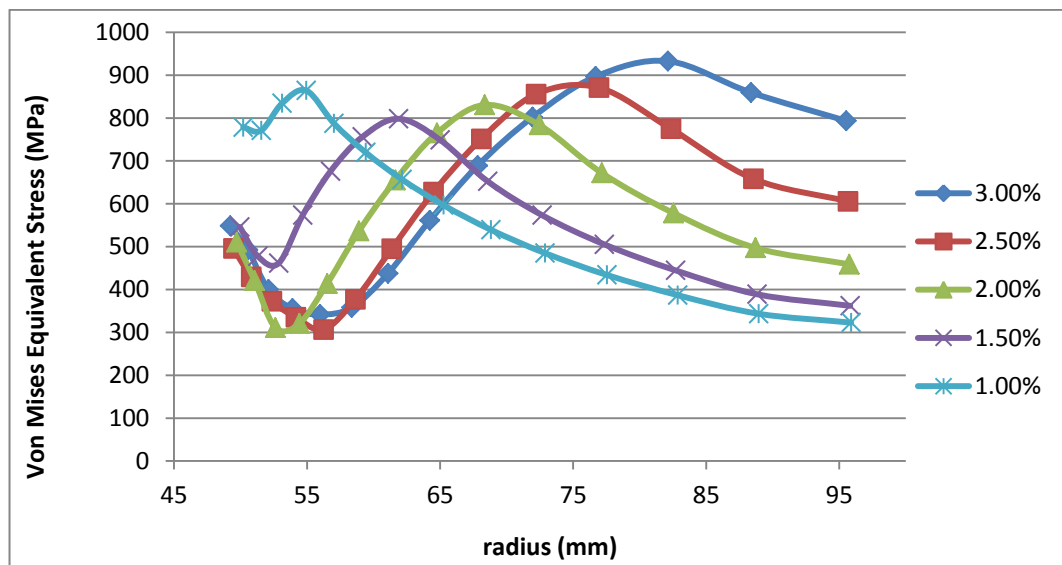


Figure 4.38 Von Mises equivalent stresses occurring in the service pressure

### 4.3 Comparison of Results of Analytical Model and Finite Element Model

#### 4.3.1 Residual Stresses

##### 4.3.1.1 Radial Stresses

When Figures 4.39-4.40-4.41 are examined, it is seen that the residual radial stresses have higher values in results of finite element model than the ones in results of analytical model. Especially, it is seen that the difference between results of finite element model and analytical analytical model is more significant in the regions where exist the largest compressive stresses.

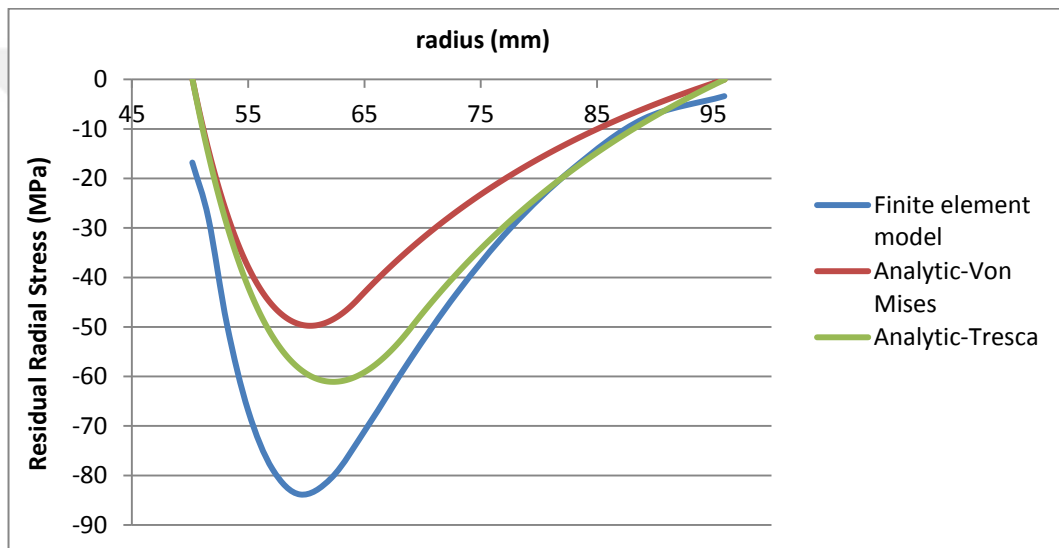


Figure 4.39 Residual radial stresses for 1% interference ratio

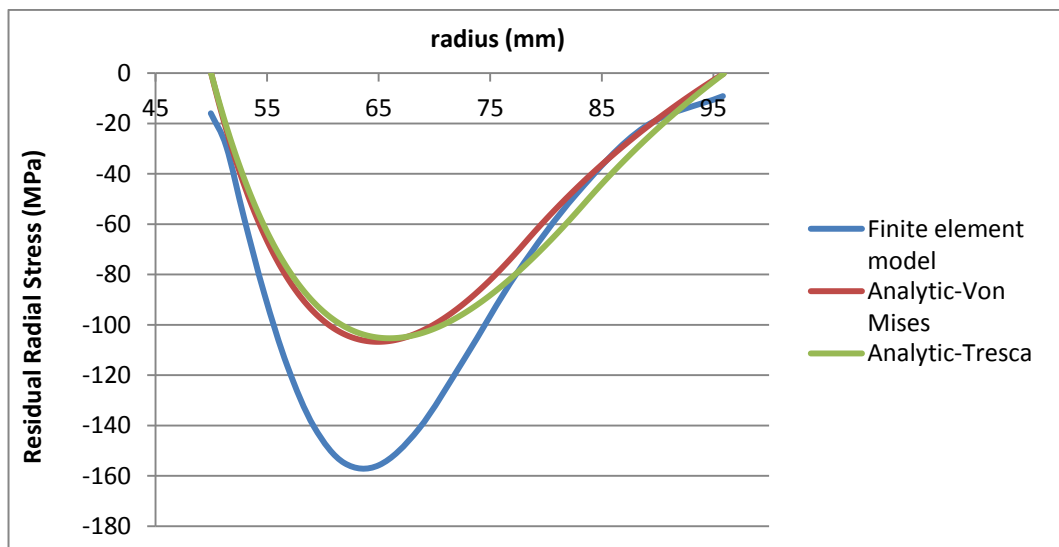
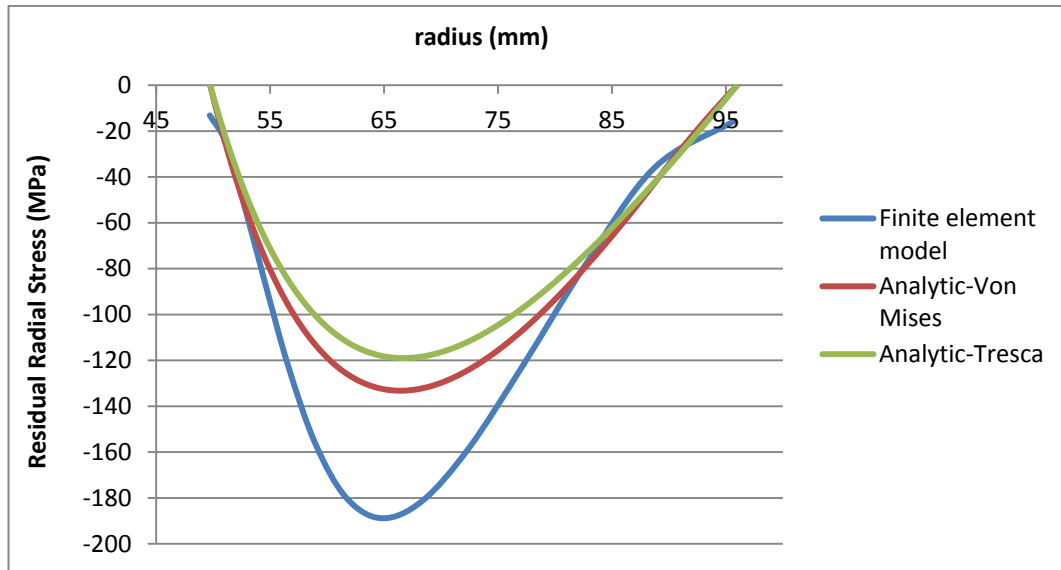


Figure 4.40 Residual radial stresses for 1.5% interference ratio



**Figure 4.41 Residual radial stresses for 2% interference ratio**

#### 4.3.1.2 Hoop Stresses

When Figures 4.42-4.43-4.44 are examined, it is seen that results of finite element model and analytical model are in compliance with each other. Some curvatures arise at the end portions of the numerically obtained graphics. These curvatures are the indicators that a secondary yielding occurred. Secondary yielding could not be determined in the analytical method.

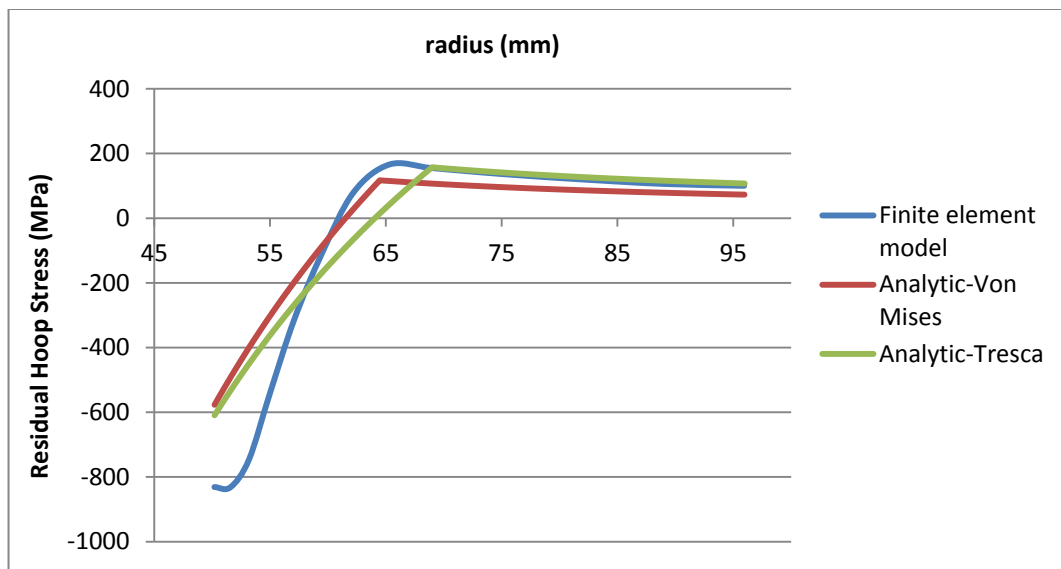


**Figure 4.42 Residual hoop stresses for 1% interference ratio**

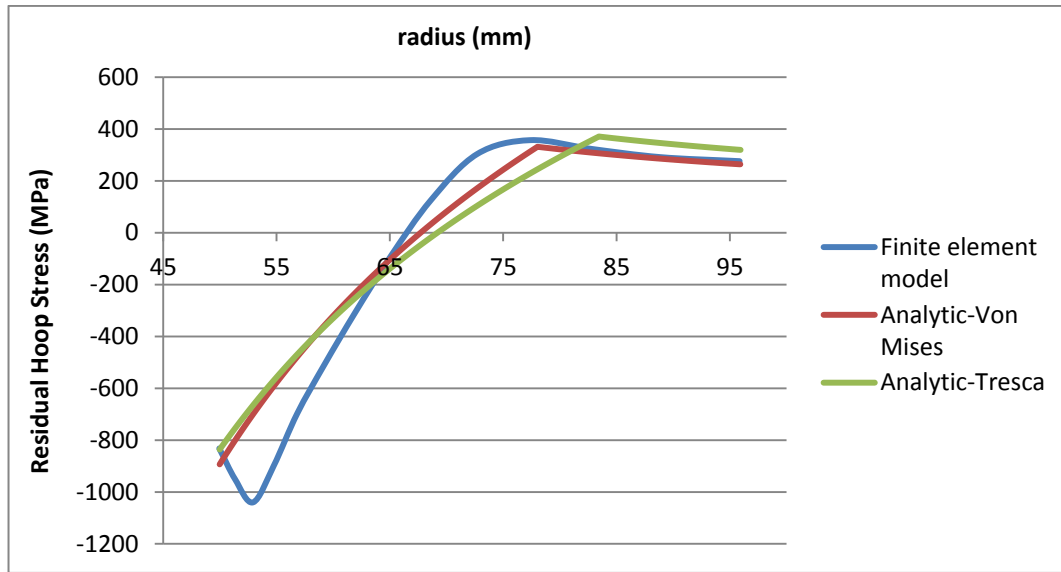


**Figure 4.43 Residual hoop stresses for 1.5% interference ratio**

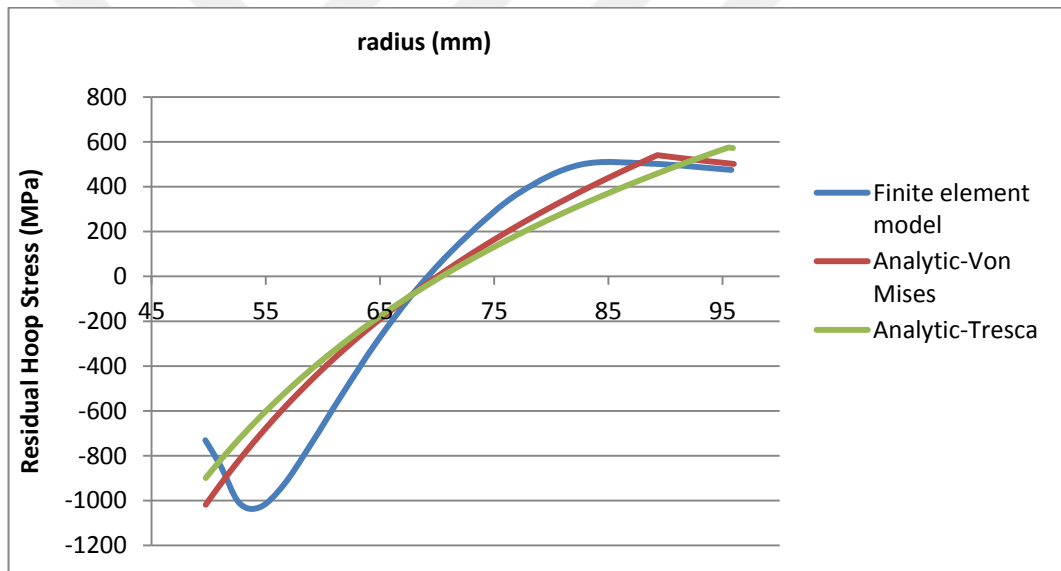


**Figure 4.44 Residual hoop stresses for 2% interference ratio**

#### 4.3.1.3 Axial Stresses

When Figures 4.45-4.46-4.47 are examined, it is seen that results of finite element model and analytical model overlap in a small interval and there are dramatic differences in the other regions.

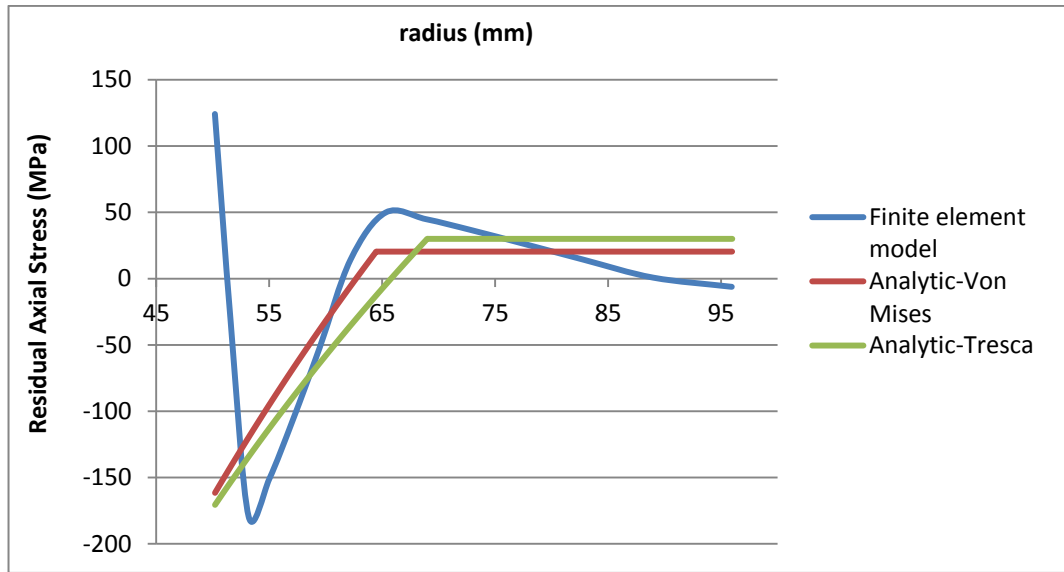


Figure 4.45 Residual axial stresses for 1% interference ratio

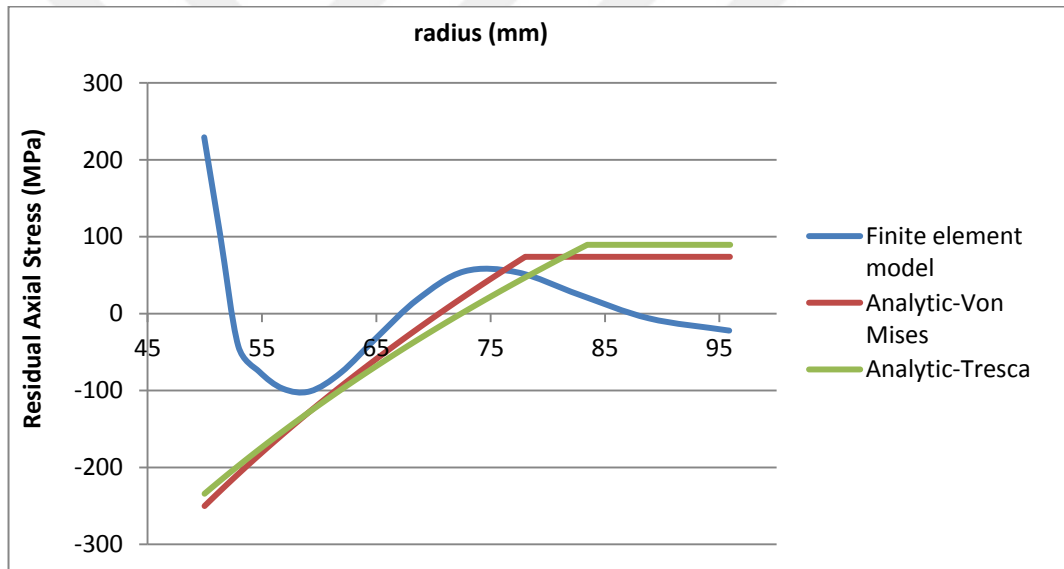


Figure 4.46 Residual axial stresses for 1.5% interference ratio

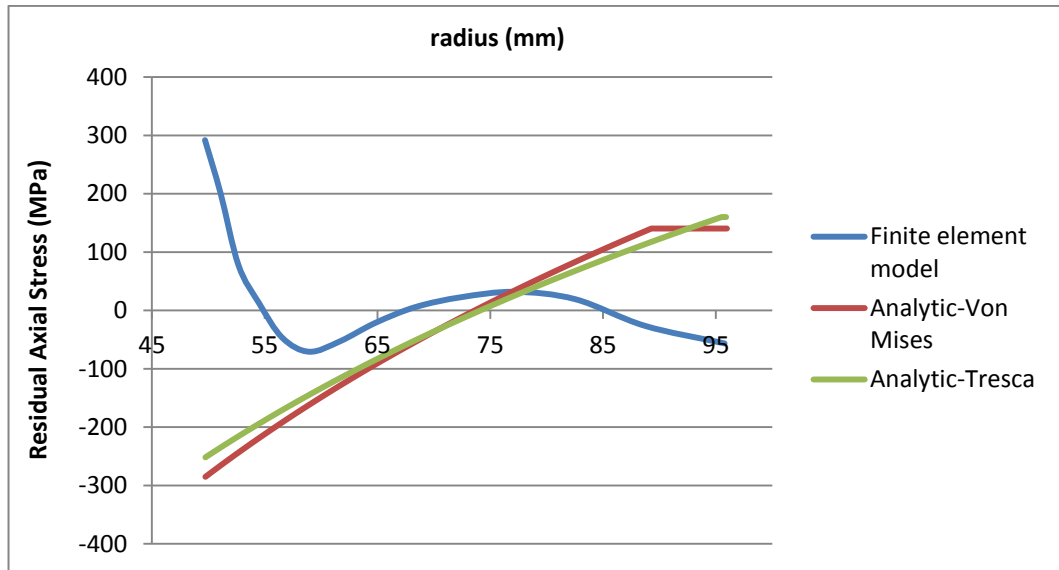


Figure 4.47 Residual axial stresses for 2% interference ratio

#### 4.3.1.4 The Comparison of Elastic-Plastic Radius Values

Table 4.9 Comparison of elastic-plastic radius values

% Interference	Tresca Elastic-Plastic Radius (mm)	Von Mises Elastic-Plastic Radius (mm)	Elastic-Plastic Radius according to Finite Element Model
1 %	68.9921	64.4771	68.8772
1.5 %	83.4477	78.0227	77.3804
2 %	95.5099	89.2869	88.7117
2.5 %	wholly plastic	wholly plastic	wholly plastic

When Table 4.9 is examined, it is seen that Von Mises criterion has more compatible results with finite element model.

#### 4.4 Conclusions

1. A significant strength increase is gained with the autofrettage of thick walled cylinders. As a result of the analytical calculations, it was determined that a minimum 54% increase in the pressure holding capacity was gained due to the autofrettage process at 1% interference ratio.

2. The failure risk on the plastic junction increases with the compression ratios on the optimum interference ratio, whereas a bigger strength increase is gained on the inner wall.

3. In case of the secondary yielding, a certain amount of decrease in the strength gain on the inner wall is met depending on the size of the secondary region. However, no significant strength gain difference is observed except the secondary plastic region.

4. Results of finite element model and analytical model are consistent with each other at a significant level. There is a remarkable inconsistency between results of finite element model and analytical model for residual axial stresses. It is thought that the reason of this inconsistency is that the physical conditions can not be reflected to the mathematical model exactly.

#### **4.5 Recommendations**

1. The plasticity theory which is used in the this thesis study for the analytical calculations is Henky's deformation theory. This theory is a simplified theory of plasticity. Incremental theory of plasticity can be used to obtain more precise results.

2. One of the most important benefits of the autofrettage process is that this process prolongs the container's fatigue life. In this thesis study, the contribution of the autofrettage process to increase of the pressure bearing capacity of the thick walled cylindrical containers is investigated. However, its contribution to fatigue life is not discussed. Fatigue life should also be discussed to examine the autofrettage process in total.

3. The autofrettage process that will be applied to the barrel was studied by analytical and numerical methods. The experiments that have the real physical conditions should be performed in order to obtain more realistic results.

## REFERENCES

- Abdelsalam, O., *Analysis and optimization of autofrettaged and shrink-fitted compound cylinders under thermo-mechanical loads*, Concordia University, 2012
- Ali, A.R.M., Ghosh, N.C., & Alam, T.E., *Optimum design of pressure vessel subjected to autofrettage process*, International Scholarly and Scientific Research & Innovation, 4(10), 582-587, 2010
- Ayob, A., & Elbasheer, M.K., *Optimum autofrettage pressure in thick cylinders*, Jurnal Mekanikal, 24, 1-14, 2007
- Babu, D.D., & Balaji, T.J., *Theoretical and finite element analysis of high pressure components*, Journal of Engineering, 3, 25-34, 2013
- Basara, A., *Evaluation of high pressure components of fuel injection systems using speckle interferometry*, Thesis (PhD), Universität Erlangen-Nürnberg, 2007
- Chakrabarty, J., *Theory of plasticity*, (3th ed.), Elsevier, UK, 1996
- Chang, L., Pan, Y., & Ma, X., *Residual stress calculation of swage autofrettage gun barrel*, International Journal of Computer Science Issues, 10, 52-59, 2013
- Chang, L., Pan, Y., & Ma, X., *Residual stress calculation of swage autofrettage gun barrel*, International Journal of Computer Science Issues, 10, 52-59, 2013
- Chen, Peter C.T., *A simple analysis of swage autofrettage process*, Technical Report ARCCB-TR-88030, US Army Armament Research Development and Engineering Center, Close Combat Armaments Center, Benet Laboratories, Newyork, USA, 1988
- Chen, Peter C.T., *Analytical solution of elastic-plastic thick-walled cylinders with general hardening*, Technical Report ARCCB-TR-92010, US Army Armament Research Development and Engineering Center, Close Combat Armaments Center, Benet Laboratories, Newyork, USA, 1992
- Clark, G., *Residual stresses in swage-autofrettged thick-walled cylinders*, Report MRL-R-847, Defence Science and Technology Organisation, Materials Research Laboratories, Melbourne, Australia, 1982
- Davidson, T.E., Kendall, D.P., & Reiner, A.N., *Residual stresses in thick-walled cylinders resulting from mechanically induced overstrain*, Experimental Mechanics, 253-268, 1963



Farhangdoost, K.H., & Hosseini, A., *The effect of mandrel speed upon the residual stress distribution around cold expanded hole*, Procedia Engineering, 10, 2184-2189, 2011

Gao, X.L., *Elasto-plastic analysis of an internally pressurized thick-walled cylinder using a strain gradient plasticity theory*, International Journal of Solids and Structures, 40, 6445-6455, 2003

Gibson, M.C., *Determination of residual stress distributions in autofrettaged thick-walled cylinders*, Thesis (PhD), Cranfield University, 2008

Ghosh, N.C., Alam, T.E., & Ali, A.R.M., *Theoretical and numerical optimization of autofrettage in strain hardened thick-walled cylinders*, Proceedings of the 8th International Conference on Mechanical Engineering 2009, 26- 28 December 2009 Bangladesh, 1-6, 2009

Gündüzer, O., *Namlu cidarı boyutlandırılmasına iç balistik davranışın etkisi*, Thesis (M.S.), Gazi University, 2011

Hosford, W.F., Caddell, R.M., *Metal forming*, (3th ed.), Cambridge University Press, 2007

Hu, Z., & Puttagunta, S., *Computer modeling of internal pressure autofrettage process of a thick-walled cylinder with the bausinger effect*, American Transactions on Engineering & Applied Sciences, 1, 143-161, 2012

Hu, Z., & Penumarthy, C., *Computer modeling and optimization of swage autofrettage process of a thick-walled cylinder incorporating bausinger effect*, American Transactions on Engineering & Applied Sciences, 3, 31-63, 2014

Huang, X.P., & Cui, W.C., *Effect of bausinger effect and yield criterion on residual stress distribution of autofrettaged tube*, Journal of Pressure Vessel Technology, 128, 212-216, 2006

Islam, M.R., *A comparative elasto-plastic study of autofrettaged cylindrical pressure vessel (al & steel) by finite element analysis*, Thesis (M.S.), Jadavpur University, 2013

Jahed, H., *A variable material approach for elastic-plastic analysis of proportional and nonproportional loading*, Thesis (PhD), University of Waterloo, 1997

Jahed, H., & Ghanbari, G., *Actual unloading behavior and its significance on residual stress in machined autofrettaged tubes*, Journal of Pressure Vessel Technology, 125, 321-325, 2003

Jost, G.S., *Stresses and strains in a cold-worked annulus*, Aircraft Structures Report 434, Defence Science and Technology Organisation, Aeronautical Research Laboratory, Melbourne, Australia, 1988

Khan, A.S., & Huang, S., *Continuum theory of plasticity*, John Wiley & Sons, 1995

Kim, N.H., *Derivation of von Mises Criterion*, University of Florida, <http://www2.mae.ufl.edu/nkim/eas4200c/>

Lee, E.Y., Lee, Y.S., Yang, Q.M., Kim, J.H., Cha, K.U., & Hong, S.K., *Autofrettage process analysis of a compound cylinder based on the elastic-perfectly plastic and strain hardening stress-strain curve*, Journal of Mechanical Science and Technology, 23, 3153-3160, 2009

Loghman, A., & Wahab, W.A., *Loading and unloading of thick-walled cylindrical pressure vessels of strain-hardening material*, Journal of Pressure Vessel Technology, 116, 105-109, 1994

Majzoobi, G.H., & Ghomi, A., *Optimisation of autofrettage in thick-walled cylinders*, Journal of Achievements in Materials and Manufacturing Engineering, 16, 124-131, 2006

Marciniak, Z., Duncan, J.L., & Hu, S.J., *Mechanics of sheet metal forming*, (2th ed.), Butterworth-Heinemann, 2002

Milligan, R.V., Koo, W.H., & Davidson, T.E., *The Bauschinger effect in a high strength-steel*, Journal of Basic Engineering, 480-488, 1966

Öztörün, D., *Bir ağır silah namlusunun sonlu elemanlar yöntemi ile elastik-plastik gerilme analizi*, Thesis (M.S.), Gazi University, 2013

Parker, Anthony P., Underwood, John H., *Influence of the bauschinger effect on residual stress and fatigue lifetimes in autofrettaged thick-walled cylinders*, Technical Report ARCCB-TR-97020, US Army Armament Research Development and Engineering Center, Close Combat Armaments Center, Benet Laboratories, Newyork, USA, 1997

Parker, A.P., *Autofrettage of open-end tubes-pressures, stresses, strains, and code comparisons*, Journal of Pressure Vessel Technology, 123, 271-281, 2001

Partovi, A., & Saadat, S.S., *Analysis of autofrettaged high pressure components*, Thesis (M.S.), Blekinge Institute of Technology of Technology, 2012

Perry, J., & Aboudi, J., *Elasto-plastic stresses in thick walled cylinders*, Journal of Pressure Vessel Technology, 125, 248-252, 2003

Sitharam, T.G., & Govindaraju, G., *Applied elasticity for engineers*, <http://www.nptel.ac.in/courses/105108070/12>, 01.07.2015

Sönmez, U., *Obüs namlusu yanma odasında atış esnasında ortaya çıkan gerilmelerin matematiksel modellenmesi ve analizi*, Thesis (M.S.), Sakarya University, 2009

Sun, Q.P., *Thick walled cylinders and spinning disks*, <http://www.me.ust.hk/~meqpsun/>, 01.07.2015

Ugural, A.C., & Fenster, S.K., *Advanced mechanics of materials and applied elasticity*, (5th ed.), Pearson Education, 2012

Vullo, V., *Circular cylinders and pressure vessels-stress analysis and design*, Springer, 2014

Wahi, N., Ayob, A., & Elbasheer, M.K., *Effect of optimum autofrettage on pressure limits of thick-walled cylinder*, International Journal of Environmental Science and Development, 329-333, 2011

Wikipedia, *Filament Winding*, The Free Encyclopedia, 30 April 2015, 12:29, Wikimedia Foundation, 30 January 2015 <<http://en.wikipedia.org>>

Yayla, P., *Uygulamalı elastisite teorisi*, Nobel, 2014

Zhao, W., Seshadri, R., & Dubey, R.N., *On thick-walled cylinder under internal pressure*, Journal of Pressure Vessel Technology, 125, 267-273, 2003

Zhu, R., & Zhu, G., *On autofrettage of cylinders by limiting circumferential residual stress based on mises yield criterion*, Journal of Theoretical and Applied Mechanics, 51, 697-710, 2013

## CURRICULUM VITAE

### **Personal Information**

**Name :** Halil Yıldırım  
**Marital Status :** Married  
**Nationality :** Republic of Turkey  
**Date of Birth :** 18.01.1988  
**Driver's license :** B  
**e-mail :** hyildirim@ybu.edu.tr

### **Job Experience**

#### **Research Assistant**

**Yıldırım Beyazıt University**

**09.2012-... Ankara - Turkey**

Working as teaching assistant in Engineering Mathematics I, Engineering Mathematics II, Strength of Materials

### **Education Information**

**University (Master's Degree) :** Yıldırım Beyazıt University  
Mechanical Engineering  
2012-2015

**University (Bachelor's Degree) :** Kırıkkale University  
Mechanical Engineering  
2007-2011

### **Competencies**

Microsoft Office  
SolidWorks  
Matlab  
Ansys  
Abaqus  
C programming

### **Foreign Language**

English